



Yifei Wang

Implementation and Investigation of Stress-Recovery-Algorithms in the Finite Element Toolbox AMfe

Semesterarbeit

30. 05. 2016

Supervisor:

Johannes Rutzmoser

Abstract

The motivation of this paper is to implement Python code in Finite Element Toolbox AMfe for the purpose of achieving an relatively exact approximation of strain and stress. The assignment we are trying to complete in this paper is the expansion of Finite Element Toolbox AMfe, which will make it possible to solve the nodal strain and stress. The approach we adopted to solve the problem is Stress-Recovery-Algorithms. This is a method based on extrapolation from Gauss points in contrast to the Direct-Evaluation-Algorithms, which directly evaluate the stress at nodes. The objects of my analysis for stress recovery in this research are six element types in AMfe Toolbox: quadrilateral element with four nodes (Quad4), quadrilateral element with eight nodes (Quad8), triangular element with three nodes (Tri3), triangular element with six nodes (Tri6), tetrahedral element with four nodes (Tet4), and tetrahedral element with four nodes (Tet10). The procedure of extrapolation for each element types will be discussed in detail in this paper. After the computing of the nodal stress, the patch test for both algorithms (Stress-Recovery-Algorithm and Direct-Evaluation-Algorithms) and a convergence analysis for all six element types will be also presented in this paper. Towards the end of this paper, the strain and stress contour plots by both algorithms will be compared to the solution calculated by the commercial Finite Element software ANSYS. The significance of our obtained results is that the solution of Stress-Recovery-Algorithms is closer to the analytical solution than the solution of Direct-Evaluation-Algorithms for Tri6, Quad4, Quad8, and Tet10. For both element types Tri3 and Quad4, the respective results for nodal stress from the Stress-Recovery-Algorithms and the Direct-Evaluation-Algorithms are exactly the same.

Acknowledgements

First of all, I would like to express my sincere gratitude to my supervisor Johannes Rutzmoser for the continuous support of my study and related research, for his patience, motivation, and immense knowledge I am deeply grateful of his help in the completion of this thesis. His guidance helped me in all the time of finite element research and get in with Finite- Element- Research-code. I could not have imagined having a better advisor and mentor for my study in Finite-Element- Method.

Contents

1	Introduction	1
1.1	Motivation	1
1.2	Structure of Study	2
2	Numerical Aspect for Finite Element Formulation	5
2.1	Shape Function	5
2.1.1	Quadrilateral Elements	5
2.1.2	Triangular and Tetrahedral Elements	6
2.2	Non-linear Element Formulation	7
2.3	Stress Recovery	13
2.3.1	Extrapolation of Stress from Gauss points	13
2.3.2	Quadrilateral element with four nodes: Quad4	15
2.3.3	Quadrilateral element with eight nodes: Quad8	19
2.3.4	Triangular element with three nodes: Tri3	21
2.3.5	Triangular element with six nodes: Tri6	24
2.3.6	Tetrahedral element with four nodes: Tet4	27
2.3.7	Tetrahedral element with ten nodes: Tet10	28
2.4	Assembly	31
3	Programming Implementation and Investigation	39
3.1	Pre-Processing with ANSYS	39
3.2	Unit Testing with Python	40
3.3	The Patch Test	43
3.4	Convergence Analysis	44
3.5	Complex Model Test	46
4	Conclusion	105
4.1	Summary	105
4.2	Recommendation	106
References		107

List of Figures

1.1	Stress-Strain curve for steel	2
1.2	Flow chart of structure	3
1.3	Overview of this essay structure	4
2.1	Linear shape function and quadratic shape function.	6
2.2	triangular and tetradral elemnets.	7
2.3	Quadrangle with four nodes	15
2.4	Quad4 in element coordinate and Gauss element coordinate.	16
2.5	Equation of side opposite corner 1 for Quad4.	17
2.6	Equation of side opposite corner 1 for Quad4.	18
2.7	Quad8 in element coordinate and Gauss element coordinate.	22
2.8	Equation of side opposite corner 1 for Quad8.	23
2.9	Tri3 in element coordinate and Gauss element coordinate.	24
2.10	Equation of side opposite corner 1 for Tri3.	25
2.11	Tri6 in element coordinate and Gauss element coordinate.	27
2.12	Equation of side opposite corner 1 for Tri6.	28
2.13	Tet4 in element coordinate and Gauss element coordinate.	29
2.14	Tet10 in element coordinate and Gauss element coordinate.	33
2.15	Two Tri6 elements in global and local perspective.	35
3.1	A simple meshed geometry	40
3.2	A model for test of 3D elements	42
3.3	A model for test of 2D elements	45
3.4	left: Contour plot of ϵ_{xx} from ANSYS (SMN: minimal value; SMX: maximal value); right: Contour plot of ϵ_{xx} calculated in AMfe, demonstrate in ParaView	46
3.5	Patch Test of Tet4	47
3.6	Convergence analysis	47
3.7	2D model meshing with Tri3 for displacement convergence analysis; P as observer point	48
3.8	3D model meshing with Tet4 for displacement convergence analysis; P as observer point	49
3.9	Convergence plot of Tri3 and Tri6	49
3.10	Convergence plot of Quad4 and Quad8	50

3.11 Convergence plot of Tet4 and Tet10	50
3.12 Convergence analysis of Von Mises stress in a 2D model	51
3.13 Left: Top view of the tank; Right: the 1/16 model of the tank, point D is regarded as the observer point for analysis	51
3.14 Convergence analysis of Von Mises stress, the analytical solutions are 2147.43N/mm^2 for 2D model and 68.94N/mm^2 for 3D model	54
3.15 Chromatic aberration between ParaView and ANSYS	54
3.16 Mesh with Tri3, upper: contour plot of ϵ_{xx} in ANSYS; lower left: contour plot of ϵ_{xx} calculated without stress recovery in AMfe; lower right: contour plot of ϵ_{xx} calculated with stress recovery in AMfe	57
3.17 Mesh with Tri3, upper: contour plot of ϵ_{yy} in ANSYS; lower left: contour plot of ϵ_{yy} calculated without stress recovery in AMfe; lower right: contour plot of ϵ_{yy} calculated with stress recovery in AMfe	58
3.18 Mesh with Tri3, upper: contour plot of ϵ_{xy} in ANSYS; lower left: contour plot of ϵ_{xy} calculated without stress recovery in AMfe; lower right: contour plot of ϵ_{xy} calculated with stress recovery in AMfe	59
3.19 Mesh with Tri3, upper: contour plot of σ_{xx} in ANSYS; lower left: contour plot of σ_{xx} calculated without stress recovery in AMfe; lower right: contour plot of σ_{xx} calculated with stress recovery in AMfe	60
3.20 Mesh with Tri3, upper: contour plot of σ_{yy} in ANSYS; lower left: contour plot of σ_{yy} calculated without stress recovery in AMfe; lower right: contour plot of σ_{yy} calculated with stress recovery in AMfe	61
3.21 Mesh with Tri3, upper: contour plot of σ_{xy} in ANSYS; lower left: contour plot of σ_{xy} calculated without stress recovery in AMfe; lower right: contour plot of σ_{xy} calculated with stress recovery in AMfe	62
3.22 Mesh with Tri6, upper: contour plot of ϵ_{xx} in ANSYS; lower left: contour plot of ϵ_{xx} calculated without stress recovery in AMfe; lower right: contour plot of ϵ_{xx} calculated with stress recovery in AMfe	63
3.23 Mesh with Tri6, upper: contour plot of ϵ_{yy} in ANSYS; lower left: contour plot of ϵ_{yy} calculated without stress recovery in AMfe; lower right: contour plot of ϵ_{yy} calculated with stress recovery in AMfe	64
3.24 Mesh with Tri6, upper: contour plot of ϵ_{xy} in ANSYS; lower left: contour plot of ϵ_{xy} calculated without stress recovery in AMfe; lower right: contour plot of ϵ_{xy} calculated with stress recovery in AMfe	65
3.25 Mesh with Tri6, upper: contour plot of σ_{xx} in ANSYS; lower left: contour plot of σ_{xx} calculated without stress recovery in AMfe; lower right: contour plot of σ_{xx} calculated with stress recovery in AMfe	66
3.26 Mesh with Tri6, upper: contour plot of σ_{yy} in ANSYS; lower left: contour plot of σ_{yy} calculated without stress recovery in AMfe; lower right: contour plot of σ_{yy} calculated with stress recovery in AMfe	67
3.27 Mesh with Tri6, upper: contour plot of σ_{xy} in ANSYS; lower left: contour plot of σ_{xy} calculated without stress recovery in AMfe; lower right: contour plot of σ_{xy} calculated with stress recovery in AMfe	68

3.28 Mesh with Quad4, upper: contour plot of ϵ_{xx} in ANSYS; lower left: contour plot of ϵ_{xx} calculated without stress recovery in AMfe; lower right: contour plot of ϵ_{xx} calculated with stress recovery in AMfe	69
3.29 Mesh with Quad4, upper: contour plot of ϵ_{yy} in ANSYS; lower left: contour plot of ϵ_{yy} calculated without stress recovery in AMfe; lower right: contour plot of ϵ_{yy} calculated with stress recovery in AMfe	70
3.30 Mesh with Quad4, upper: contour plot of ϵ_{xy} in ANSYS; lower left: contour plot of ϵ_{xy} calculated without stress recovery in AMfe; lower right: contour plot of ϵ_{xy} calculated with stress recovery in AMfe	71
3.31 Mesh with Quad4, upper: contour plot of σ_{xx} in ANSYS; lower left: contour plot of σ_{xx} calculated without stress recovery in AMfe; lower right: contour plot of σ_{xx} calculated with stress recovery in AMfe	72
3.32 Mesh with Quad4, upper: contour plot of σ_{yy} in ANSYS; lower left: contour plot of σ_{yy} calculated without stress recovery in AMfe; lower right: contour plot of σ_{yy} calculated with stress recovery in AMfe	73
3.33 Mesh with Quad4, upper: contour plot of σ_{xy} in ANSYS; lower left: contour plot of σ_{xy} calculated without stress recovery in AMfe; lower right: contour plot of σ_{xy} calculated with stress recovery in AMfe	74
3.34 Mesh with Quad8, upper: contour plot of ϵ_{xx} in ANSYS; lower left: contour plot of ϵ_{xx} calculated without stress recovery in AMfe; lower right: contour plot of ϵ_{xx} calculated with stress recovery in AMfe	75
3.35 Mesh with Quad8, upper: contour plot of ϵ_{yy} in ANSYS; lower left: contour plot of ϵ_{yy} calculated without stress recovery in AMfe; lower right: contour plot of ϵ_{yy} calculated with stress recovery in AMfe	76
3.36 Mesh with Quad8, upper: contour plot of ϵ_{xy} in ANSYS; lower left: contour plot of ϵ_{xy} calculated without stress recovery in AMfe; lower right: contour plot of ϵ_{xy} calculated with stress recovery in AMfe	77
3.37 Mesh with Quad8, upper: contour plot of σ_{xx} in ANSYS; lower left: contour plot of σ_{xx} calculated without stress recovery in AMfe; lower right: contour plot of σ_{xx} calculated with stress recovery in AMfe	78
3.38 Mesh with Quad8, upper: contour plot of σ_{yy} in ANSYS; lower left: contour plot of σ_{yy} calculated without stress recovery in AMfe; lower right: contour plot of σ_{yy} calculated with stress recovery in AMfe	79
3.39 Mesh with Quad8, upper: contour plot of σ_{xy} in ANSYS; lower left: contour plot of σ_{xy} calculated without stress recovery in AMfe; lower right: contour plot of σ_{xy} calculated with stress recovery in AMfe	80
3.40 Mesh with Tet4, upper: contour plot of ϵ_{xx} in ANSYS; lower left: contour plot of ϵ_{xx} calculated without stress recovery in AMfe; lower right: contour plot of ϵ_{xx} calculated with stress recovery in AMfe	81
3.41 Mesh with Tet4, upper: contour plot of ϵ_{yy} in ANSYS; lower left: contour plot of ϵ_{yy} calculated without stress recovery in AMfe; lower right: contour plot of ϵ_{yy} calculated with stress recovery in AMfe	82

3.42 Mesh with Tet4, upper: contour plot of ϵ_{zz} in ANSYS; lower left: contour plot of ϵ_{zz} calculated without stress recovery in AMfe; lower right: contour plot of ϵ_{zz} calculated with stress recovery in AMfe	83
3.43 Mesh with Tet4, upper: contour plot of ϵ_{xy} in ANSYS; lower left: contour plot of ϵ_{xy} calculated without stress recovery in AMfe; lower right: contour plot of ϵ_{xy} calculated with stress recovery in AMfe	84
3.44 Mesh with Tet4, upper: contour plot of ϵ_{yz} in ANSYS; lower left: contour plot of ϵ_{yz} calculated without stress recovery in AMfe; lower right: contour plot of ϵ_{yz} calculated with stress recovery in AMfe	85
3.45 Mesh with Tet4, upper: contour plot of ϵ_{xz} in ANSYS; lower left: contour plot of ϵ_{xz} calculated without stress recovery in AMfe; lower right: contour plot of ϵ_{xz} calculated with stress recovery in AMfe	86
3.46 Mesh with Tet4, upper: contour plot of σ_{xx} in ANSYS; lower left: contour plot of σ_{xx} calculated without stress recovery in AMfe; lower right: contour plot of σ_{xx} calculated with stress recovery in AMfe	87
3.47 Mesh with Tet4, upper: contour plot of σ_{yy} in ANSYS; lower left: contour plot of σ_{yy} calculated without stress recovery in AMfe; lower right: contour plot of σ_{yy} calculated with stress recovery in AMfe	88
3.48 Mesh with Tet4, upper: contour plot of σ_{zz} in ANSYS; lower left: contour plot of σ_{zz} calculated without stress recovery in AMfe; lower right: contour plot of σ_{zz} calculated with stress recovery in AMfe	89
3.49 Mesh with Tet4, upper: contour plot of σ_{xy} in ANSYS; lower left: contour plot of σ_{xy} calculated without stress recovery in AMfe; lower right: contour plot of σ_{xy} calculated with stress recovery in AMfe	90
3.50 Mesh with Tet4, upper: contour plot of σ_{yz} in ANSYS; lower left: contour plot of σ_{yz} calculated without stress recovery in AMfe; lower right: contour plot of σ_{yz} calculated with stress recovery in AMfe	91
3.51 Mesh with Tet4, upper: contour plot of σ_{xz} in ANSYS; lower left: contour plot of σ_{xz} calculated without stress recovery in AMfe; lower right: contour plot of σ_{xz} calculated with stress recovery in AMfe	92
3.52 Mesh with Tet10, upper: contour plot of ϵ_{xx} in ANSYS; lower left: contour plot of ϵ_{xx} calculated without stress recovery in AMfe; lower right: contour plot of ϵ_{xx} calculated with stress recovery in AMfe	93
3.53 Mesh with Tet10, upper: contour plot of ϵ_{yy} in ANSYS; lower left: contour plot of ϵ_{yy} calculated without stress recovery in AMfe; lower right: contour plot of ϵ_{yy} calculated with stress recovery in AMfe	94
3.54 Mesh with Tet10, upper: contour plot of ϵ_{zz} in ANSYS; lower left: contour plot of ϵ_{zz} calculated without stress recovery in AMfe; lower right: contour plot of ϵ_{zz} calculated with stress recovery in AMfe	95
3.55 Mesh with Tet10, upper: contour plot of ϵ_{xy} in ANSYS; lower left: contour plot of ϵ_{xy} calculated without stress recovery in AMfe; lower right: contour plot of ϵ_{xy} calculated with stress recovery in AMfe	96

3.56	Mesh with Tet10, upper: contour plot of ϵ_{yz} in ANSYS; lower left: contour plot of ϵ_{yz} calculated without stress recovery in AMfe; lower right: contour plot of ϵ_{yz} calculated with stress recovery in AMfe	97
3.57	Mesh with Tet10, upper: contour plot of ϵ_{xz} in ANSYS; lower left: contour plot of ϵ_{xz} calculated without stress recovery in AMfe; lower right: contour plot of ϵ_{xz} calculated with stress recovery in AMfe	98
3.58	Mesh with Tet10, upper: contour plot of σ_{xx} in ANSYS; lower left: contour plot of σ_{xx} calculated without stress recovery in AMfe; lower right: contour plot of σ_{xx} calculated with stress recovery in AMfe	99
3.59	Mesh with Tet10, upper: contour plot of σ_{yy} in ANSYS; lower left: contour plot of σ_{yy} calculated without stress recovery in AMfe; lower right: contour plot of σ_{yy} calculated with stress recovery in AMfe	100
3.60	Mesh with Tet10, upper: contour plot of σ_{zz} in ANSYS; lower left: contour plot of σ_{zz} calculated without stress recovery in AMfe; lower right: contour plot of σ_{zz} calculated with stress recovery in AMfe	101
3.61	Mesh with Tet10, upper: contour plot of σ_{xy} in ANSYS; lower left: contour plot of σ_{xy} calculated without stress recovery in AMfe; lower right: contour plot of σ_{xy} calculated with stress recovery in AMfe	102
3.62	Mesh with Tet10, upper: contour plot of σ_{yz} in ANSYS; lower left: contour plot of σ_{yz} calculated without stress recovery in AMfe; lower right: contour plot of σ_{yz} calculated with stress recovery in AMfe	103
3.63	Mesh with Tet10, upper: contour plot of σ_{xz} in ANSYS; lower left: contour plot of σ_{xz} calculated without stress recovery in AMfe; lower right: contour plot of σ_{xz} calculated with stress recovery in AMfe	104

List of Tables

2.1	Gauss-Legendre points and weights	14
2.2	Natural Coordinate of Quad4	19
2.3	Natural Coordinate of Tri3	24
2.4	Tetrahedral Coordinate of Tet4	30
2.5	Coordinate system of Tet10	32
3.1	Node list exported from ANSYS	41
3.2	Element list exported from ANSYS	41
3.3	Unit testing of the result using Direct-Evaluation-Algorithms	43
3.4	Unit testing of the extrapolate result using Stress-Recovery-Algorithms	44
3.5	Convergence analysis of displacement for triangular element	52
3.6	Convergence analysis of displacement for quadrilateral element	53
3.7	Convergence analysis of displacement for tetrahedral element	55
3.8	Convergence analysis of Von Mises stress	56

Chapter 1

Introduction

1.1 Motivation

The Finite Element Method (FEM) is a numerical technique for finding approximate solutions to boundary value problems for partial differential equations. FEM contains linear FEM and non-linear FEM. Linear analysis follows the equation $K \cdot D = F$, in which K stands for stiffness matrix, D stands for displacement, and F stands for force. It means that the correlation of force and displacement is linear. This relation between force and displacement is only valid for materials that have elastic linear property. But in real situation, elastic materials such as steel has also non- linear region. (see the Figure 1.1). The property of steel is elastic linear up until yield point. Then the steel is yielding and becomes non-linear. Non-linear states include geometry non-linear and material non-linear. The example in Figure 1.1 describes a non-linear case and it also the main topic of this thesis. In the fields of engineering and science, FEM is a powerful tool in producing strength visualization and can help engineers to minimize weight, materials and costs. The accuracy of solution are only limited by the quality of model and by the available computational power. Ever since the computational power has been improved enormously, the FEM software has offered a wide range of simulations of complex model designs and system analyses.

AMfe is a nonlinear finite element code for structural application at the chair of applied mechanics in Technical University of Munich. AMfe Toolbox is developed in Python and Fortran. Python is a high-level, interpreted, and dynamically-typed programming language. There are many numerical packages built on Python, such as Numpy, Scipy, Pandas. These packages provide high-performance and easy to use data structures, both of which match the FEM developing work. The fact that Python is a high-level programming language makes it less time-consuming to develop the code. However, Python is slow for repeated execution of low-level task. Each Python operation comes with a small type-checking overhead, and when many repeated small operations add up, the overhead becomes significant. For this reason, A part of the AMfe code is rewritten in Fortran. Fortran is a general-purpose and imperative programming language that is specially tailored for numeric computation and scientific computing. Therefore, the combination of Python and Fortran retains the advantages of both - the easy-to-develop nature of Python and the fast numeric computation in Fortran. The aim of AMfe Toolbox is to solve and anal-

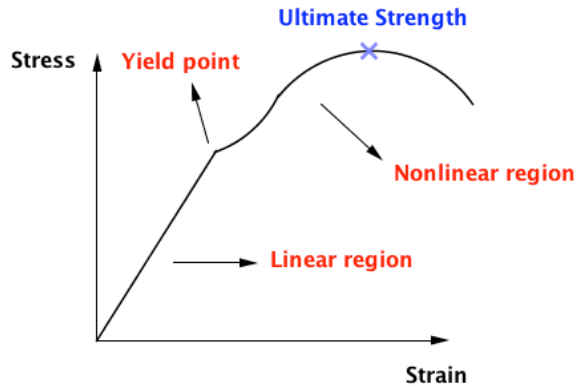


Figure 1.1: Stress-Strain curve for steel

use FEM problems, especially structural mechanical problems. The toolbox contains several modules with different functions to solve problems step by step. A simple structure of AMfe is depicted in Figure 1.3. Displacement, stress, and strain are three important factors in structural mechanical engineering. The function for calculating nodal displacements is completed in AMfe Toolbox, but functions for calculating nodal stress and strain remain blank. Strain and stress calculations are important in structural mechanical analysis and geometric design. For this reason, functions for solving of stress and strain will be added to AMfe Toolbox. When strain and stress calculations are completed, the aim of research is then shifted to improving the accuracy of these results. In order to do so, stress recovery is an approach to extrapolate the element solution to nodal solution. The goal is to be as accurate as possible in the computed displacements while keeping the computational effort reasonable. When the most important functions are completed and running well, it is time to check if AMfe Toolbox exports the reasonable results. The results of stress and strain from AMfe Toolbox will be compared with a commercial FEM software - ANSYS. The comparison of each element type will be recorded and discussed.

1.2 Structure of Study

This study can be divided into three parts. Figure 1.2 shows the structural flow chart in this study. The first part is marked with a green box. The main function for this part is to export the data of a meshed geometry using ANSYS Parametric Design Language(APDL) code and import the data into the AMfe Toolbox. This procedure, which is called Pre-Processing, is the first step in solving a problem in Finite Element Analysis. This step also ensures the analyses from both ANSYS and AMfe Toolbox have the same set of elements and nodes. The processing step comes next, which is marked with a yellow box. AMfe Toolbox has several modules with different functions. These modules combined provides all calculation functions needed for processing. This study is focusing on calculating stress and strain. The last part marked by blue is to check the accuracy of strain and stress using different types of elements.

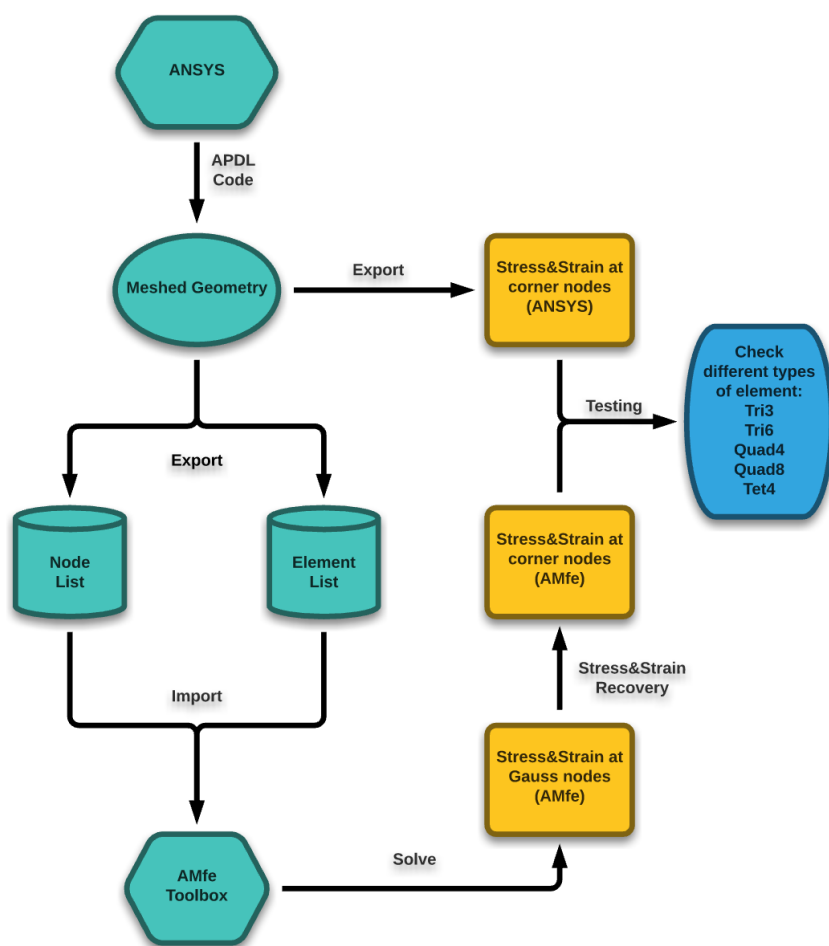


Figure 1.2: Flow chart of structure

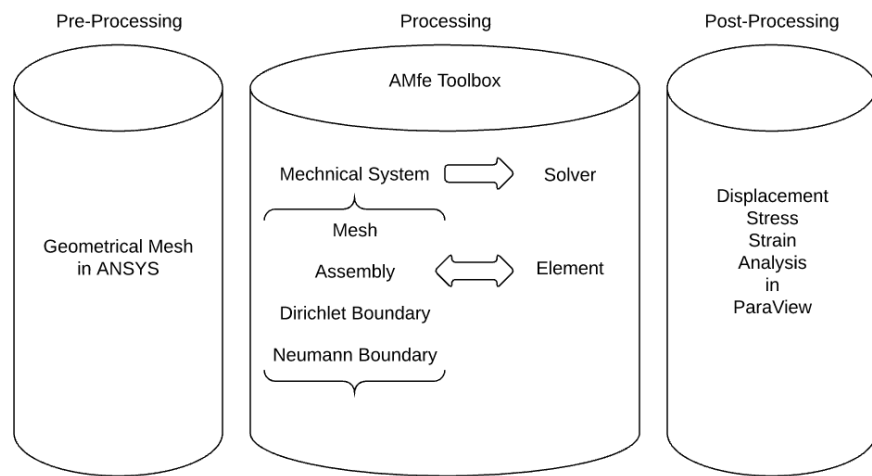


Figure 1.3: Overview of this essay structure

Chapter 2

Numerical Aspect for Finite Element Formulation

2.1 Shape Function

2.1.1 Quadrilateral Elements

The goal of the AMfe Code in the structural mechanical field is to get the approximate solutions to position, displacement, stress, and strain. According to the Finite Element theory of W. A. Wall [Wall 2014 p.75], the approximation is dependent on the shape function N . The standard approach to define the shape functions is choosing them as simple polynomials that are associated to nodes. There are n nodes and n shape functions in one single element. The i -th shape function takes the value of 1 at the i -th node in reference coordinates, then the j -th shape function can be written like this:

$$\begin{aligned} \text{if } j = i \text{ then } N_j(\hat{\xi}_i) &= 1 \\ \text{if } j \neq i \text{ then } N_j(\hat{\xi}_i) &= 0 \end{aligned}$$

for $i, j = 1, \dots, n$.

In Figure 2.1, linear and quadratic shape functions are expressed together with corresponding node positions. When referring to an element with three nodes, as shown in the right of Figure 2.1, there are three restrictions for each shape functions:

$$\begin{aligned} N_1(\hat{\xi}_1 = -1) &= 1, N_1(\hat{\xi}_2 = 0) = 0, N_1(\hat{\xi}_3 = 1) = 0; \\ N_2(\hat{\xi}_1 = -1) &= 0, N_2(\hat{\xi}_2 = 0) = 1, N_2(\hat{\xi}_3 = 1) = 0; \\ N_3(\hat{\xi}_1 = -1) &= 0, N_3(\hat{\xi}_2 = 0) = 0, N_3(\hat{\xi}_3 = 1) = 1 \end{aligned}$$

For quadratic polynomial, the shape function has three coefficients, and it can be constructed as follows:

$$p_{quad}(\xi) = c_0 + c_1\xi + c_2\xi^2$$

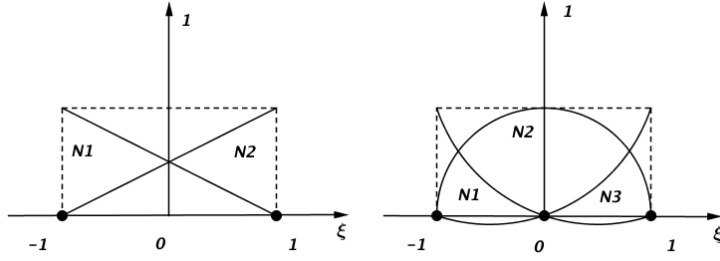


Figure 2.1: Linear shape function and quadratic shape function.

According to the work of W. A. Wall [Wall 2014 p. 75], Lagrange polynomials are a general group of polynomials with the node undermentioned association property: a Lagrange polynomial l_k^{n-1} of order $n-1$ transits n nodes with coordinates $\bar{\xi}^j$ ($j = 1, \dots, n$) of which the single node k equals one ($l_k^{n-1}(\bar{\xi}^k) = 1$) and every other node equals zero ($l_k^{n-1}(\bar{\xi}^j) = 0 \quad \text{for all } j \neq k$).

$$l_k^{n-1}(\xi) = \prod_{j=1, j \neq k}^n \frac{\xi - \bar{\xi}^j}{\bar{\xi}^k - \bar{\xi}^j} = \frac{(\xi - \bar{\xi}^1) \cdots (\xi - \bar{\xi}^{k-1})(\xi - \bar{\xi}^{k+1}) \cdots (\xi - \bar{\xi}^n)}{(\bar{\xi}^k - \bar{\xi}^1) \cdots (\bar{\xi}^k - \bar{\xi}^{k-1})(\bar{\xi}^k - \bar{\xi}^{k+1}) \cdots (\bar{\xi}^k - \bar{\xi}^n)}$$

$$k = 1, 2, \dots, n$$

For instance, to calculate linear, i.e. order 1, Lagrange polynomials can be calculated by $n-1 = 1 \Rightarrow n = 2$. Using $\bar{\xi}^1 = -1$ and $\bar{\xi}^2 = +1$ we can get the shape functions as: $l_1^1(\xi) = -1/2(\xi - 1)$ and $l_2^1(\xi) = 1/2(\xi + 1)$. Then the linear shape functions can be simply constructed as $N_1 = l_1^1 = 1/2(1 - \xi)$ and $N_2 = l_2^1 = 1/2(1 + \xi)$.

2.1.2 Triangular and Tetrahedral Elements

According to the work of Carlos A. Felippa [Felippa 2004 p.79], triangular and tetrahedral elements have higher flexibility than that of quadrilateral and hexahedral elements in meshing complex geometries, thus the former is often preferred to the latter. The shape functions can be solved by an analogous method, but triangular and tetrahedral elements are expressed in area and volume coordinates, respectively. Figure 2.2 shows the geometries and shape functions. A visualization of the coordinates representing area and volume fractions is expressed below:

$$L_1 = \frac{\text{areaP23}}{\text{area123}}, \quad V_1 = \frac{\text{areaP234}}{\text{area1234}}$$

$$\sum L_i = 1 \quad \sum V_i = 1$$

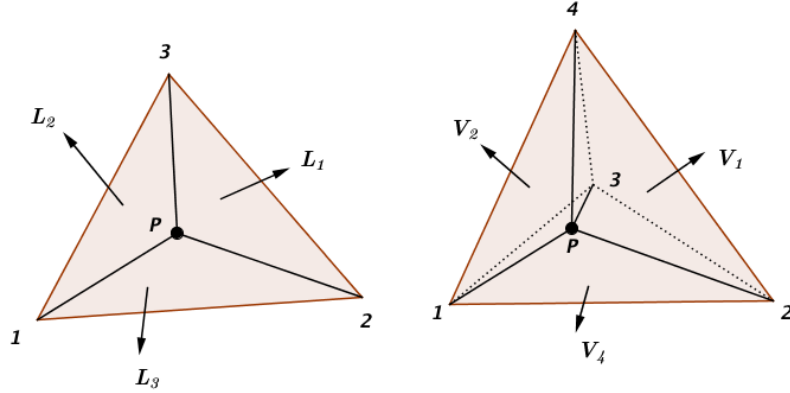


Figure 2.2: triangular and tetradral elemnets.

2.2 Non-linear Element Formulation

This section provides an introduction to the most common model and simulation technique for both 2D and 3D solid bodies in Non-Finite-Element-Method. The following section is based on the work of Johanness Rutzmoser [Rutzmoser 2016 p.1-5] in non-linear element formulation. In the first part of this introduction, we will pick a fictional 3D element with five nodes as our object of study. The coordinate system is based on three coordinate, namely ξ_1 , ξ_2 , and ξ_3 . The shape function of this 3D element can be ordered in Voigt notation as follows:

$$N(\xi) = \begin{pmatrix} N_1(\xi) \\ N_2(\xi) \\ N_3(\xi) \\ N_4(\xi) \\ N_5(\xi) \end{pmatrix} \quad (2.1)$$

We can denote the coordinate of this element as vector \mathbf{X}^e . The columns of \mathbf{X}^e stands for its axis direction and the rows of \mathbf{X}^e stands for the index of nodes. The matrix of \mathbf{X}^e is shown as:

$$\mathbf{X}^e = \begin{pmatrix} X_1 & Y_1 & Z_1 \\ X_2 & Y_2 & Z_2 \\ X_3 & Y_3 & Z_3 \\ X_4 & Y_4 & Z_5 \\ X_5 & Y_5 & Z_6 \end{pmatrix} \quad (2.2)$$

The coordinates \mathbf{X} of this element in the initial configuration relies on the local coordinate of the element ξ and the shape function N . It can be described as:

$$\mathbf{X}(\xi) = \begin{pmatrix} \mathbf{X} \\ \mathbf{Y} \\ \mathbf{Z} \end{pmatrix} = (\mathbf{X}^e)^T N = \begin{pmatrix} X_1 & X_2 & X_3 & X_4 & X_5 \\ Y_1 & Y_2 & Y_3 & Y_4 & Y_5 \\ Z_1 & Z_2 & Z_3 & Z_4 & Z_5 \end{pmatrix} \begin{pmatrix} N_1 \\ N_2 \\ N_3 \\ N_4 \\ N_5 \end{pmatrix} \quad (2.3)$$

The displacements \mathbf{u} at any points of the element are interpolated from the nodal coordinate, in the same manner that was completed for the coordinate \mathbf{X} above. Then the displacement field

can be shown as:

$$\mathbf{u}(\xi) = \begin{pmatrix} u_x(\xi) \\ u_y(\xi) \\ u_z(\xi) \end{pmatrix} = (\mathbf{u}^e)^T N = \begin{pmatrix} u_{x1} & u_{x2} & u_{x3} & u_{x4} & u_{x5} \\ u_{y1} & u_{y2} & u_{y3} & u_{y4} & u_{y5} \\ u_{z1} & u_{z2} & u_{z3} & u_{z4} & u_{z5} \end{pmatrix} \begin{pmatrix} N_1 \\ N_2 \\ N_3 \\ N_4 \\ N_5 \end{pmatrix} \quad (2.4)$$

This approach is called the isoparametric concept, which makes it possible to present the parameters at any given point within an element. The magnitude of parameters at a one of such points can be calculated through both the known values of parameters and shape functions at each node. An example of displacements can be formed like this:

$$\frac{\partial \mathbf{u}}{\partial X} = (\mathbf{u}^e)^T \frac{\partial N}{\partial X} = (\mathbf{u}^e)^T \tilde{\mathbf{B}}_0 \quad (2.5)$$

The deviation of a parameter can be passed to the shape function. Through this approach, we can define a new term $\tilde{\mathbf{B}}_0 = \frac{\partial \mathbf{u}}{\partial X}$. The expansion of $\tilde{\mathbf{B}}_0$ can be derived as:

$$\frac{\partial \mathbf{N}}{\partial X} = \tilde{\mathbf{B}}_0 = \begin{pmatrix} \frac{\partial N_1}{\partial X} & \frac{\partial N_1}{\partial Y} & \frac{\partial N_1}{\partial Z} \\ \frac{\partial N_2}{\partial X} & \frac{\partial N_2}{\partial Y} & \frac{\partial N_2}{\partial Z} \\ \frac{\partial N_3}{\partial X} & \frac{\partial N_3}{\partial Y} & \frac{\partial N_3}{\partial Z} \\ \frac{\partial N_4}{\partial X} & \frac{\partial N_4}{\partial Y} & \frac{\partial N_4}{\partial Z} \\ \frac{\partial N_5}{\partial X} & \frac{\partial N_5}{\partial Y} & \frac{\partial N_5}{\partial Z} \end{pmatrix} = \frac{\partial \mathbf{N}}{\partial \xi} \frac{\partial \xi}{\partial X} \quad (2.6)$$

The first term $\frac{\partial N}{\partial \xi}$ in Equation 2.6 can be directly expressed with shape function relating coordinate ξ . It is shown as:

$$\frac{\partial N}{\partial \xi} = \begin{pmatrix} \frac{\partial N_1}{\partial \xi_1} & \frac{\partial N_1}{\partial \xi_2} & \frac{\partial N_1}{\partial \xi_3} \\ \frac{\partial N_2}{\partial \xi_1} & \frac{\partial N_2}{\partial \xi_2} & \frac{\partial N_2}{\partial \xi_3} \\ \frac{\partial N_3}{\partial \xi_1} & \frac{\partial N_3}{\partial \xi_2} & \frac{\partial N_3}{\partial \xi_3} \\ \frac{\partial N_4}{\partial \xi_1} & \frac{\partial N_4}{\partial \xi_2} & \frac{\partial N_4}{\partial \xi_3} \\ \frac{\partial N_5}{\partial \xi_1} & \frac{\partial N_5}{\partial \xi_2} & \frac{\partial N_5}{\partial \xi_3} \end{pmatrix} \quad (2.7)$$

The second term $\frac{\partial \xi}{\partial X}$ is not straightforward to obtain. However, it is much easier to get the matrix $\frac{\partial X}{\partial \xi}$. This matrix is called Jacobian matrix J , which is a matrix of ξ with respect to x . The inverse Jacobian matrix is denoted as J^{-1} , which is the second term in the Equation 2.6.

The deformation gradient F describes the mapping of an infinitesimal fiber from its initial state to its new position in the current configuration. $F = H + I$ can be derived through the transient matrix $H = \frac{\partial u}{\partial X} = (u^e)^T \tilde{B}_0$. The Green-Lagrange strain tensor can also be written as:

$$E = \frac{1}{2} (H + H^T + H^T H) \quad (2.8)$$

$$E = \frac{1}{2} (F^T F - I) \quad (2.9)$$

The transient matrix H can be expressed in more details as:

$$H = \frac{\partial u}{\partial X} = \frac{\partial u}{\partial \xi} \frac{\partial \xi}{\partial X} = (u^e)^T \frac{\partial N}{\partial \xi} \left[(X^e)^T \frac{\partial N}{\partial \xi} \right]^{-1} \quad (2.10)$$

When we have result for strain E , It is possible to calculate stress S . One simply constitutive equation between stress S (2. Piola-Kirchhoff-Stress tensor) and E (Green-Lagrange-Strain tensor) can be formulated as:

$$S = C : E \quad (2.11)$$

The value of stress is subsequently transferred into the degrees of freedom(DOFs) at each nodes. The principle for stress calculation can be formulated as follows:

In the Total Lagrange approach, the principle of virtual work represents that the internal strain

energy $\delta W_{int} = \int \sigma : \delta \epsilon d\Omega_0 = \int S : \delta E d\Omega_0$ equals the external energy $\delta W_{ext} = (\delta u^{e,v})^T f_{int}^v$, which is caused by external nodal force. The complete equation can be expressed as:

$$\delta W = \delta W_{ext} = (\delta u^{e,v})^T f_{int}^v = \int S : \delta E d\Omega_0 = \int (\delta E^v)^T S^v \Omega_0 \quad (2.12)$$

The internal deformation energy can be computed by matrix-vector-product in voigt-notation or direct product of two matrix with notation (:). Now, we evaluate the variation of Green-Lagrange strain tensor δE . From equation 2.9, it is obvious that the variation of tensor δE is determined by the variation of deformation gradient. According to above equation 2.10, the variation of deformation gradient can be transformed into:

$$\delta F = \delta H = (\delta u^e)^T \frac{\delta N}{\delta X} = (\delta u^e)^T \tilde{B}_0 \quad (2.13)$$

Consequently, the variation of tensor δE is:

$$\delta E = \frac{1}{2} (\delta F^T F + F^T \delta F) \quad (2.14)$$

Green-Lagrange-Strain δE is often represented in a complex matrix form, thus it is often expressed in Voigt-Notation in computer programming. Then, δE^v can be coupled with B_0 -matrix as:

$$\delta E^v = B_0 \delta u^{e,v} \quad (2.15)$$

The entry of B_0 will be packed into a black box and directly implemented in the FEM simulation. By solving simultaneous equations of Equation 2.12 and Equation 2.15, the non-linear force f_{int}^v results in:

$$\delta W = (\delta u^{e,v})^T f_{int}^v = \int (\delta E^v)^T S^v d\Omega_0 = (\delta u^{e,v})^T \int B_0^T S^v d\Omega_0 \quad (2.16)$$

$$f_{int}^v = \int B_0^T S^v d\Omega_0 \quad (2.17)$$

The non-linear internal force of element concerning the coordinate of node can be integrated by B_0 -matrix with second Piola-Kirchhoff-Stress tensor in Voigt-Notation. To obtain the tangential stiffness matrix, it is necessary to calculate the partial derivative of internal force f_{int}^v in respect to the nodal degrees of freedom(DOFs) $u^{e,v}$:

$$\frac{\partial f_{int}^v}{\partial u^{e,v}} = K = \int \frac{\partial B_0^T}{\partial u^{e,v}} S^v d\Omega_0 + \int B_0^T \frac{\partial S^v}{\partial u^{e,v}} d\Omega_0 = K_{geo} + K_{mat} \quad (2.18)$$

Stiffness matrix can be divided into two terms, one of the terms is the material stiffness matrix K_{mat} , which is shown as:

$$K_{mat} = \int B_0^T \frac{\partial S^v}{\partial u^{e,v}} d\Omega_0 = \int B_0^T \frac{\partial S^v}{\partial E^v} \frac{\partial E^v}{\partial u^{e,v}} d\Omega_0 = \int B_0^T C^{SE} B_0 d\Omega_0 \quad (2.19)$$

The derivative of stress in respect to strain is considered as Tangent-Modulus $C^{SE} = \frac{\partial S^v}{\partial E^v}$ by constitutive equation. The derivative of strain is \mathbf{B}_0 as determined in equation 2.9.

The other term, the geometrical stiffness matrix, is much more complex to derive. In short, based on the relation between deformation gradient and continuum mechanics $\mathbf{P} = \mathbf{SF}^T$, the internal energy from Equation 2.12 is reformulated into:

$$\delta W = \mathbf{u}^e : \mathbf{f}_{int} = \int \delta \mathbf{F}^T : \mathbf{P} d\Omega_0 = \int \delta \mathbf{F}_{ij} \mathbf{P}_{ji} d\Omega_0 \quad (2.20)$$

The variation of deformation gradient can be written as $\delta \mathbf{F} = \delta \mathbf{u}^{eT} \mathbf{B}_0$. It can also be written in the Index-Notation form as $\delta \mathbf{F}_{ij} = \delta \mathbf{u}_{ki}^e \tilde{\mathbf{B}}_{kj}^0$. Then, the internal force in matrix notation can be derived as:

$$\delta W = \delta \mathbf{u}^e : \mathbf{f}_{int} = \mathbf{u}_{ki}^e \mathbf{f}_{ki}^{int} = \int \delta \mathbf{F}_{ji} \mathbf{P}_{ij} d\Omega_0 = \delta \mathbf{u}_{ki}^e \int \tilde{\mathbf{B}}_{kj}^0 \mathbf{P}_{ji} d\Omega_0 = \delta \mathbf{u}^e : \int \tilde{\mathbf{B}}_0 \mathbf{P} d\Omega_0 \quad (2.21)$$

$$\mathbf{f}_{int} = \int \tilde{\mathbf{B}}_0 \mathbf{P} d\Omega_0 \quad (2.22)$$

The tangential stiffness matrix is determined by variation of the force vector, which is determined by the velocity of nodal displacement $\dot{\mathbf{u}}^e$. Because Jacobian Matrix is relatively complex to build, the derivative of internal force $\dot{\mathbf{f}}_{int}$ in time is as follows:

$$\dot{\mathbf{f}}_{int} = \int \tilde{\mathbf{B}}_0 \dot{\mathbf{S}} \mathbf{F}^T d\Omega_0 + \int \tilde{\mathbf{B}}_0 \mathbf{S} \dot{\mathbf{F}}^T d\Omega_0 \quad (2.23)$$

The first term corresponds to material stiffness because the time derivative of second Piola-Kirchhoff-Stress tensor is time-dependent part. And the second term corresponds to geometrical stiffness, as is shown in equation 2.18. Because the time derivative $\dot{\mathbf{F}}$ equals $\dot{\mathbf{u}}^{eT} \tilde{\mathbf{B}}_0$, Equation 2.23 can be transformed as:

$$\dot{\mathbf{f}}_{int,geo} = \int \tilde{\mathbf{B}}_0 \mathbf{S} \tilde{\mathbf{B}}_0 \Omega_0 \dot{\mathbf{u}}^e \quad (2.24)$$

The geometrical stiffness matrix can be achieved by coupling the temporal variation of non-linear force with the displacements using the tangential stiffness matrix.

$$\dot{\mathbf{f}}_{int,geo} = \mathbf{K}_{geo} \dot{\mathbf{u}}^e = \int \tilde{\mathbf{B}}_0 \mathbf{S} \tilde{\mathbf{B}}_0 \Omega_0 \dot{\mathbf{u}}^e \quad (2.25)$$

The last step in determining the non-linear force and the tangential stiffness matrix is the integrate the non-linear force on domain $d\Omega_0$, which is the transformation from domain $d\Omega_0$ to reference coordinate system:

$$\int f(x) d\Omega = \int f(x) \frac{\partial \xi}{\partial x} d\Omega = \int f(x) \frac{\partial \Omega}{\partial \xi} d\xi = \int f(x) \det \left(\frac{\partial X}{\partial \xi} \right) d\xi \quad (2.26)$$

Numerical integration plays an important role in FEM. Gauss integration is an efficient approach compared to other numerical integration approaches. It integrates a function $f(\xi)$ on the spatial domain Ω by replacing a summation of certain function values at the so-called Gauss points $\tilde{\xi}$ that are each multiplied by a scalar (weight) w . According to the work of W. A. Wall [Wall 2014 p.73], a clear expression of Gauss integration is:

$$\int_E f(\xi) d\xi_1 d\xi_2 d\xi_3 = \sum_{i=1}^{numgp_1} \sum_{j=1}^{numgp_2} \sum_{k=1}^{numgp_3} f\left(\tilde{\xi}_1^i \tilde{\xi}_2^j \tilde{\xi}_3^k\right) \cdot w_1^i w_2^j w_3^k \quad (2.27)$$

In this expression, the corresponding weights are applied for each of the three spatial directions, which is available to take Gauss points coordinates and weights tabulated for the one-dimensional case. The locations and weights of these points can be expressed theoretically in Table 2.1.

2.3 Stress Recovery

2.3.1 Extrapolation of Stress from Gauss points

Stress recovery is an approach to achieve an approximation of nodal stress by extrapolation of stress from Gauss points. This method is regarded as advanced technique with respect to the method, which directly evaluates the stress at nodes. In this paper, we name the latter method as Direct-Evaluation-Algorithms. According to the research of Carlos A. Felippa [Felippa 2004 section 28, p.5], when referring to the Direct-Evaluation-Algorithms, the relative error are typically 10% to 20%, this is the main reason why we use the Stress-Recovery-Algorithms. An example in Figure 2.3 is good to describe the procedure of calculation. We have a quadrangle with quadratic shape function. Its four nodes are denoted as 1, 2, 3, 4. The Gauss points in this element are denoted as 1', 2', 3', 4'. The position of each Gauss points are ξ_i' , η_i' ($i = 1, 2, 3, 4$). The shape functions of each Gauss points can be written in:

$$N_1'(\xi', \eta') = \frac{1}{4} \times (1 - \xi') \times (1 - \eta') \quad (2.28)$$

$$N_2'(\xi', \eta') = \frac{1}{4} \times (1 + \xi') \times (1 - \eta') \quad (2.29)$$

$$N_3'(\xi', \eta') = \frac{1}{4} \times (1 + \xi') \times (1 + \eta') \quad (2.30)$$

$$N_4'(\xi', \eta') = \frac{1}{4} \times (1 - \xi') \times (1 + \eta') \quad (2.31)$$

We assume that the stress at Gauss points have been already calculated out in previous step and they can be written as σ_1' , σ_2' , σ_3' , σ_4' . The nodal stress components are calculated by a bilinear extrapolation based on the given values at Gauss points. We replace the coordinates of nodal points into the shape functions of Gauss points for calculating the nodal stress, which can be derived as:

$$\sigma_1 = \sigma_1' N_1'(\xi_1, \eta_1) + \sigma_2' N_2'(\xi_2, \eta_2) + \sigma_3' N_3'(\xi_3, \eta_3) + \sigma_4' N_4'(\xi_4, \eta_4) \quad (2.32)$$

Table 2.1: Gauss-Legendre points and weights

<i>numgp</i>	<i>i</i>	$\tilde{\xi}^i$	ω^i
1	1	0	2
2	1	$-1/\sqrt{3}$	1
	2	$+1/\sqrt{3}$	1
3	1	$-\sqrt{3}/5$	5/9
4	2	0	8/9
	3	$+1/\sqrt{3}/5$	5/9
4	1	$-\sqrt{(15 + \sqrt{120})/35}$	$(18 - \sqrt{30})/36$
	2	$-\sqrt{(15 - \sqrt{120})/35}$	$(18 + \sqrt{30})/36$
	3	$+\sqrt{(15 - \sqrt{120})/35}$	$(18 + \sqrt{30})/36$
	4	$+\sqrt{(15 + \sqrt{120})/35}$	$(18 - \sqrt{30})/36$
5	1	$-1/3\sqrt{5 + 2\sqrt{10/7}}$	$(332 - 13\sqrt{70})/900$
	2	$-1/3\sqrt{5 - 2\sqrt{10/7}}$	$(332 + 13\sqrt{70})/900$
5	3	0	128/255
5	4	$+1/3\sqrt{5 - 2\sqrt{10/7}}$	$(332 + 13\sqrt{70})/900$
	5	$+1/3\sqrt{5 + 2\sqrt{10/7}}$	$(332 - 13\sqrt{70})/900$

$$\sigma_2 = \sigma_1' N_1' (\xi_1, \eta_1) + \sigma_2' N_2' (\xi_2, \eta_2) + \sigma_3' N_3' (\xi_3, \eta_3) + \sigma_4' N_4' (\xi_4, \eta_4) \quad (2.33)$$

$$\sigma_3 = \sigma_1' N_1' (\xi_1, \eta_1) + \sigma_2' N_2' (\xi_2, \eta_2) + \sigma_3' N_3' (\xi_3, \eta_3) + \sigma_4' N_4' (\xi_4, \eta_4) \quad (2.34)$$

$$\sigma_4 = \sigma_1' N_1' (\xi_1, \eta_1) + \sigma_2' N_2' (\xi_2, \eta_2) + \sigma_3' N_3' (\xi_3, \eta_3) + \sigma_4' N_4' (\xi_4, \eta_4) \quad (2.35)$$

Then we can form them as:

$$\begin{pmatrix} \sigma_1 \\ \sigma_2 \\ \sigma_3 \\ \sigma_4 \end{pmatrix} = \begin{pmatrix} N_1' (\xi_1, \eta_1) & N_2' (\xi_2, \eta_2) & N_3' (\xi_3, \eta_3) & N_4' (\xi_4, \eta_4) \\ N_1' (\xi_1, \eta_1) & N_2' (\xi_2, \eta_2) & N_3' (\xi_3, \eta_3) & N_4' (\xi_4, \eta_4) \\ N_1' (\xi_1, \eta_1) & N_2' (\xi_2, \eta_2) & N_3' (\xi_3, \eta_3) & N_4' (\xi_4, \eta_4) \\ N_1' (\xi_1, \eta_1) & N_2' (\xi_2, \eta_2) & N_3' (\xi_3, \eta_3) & N_4' (\xi_4, \eta_4) \end{pmatrix} \begin{pmatrix} \sigma_1' \\ \sigma_2' \\ \sigma_3' \\ \sigma_4' \end{pmatrix} \quad (2.36)$$

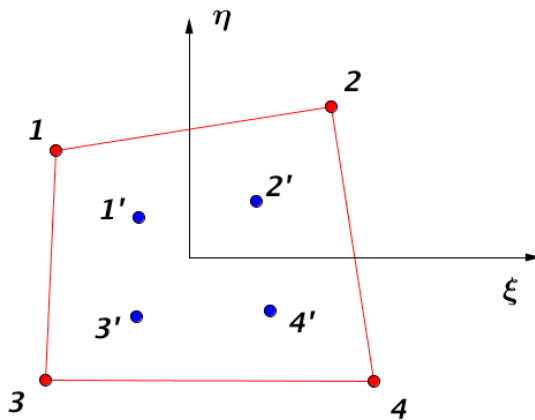


Figure 2.3: Quadrangle with four nodes

2.3.2 Quadrilateral element with four nodes: Quad4

Quad4 is used for 2D modelling of solid structure. The element can be used either as a plane element (plane stress or plane strain) or as an axisymmetric element. The element is defined by four nodes with two degrees of freedom (DOFs) at each node: translations in the nodal x and y directions. The normal Gauss integration rule for element stiffness evaluation is 2×2 , as is illustrated in Figure 2.4. According to the work of Carlos A. Felippa [Felippa 2004 section 18,

p.6], the components(strain, stress) are calculated at the Gauss points and are identified as k_1^G, k_2^G, k_3^G and k_4^G in Figure 2.4. Point k_i^G is closest to node k_i^E , and other Gauss point numbering follows element node numbering in the same counterclockwise manner. The natural coordinates of these points are listed in Table 2.2. The components are calculated at these Gauss points, at which strain and stress attain best approximated solutions. Then each strain and stress component is transported to the corner nodes k_1^E through k_4^E by a bilinear extrapolation based on the computed values at k_1^G through k_4^G . To understand the extrapolation procedure more clearly, we should consider the region bounded by the Gauss points as an internal Gauss element. This interpretation is depicted in Figure 2.4. The external element is denoted by (E). The internal Gauss element, denoted by (G), is also a four-node quadrilateral. The coordinate of node for element and Gauss element can be represented as k_i^E and k_i^G , respectively. The natural coordinates are denoted by ξ and η , and the internal Gauss coordinates are denoted by ξ' and η' . Both coordinates follow the simple relations from Gauss-Legendre quadrature in Table 2.2, here we have the coordinate relation of components for Quad4:

$$k_i^G = \frac{k_i^E}{\sqrt{3}}, \quad k_i^E = k_i^G \sqrt{3} \quad (2.37)$$

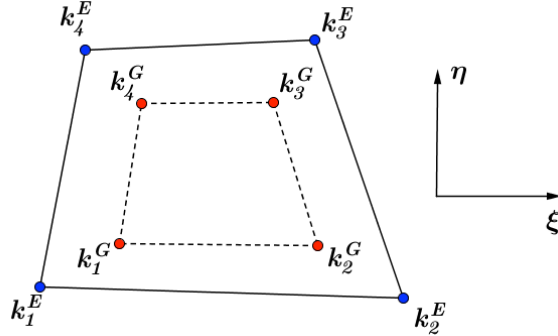


Figure 2.4: Quad4 in element coordinate and Gauss element coordinate.

The element geometry and natural coordinates are shown in Figure 2.6. There is only one type of node and associated shape function. We consider node 1 to be a typical node. From Figure 2.5 we can form:

$$N_1^e = c_1 L_{2-3} L_{3-4} \quad (2.38)$$

The equation of edge 2-3 is $\xi - 1 = 0$. The equation of edge 3-4 is $\eta - 1 = 0$. Inserting in Equation (2.38) results in:

$$N_1^e(\xi, \eta) = c_1 (\xi - 1)(\eta - 1) = c_1 (1 - \xi)(1 - \eta) \quad (2.39)$$

We evaluate the point at node 1 to find c_1 and the natural coordinates can be expressed as $\xi = \eta = -1$:

$$N_1^e(-1, -1) = c_1 \times 2 \times 2 = 4c_1 = 1 \quad (2.40)$$

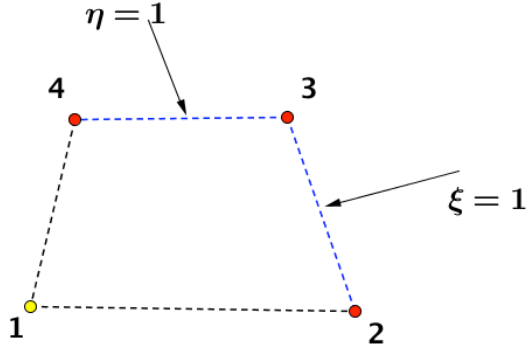


Figure 2.5: Equation of side opposite corner 1 for Quad4.

Therefore, $c_1 = \frac{1}{4}$ and the shape functions is

$$N_1^e = \frac{1}{4} (1 - \xi)(1 - \eta) \quad (2.41)$$

We can use the same approach to calculate the other three nodes. Following this general expression, the shape functions of Node 2, 3 and 4 are demonstrated as:

$$N_2^e = \frac{1}{4} (1 + \xi)(1 - \eta) \quad (2.42)$$

$$N_3^e = \frac{1}{4} (1 + \xi)(1 + \eta) \quad (2.43)$$

$$N_4^e = \frac{1}{4} (1 - \xi)(1 + \eta) \quad (2.44)$$

When we have all the shape functions for Gauss element, we are able to extrapolate the components (stress, strain, etc) from Gauss points k_i^G to corner nodes k_i^E . According to Table 2.2 and Figure 2.4, we have the corner nodes in Gauss coordinate: $k_1^E(-\sqrt{3}, -\sqrt{3})$, $k_2^E(\sqrt{3}, -\sqrt{3})$, $k_3^E(\sqrt{3}, \sqrt{3})$, $k_4^E(\sqrt{3}, \sqrt{3})$. The extrapolation process is to replace all the coordinates of corner nodes into Gauss coordinate with the shape function of each Gauss points. Then we can get the

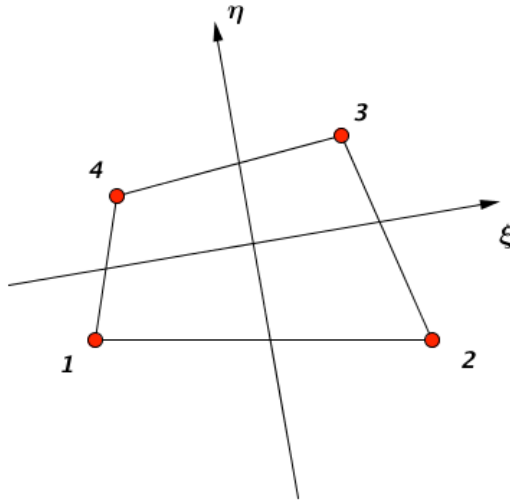


Figure 2.6: Equation of side opposite corner 1 for Quad4.

relation between corner nodes and Gauss points as:

$$\begin{pmatrix} w_1 \\ w_2 \\ w_3 \\ w_4 \end{pmatrix} = \begin{pmatrix} 1 + \frac{1}{2}\sqrt{3} & -\frac{1}{2} & 1 - \frac{1}{2}\sqrt{3} & -\frac{1}{2} \\ -\frac{1}{2} & 1 + \frac{1}{2}\sqrt{3} & -\frac{1}{2} & 1 - \frac{1}{2}\sqrt{3} \\ 1 - \frac{1}{2}\sqrt{3} & -\frac{1}{2} & 1 + \frac{1}{2}\sqrt{3} & -\frac{1}{2} \\ -\frac{1}{2} & 1 - \frac{1}{2}\sqrt{3} & -\frac{1}{2} & 1 + \frac{1}{2}\sqrt{3} \end{pmatrix} \begin{pmatrix} w_1' \\ w_2' \\ w_3' \\ w_4' \end{pmatrix} \quad (2.45)$$

Here w' means strains and stresses in this paper. So the w' part can be written as:

$$\begin{pmatrix} w_1' \\ w_2' \\ w_3' \\ w_4' \end{pmatrix} = \begin{pmatrix} \epsilon_{1xx} & \epsilon_{1yy} & \epsilon_{1zz} & 2\epsilon_{1yz} & 2\epsilon_{1xz} & 2\epsilon_{1xy} \\ \epsilon_{2xx} & \epsilon_{2yy} & \epsilon_{2zz} & 2\epsilon_{2yz} & 2\epsilon_{2xz} & 2\epsilon_{2xy} \\ \epsilon_{3xx} & \epsilon_{3yy} & \epsilon_{3zz} & 2\epsilon_{3yz} & 2\epsilon_{3xz} & 2\epsilon_{3xy} \\ \epsilon_{4xx} & \epsilon_{4yy} & \epsilon_{4zz} & 2\epsilon_{4yz} & 2\epsilon_{4xz} & 2\epsilon_{4xy} \end{pmatrix} \quad (2.46)$$

Table 2.2: Natural Coordinate of Quad4

Corner node	ξ	η	ξ'	η'	Gauss node	ξ	η	ξ'	η'
1	-1	-1	$-\sqrt{3}$	$-\sqrt{3}$	1'	$+1/\sqrt{3}$	$-1/\sqrt{3}$	-1	-1
2	+1	-1	$+\sqrt{3}$	$-\sqrt{3}$	2'	$+1/\sqrt{3}$	$+1/\sqrt{3}$	+1	-1
3	+1	+1	$+\sqrt{3}$	$+\sqrt{3}$	3'	$+1/\sqrt{3}$	$+1/\sqrt{3}$	+1	+1
4	-1	+1	$-\sqrt{3}$	$+\sqrt{3}$	4'	$-1/\sqrt{3}$	$+1/\sqrt{3}$	-1	+1

$$\begin{pmatrix} w_1' \\ w_2' \\ w_3' \\ w_4' \end{pmatrix} = \begin{pmatrix} \sigma_{1xx} & \sigma_{1yy} & \sigma_{1zz} & \sigma_{1yz} & \sigma_{1xz} & \sigma_{1xy} \\ \sigma_{2xx} & \sigma_{2yy} & \sigma_{2zz} & \sigma_{2yz} & \sigma_{2xz} & \sigma_{2xy} \\ \sigma_{3xx} & \sigma_{3yy} & \sigma_{3zz} & \sigma_{3yz} & \sigma_{3xz} & \sigma_{3xy} \\ \sigma_{4xx} & \sigma_{4yy} & \sigma_{4zz} & \sigma_{4yz} & \sigma_{4xz} & \sigma_{4xy} \end{pmatrix} \quad (2.47)$$

2.3.3 Quadrilateral element with eight nodes: Quad8

Quad8 is a higher order 2D, 8 node element. This element is defined by 8 nodes with two degrees of freedom (DOFs) at each node: translation in the nodal x and y direction. The element may be used as a plane element (plane stress, plane strain) or as an axisymmetric element. For Quad8, we can choose different types of Gauss element for extrapolation. We can chose from four, eight or nine nodes Gauss element as quadrilateral elements. In this paper, we use the Gauss element with nine nodes. The nine-nodes quadrilateral Gauss element has three types of shape functions, which are associated with corner midpoint, and, center nodes, respectively. The element coordinate and Gauss element coordinate are illustrated in Figure 2.7.

According to the work of Carlos A. Felippa [Felippa 2004 section 18, p.8], the three types of shape functions are illustrated in Figure for nodes 1, 5, and 9, respectively. The procedure for calculating shape function has been clearly expressed in Section 2.3.2. Here we summarize the calculation for three typical types, represented by nodes 1, 5 and 9. The three types are illustrated in Figure 2.8.

$$N_1^e = c_1 L_{2-3} L_{3-4} L_{5-7} L_{6-8} = c_1 (\xi - 1)(\eta - 1) \xi \eta \quad (2.48)$$

$$N_5^e = c_5 L_{2-3} L_{1-4} L_{6-8} L_{3-4} = c_5 (\xi - 1) (\xi + 1) \eta (\eta - 1) = c_5 (1 - \xi^2) \eta (1 - \eta) \quad (2.49)$$

$$N_9^e = c_9 L_{1-2} L_{2-3} L_{3-4} L_{4-1} = c_9 (\xi - 1) (\eta - 1) (\xi + 1) (\eta + 1) = c_9 (1 - \xi^2) (1 - \eta^2) \quad (2.50)$$

By applying the normalization conditions, the results are:

$$c_1 = \frac{1}{4}, \quad c_5 = -\frac{1}{2}, \quad c_9 = 1$$

By following this approach, all the shape functions can be calculated:

$$N_1 = \frac{1}{4} (\xi - 1) (\eta - 1) \cdot \xi \cdot \eta \quad (2.51)$$

$$N_2 = \frac{1}{4} (\xi + 1) (\eta - 1) \cdot \xi \cdot \eta \quad (2.52)$$

$$N_3 = \frac{1}{4} (\xi + 1) (\eta + 1) \cdot \xi \cdot \eta \quad (2.53)$$

$$N_4 = \frac{1}{4} (\xi - 1) (\eta + 1) \cdot \xi \cdot \eta \quad (2.54)$$

$$N_5 = \frac{1}{2} (1 + \xi) (1 + \xi) (\eta - 1) \cdot \eta \quad (2.55)$$

$$N_6 = \frac{1}{2} (1 + \eta) (1 - \eta) (\xi + 1) \cdot \xi \quad (2.56)$$

$$N_7 = \frac{1}{2} (1 + \xi) (1 + \xi) (\eta + 1) \cdot \eta \quad (2.57)$$

$$N_8 = \frac{1}{2} (1 + \eta) (1 - \eta) (\xi - 1) \cdot \xi \quad (2.58)$$

$$N_9 = (1 + \xi) (1 - \xi) (1 + \eta) (1 - \eta) \quad (2.59)$$

Same as in Quad4, the extrapolation function can be expressed by inserting corner nodes in Gauss coordinate into the shape function of Gauss points:

$$\begin{pmatrix} w_1 \\ w_2 \\ w_3 \\ w_4 \\ w_5 \\ w_6 \\ w_7 \\ w_8 \end{pmatrix} = \begin{pmatrix} a_1 & a_2 & a_3 & a_2 & a_4 & a_5 & a_5 & a_4 & a_6 \\ a_2 & a_1 & a_2 & a_3 & a_4 & a_4 & a_5 & a_5 & a_6 \\ a_3 & a_2 & a_1 & a_2 & a_5 & a_4 & a_4 & a_5 & a_6 \\ a_2 & a_3 & a_2 & a_1 & a_5 & a_5 & a_4 & a_4 & a_6 \\ 0 & 0 & 0 & 0 & a_7 & 0 & a_8 & 0 & a_9 \\ 0 & 0 & 0 & 0 & 0 & a_7 & 0 & a_8 & a_9 \\ 0 & 0 & 0 & 0 & a_8 & 0 & a_7 & 0 & a_9 \\ 0 & 0 & 0 & 0 & 0 & a_8 & 0 & a_7 & a_9 \end{pmatrix} \begin{pmatrix} w'_1 \\ w'_2 \\ w'_3 \\ w'_4 \\ w'_5 \\ w'_6 \\ w'_7 \\ w'_8 \\ w'_9 \end{pmatrix} \quad (2.60)$$

$$a_1 = +2.1869398$$

$$a_2 = +0.2777778$$

$$a_3 = +0.0352824$$

$$a_4 = -0.9858870$$

$$a_5 = -0.1252241$$

$$a_6 = +0.4444444$$

$$a_7 = +1.4788331$$

$$a_8 = +0.1878361$$

$$a_9 = -0.6666666$$

2.3.4 Triangular element with three nodes: Tri3

Tri3 is used for 2D modelling of solid structure. This element is defined by 3 nodes with two degrees of freedom (DOFs) at each node: translation in the nodal x and y direction. The geometry

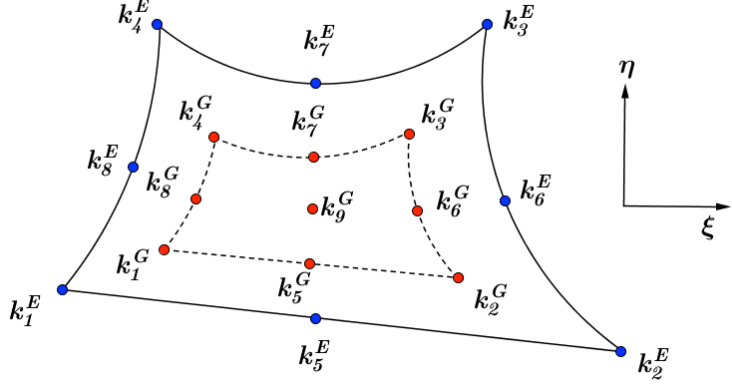


Figure 2.7: Quad8 in element coordinate and Gauss element coordinate.

of a 3-node triangle, as is shown in Figure 2.9, is specified by the location of its three corner nodes on the $\{x, y\}$ plane. The shape functions for triangular element has a different form, in comparison to quadrilateral elements. The triangular element has its own coordinates, named the triangular coordinates. According to the work of Carlos A. Felippa [Felippa 2004 section 18, p.4-5], the shape functions based on this coordinate can be formed as: $N_i = \xi_i$ for $i = 1, 2, 3$. The shape function can be derived from the following approach: the equation of the triangle edge corresponding to node i is $L_{j-k} = \xi_i = 0$, in which j and k stand for the cyclic permutations of i . See Figure 2.10 for $i = 1, j = 2$ and $k = 3$. Hence the general equation can be formed as:

$$N_i^e = c_i L_i \quad (2.61)$$

For finding c_1 , we can evaluate $N_1^e(\xi_1, \xi_2, \xi_3)$ at node 1, which the triangular coordinates are $\xi_1 = 1, \xi_2 = \xi_3 = 0$. Hence the shape function of this node can be expressed as $N_1^e(1, 0, 0) = c_1 \times 1 = 1$. Therefore $c_1 = 1$, using the same approach, $c_2 = 1, c_3 = 1$. Thus the shape functions are:

$$N_1^e = L_1, \quad N_2^e = L_2, \quad N_3^e = L_3 \quad (2.62)$$

By combining the shape function and corner coordinate in Gauss element from Table 2.3, the extrapolation of Tri3 can be written as:

$$\begin{pmatrix} w_1 \\ w_2 \\ w_3 \end{pmatrix} = \begin{pmatrix} 5/3 & -1/3 & -1/3 \\ -1/3 & 5/3 & -1/3 \\ -1/3 & -1/3 & 5/3 \end{pmatrix} \begin{pmatrix} w_1' \\ w_2' \\ w_3' \end{pmatrix} \quad (2.63)$$

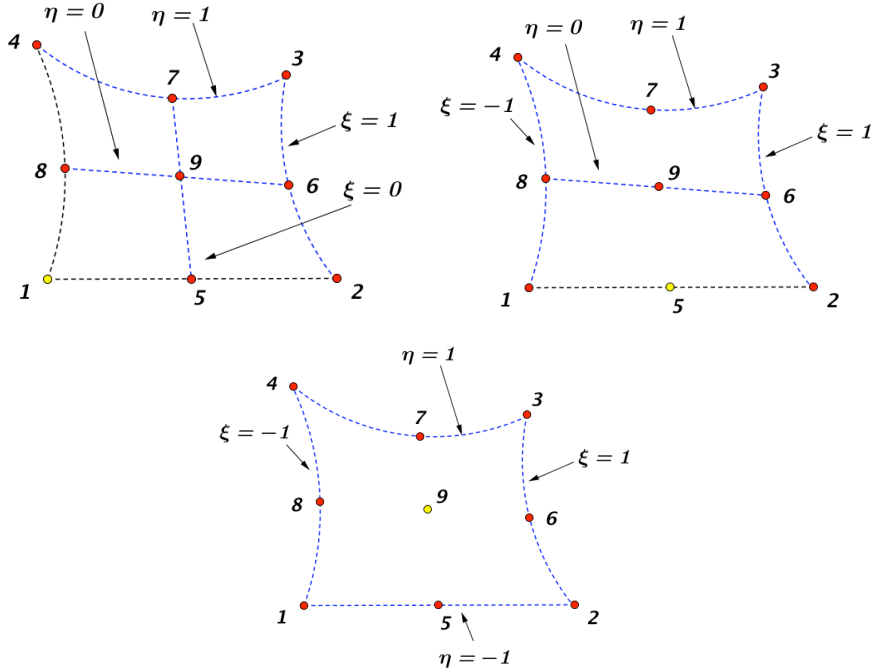


Figure 2.8: Equation of side opposite corner 1 for Quad8.

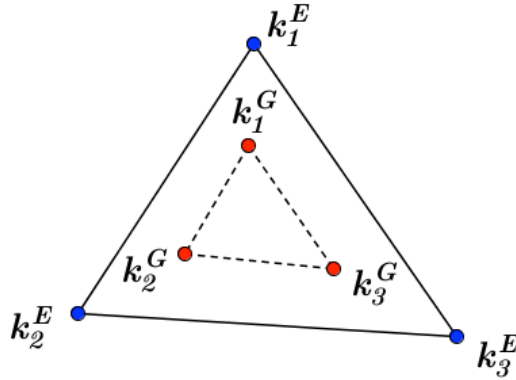
According to the work of Carlos A. Felippa [Felippa 2004 section 15 p.5-6], it is good to express the quantities in triangular coordinates when the type of element are formed by triangular. However, quantities such as displacements, strains and stresses are often calculated in the Cartesian coordinate system. Thus, the transformation functions from Cartesian coordinate system to the triangular coordinate system is necessary. The following equation shows the relation between this two systems:

$$\begin{pmatrix} 1 \\ x \\ y \end{pmatrix} = \begin{pmatrix} 1 & 1 & 1 \\ x_1 & x_2 & x_3 \\ y_1 & y_2 & y_3 \end{pmatrix} \begin{pmatrix} \xi_1 \\ \xi_2 \\ \xi_3 \end{pmatrix} \quad (2.64)$$

Table 2.3: Natural Coordinate of Tri3

Corner node	ξ	η	ξ'	η'	Gauss node	ξ	η	ξ'	η'
1	-1	-1	-5/3	-5/3	1'	-2/3	-2/3	-1	-1
2	+1	-1	+7/3	-5/3	2'	+1/3	-2/3	+1	-1
3	-1	+1	-5/3	+7/3	3'	-2/3	+1/3	-1	+1

$$\begin{pmatrix} \xi_1 \\ \xi_2 \\ \xi_3 \end{pmatrix} = \frac{1}{2A} \begin{pmatrix} x_2y_3 - x_3y_2 & y_2 - y_3 & x_3 - x_2 \\ x_3y_1 - x_1y_3 & y_3 - y_1 & x_1 - x_3 \\ x_1y_2 - x_2y_1 & y_1 - y_2 & x_2 - x_1 \end{pmatrix} \begin{pmatrix} 1 \\ x \\ y \end{pmatrix} = \frac{1}{2A} \begin{pmatrix} 2A_{23} & y_{23} & x_{32} \\ 2A_{31} & y_{31} & x_{13} \\ 2A_{12} & y_{12} & x_{21} \end{pmatrix} \begin{pmatrix} 1 \\ x \\ y \end{pmatrix} \quad (2.65)$$

**Figure 2.9:** Tri3 in element coordinate and Gauss element coordinate.

2.3.5 Triangular element with six nodes: Tri6

Tri6 is a higher order 2D, 6 node element. This element is defined by 6 nodes with two degrees of freedom (DOFs) at each node: translation in the nodal x and y direction. The geometry of

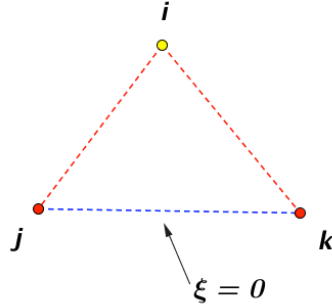


Figure 2.10: Equation of side opposite corner 1 for Tri3.

Tri6 is shown in Figure 2.11. Two kinds of Gauss elements can be applied in this case, namely, triangle with three nodes and triangle with six nodes. Here we explain the case with six nodes. According to the work of Carlos A. Felippa [Felippa 2004 section 18, p.5-6], there are two types of nodes within Tri6: corners nodes(1, 2 and 3) and midside nodes(4, 5 and 6). In both cases, we calculate the product of the two linear functions in the triangular coordinates because the shape function should be quadratic. The both types of shape function are depicted in Figure 2.12. For corner node 1, we can derive the shape function, which refers to Figure 2.12 at left hand side.

$$N_1^e = c_1 L_{2-3} L_{4-6} \quad (2.66)$$

For calculating N_1^e will take edge 2-5-3 and edge 4-6 into consideration. This makes the function zero at node 2,3,4,5,6 and nonzero at node 1. The value of function can be adjusted to 1 if c_1 is appropriately chosen. The equations of the edges that show in Equation 2.66 are:

$$L_{2-3} : \xi_1 = 0, \quad L_{4-6} : \xi_1 - \frac{1}{2} = 0 \quad (2.67)$$

Inserting the above functions into Equation 2.66:

$$N_1^e = c_1 \xi_1 \left(\xi_1 - \frac{1}{2} \right) \quad (2.68)$$

Same as in Tri3, $N_1^e(1, 0, 0) = c_1 \times 1 \times \frac{1}{2} = 1$. Then the result $c_1 = 2$ can be achieved and the corresponding shape function can be expressed as:

$$N_1^e = 2 \xi_1 \left(\xi_1 - \frac{1}{2} \right) = \xi_1 (2\xi_1 - 1) \quad (2.69)$$

For midside node 4, we can express the shape function by observation of Figure 2.12:

$$N_4^e = c_4 L_{2-3} L_{1-3} \quad (2.70)$$

The equations of edges L_{2-3} and L_{1-3} are $\xi_1 = 0$ and $\xi_2 = 0$, respectively. Therefore, $N_4^e(\xi_1, \xi_2, \xi_3) = c_4 \xi_1 \xi_2$. We evaluate this function at node 4 to find c_4 , and its triangular coordinates are $\xi_1 = \xi_2 =$

$\frac{1}{2}, \xi_3 = 0$. Then $N_4^e\left(\frac{1}{2}, \frac{1}{2}, 0\right) = c_4 \times \frac{1}{2} \times \frac{1}{2} = 1$. Hence $c_4 = 4$ and the shape function can be formed as:

$$N_4^e = 4\xi_1\xi_2 \quad (2.71)$$

The rest of the shape functions can be solved with by the same approach. They can be expressed as:

$$N_2^e = \xi_2(2\xi_2 - 1) \quad (2.72)$$

$$N_3^e = \xi_3(2\xi_3 - 1) \quad (2.73)$$

$$N_5^e = 4\xi_2\xi_3 \quad (2.74)$$

$$N_6^e = 4\xi_1\xi_3 \quad (2.75)$$

From the above functions, the extrapolation function of Tri6 can be written as:

$$\begin{pmatrix} w_1 \\ w_2 \\ w_3 \\ w_4 \\ w_5 \\ w_6 \end{pmatrix} = \begin{pmatrix} a_1 & a_1 & a_2 & a_3 & a_4 & a_4 \\ a_1 & a_2 & a_1 & a_4 & a_4 & a_3 \\ a_2 & a_1 & a_1 & a_4 & a_3 & a_4 \\ a_1 & a_7 & a_7 & a_5 & a_6 & a_5 \\ a_7 & a_7 & a_1 & a_6 & a_5 & a_5 \\ a_7 & a_1 & a_7 & a_5 & a_5 & a_6 \end{pmatrix} \begin{pmatrix} w_1' \\ w_2' \\ w_3' \\ w_4' \\ w_5' \\ w_6' \end{pmatrix} \quad (2.76)$$

$$a_1 = +0.55555556$$

$$a_2 = +3.88888889$$

$$a_3 = +0.44444444$$

$$a_4 = -2.22222222$$

$$a_5 = -0.88888889$$

$$a_6 = +1.77777778$$

$$a_7 = +0.22222222$$

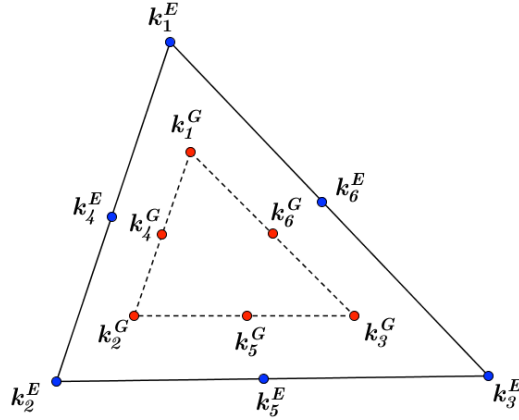


Figure 2.11: Tri6 in element coordinate and Gauss element coordinate.

2.3.6 Tetrahedral element with four nodes: Tet4

Tet4 is a higher order 3D 4-node solid element. The element is defined by 4 nodes with three degrees of freedom (DOFs) per node: translation in the nodal x , y and z directions. The geometry of Tet4 is shown in Figure 2.13. For the tetrahedron element, it is beneficial to use its own coordinate. The shape functions of Tet4 are:

$$N_1 = L_1 \quad (2.77)$$

$$N_2 = L_2 \quad (2.78)$$

$$N_3 = L_3 \quad (2.79)$$

$$N_4 = L_4 \quad (2.80)$$

We take a tetrahedron element with four nodes as Gauss element for Gauss integration. The relation between Gauss and nodal coordinate are represented in Table 2.4. From this table, we can conclude four corner nodes in Gauss coordinate: $k_1^E(j, k, k, k)$, $k_2^E(k, j, k, k)$, $k_3^E(k, k, j, k)$, $k_4^E(k, k, k, j)$ ($j = 1.927051, k = -0.309017$). The procedure to calculate the extrapolation function of Tet4 is similar as Tri3, because they both use their own coordinate system. After

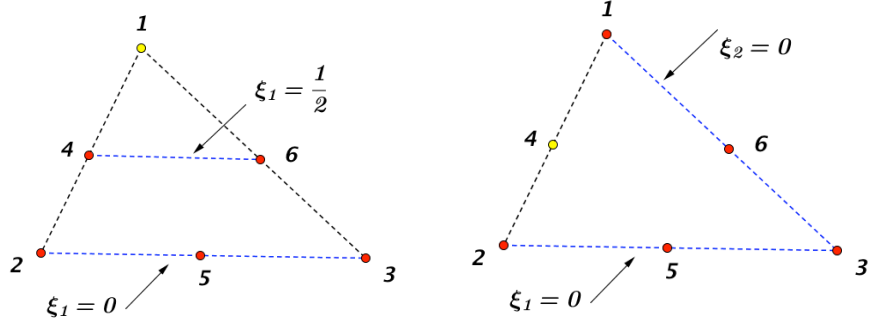


Figure 2.12: Equation of side opposite corner 1 for Tri6.

inserting the corner points into shape function, the extrapolation of Tet4 is shown as:

$$\begin{pmatrix} w_1 \\ w_2 \\ w_3 \\ w_4 \end{pmatrix} = \begin{pmatrix} a_1 & a_2 & a_2 & a_2 \\ a_2 & a_1 & a_2 & a_2 \\ a_2 & a_2 & a_1 & a_2 \\ a_2 & a_2 & a_2 & a_1 \end{pmatrix} \begin{pmatrix} w_1' \\ w_2' \\ w_3' \\ w_4' \end{pmatrix} \quad (2.81)$$

$$a_1 = +1.927051$$

$$a_2 = -0.309017$$

2.3.7 Tetrahedral element with ten nodes: Tet10

Tet10 is a higher order 3D 10-node solid element. The element is defined by 10 nodes with three degrees of freedom (DOFs) per node: translation in the nodal x , y and z directions. The geometry, node location, and coordinate system for this element are shown in Figure 2.14. According to the work of Carlos A. Felippa [Felippa 2004 section 10 p.21], for Tet10 it is possible to choose different types of Gauss element, which contains 1, 4, 6, 14, 15 and 24 integration points. We choose a tetrahedron with four nodes as internal Gauss element for this paper. The shape function of this type of Gauss element is same as the shape functions of Tet4:

$$N_1 = L_1 \quad (2.82)$$

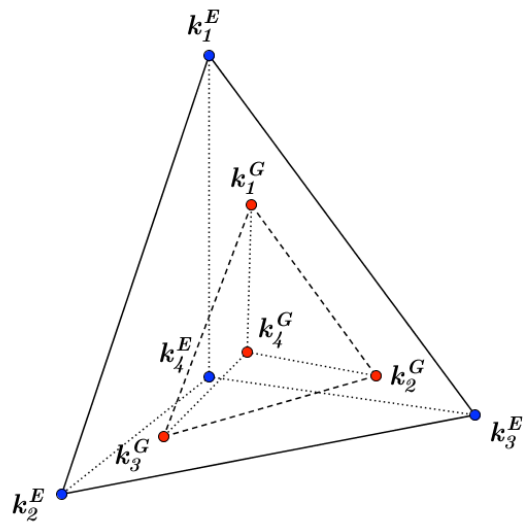


Figure 2.13: Tet4 in element coordinate and Gauss element coordinate.

$$N_2 = L_2 \quad (2.83)$$

$$N_3 = L_3 \quad (2.84)$$

$$N_4 = L_4 \quad (2.85)$$

Table 2.4: Tetrahedral Coordinate of Tet4

Corner node	L1	L2	L3	L4	L1'	L2'	L3'	L4'
1	1	0	0	0	α	β	β	β
2	0	1	0	0	β	α	β	β
3	0	0	1	0	β	β	α	β
4	0	0	0	1	β	β	β	α

Gauss node	L1	L2	L3	L4	L1'	L2'	L3'	L4'
1'	α	β	β	β	1	0	0	0
2'	β	α	β	β	0	1	0	0
3'	β	β	α	β	0	0	1	0
4'	β	β	β	α	0	0	0	1

$$\alpha = 0.58541020; \beta = 0.13819660$$

The relation between Gauss and natural coordinate of Tet10 has a similar basic frame as Tet4. The new appended six corner nodes are picked as midpoint of each edges. Table 2.5 shows the details of Gauss and nodal coordinate system, respectively. Then the extrapolation of Tet10 can be formed as:

$$\begin{pmatrix} w_1 \\ w_2 \\ w_3 \\ w_4 \\ w_5 \\ w_6 \\ w_7 \\ w_8 \\ w_9 \\ w_{10} \end{pmatrix} = \begin{pmatrix} a_1 & a_2 & a_2 & a_2 \\ a_2 & a_1 & a_2 & a_2 \\ a_2 & a_2 & a_1 & a_2 \\ a_2 & a_2 & a_2 & a_1 \\ a_3 & a_3 & a_2 & a_2 \\ a_3 & a_2 & a_3 & a_2 \\ a_3 & a_2 & a_2 & a_3 \\ a_2 & a_3 & a_3 & a_2 \\ a_2 & a_3 & a_2 & a_3 \\ a_2 & a_2 & a_3 & a_3 \end{pmatrix} \begin{pmatrix} w_1' \\ w_2' \\ w_3' \\ w_4' \\ \\ \\ \\ \\ \\ \\ \end{pmatrix} \quad (2.86)$$

$$a_1 = +1.927051$$

$$a_2 = -0.309017$$

$$a_3 = +0.809017$$

2.4 Assembly

In the previous chapter, we have solved the value of strain and stress in one element. The next step is to assemble strain and stress at each node from the local view to the global view. Meanwhile,

Table 2.5: Coordinate system of Tet10

Corner node	L1	L2	L3	L4	L1'	L2'	L3'	L4'
1	1	0	0	0	α	β	β	β
2	0	1	0	0	β	α	β	β
3	0	0	1	0	β	β	α	β
4	0	0	0	1	β	β	β	α
5	0.5	0.5	0	0	$\frac{\alpha+\beta}{2}$	$\frac{\alpha+\beta}{2}$	β	β
6	0.5	0	0.5	0	$\frac{\alpha+\beta}{2}$	β	$\frac{\alpha+\beta}{2}$	β
7	0.5	0	1	0.5	$\frac{\alpha+\beta}{2}$	β	β	$\frac{\alpha+\beta}{2}$
8	0	0.5	0.5	0	β	$\frac{\alpha+\beta}{2}$	$\frac{\alpha+\beta}{2}$	β
9	0	0.5	0	0.5	β	$\frac{\alpha+\beta}{2}$	β	$\frac{\alpha+\beta}{2}$
10	0	0	0.5	0.5	β	β	$\frac{\alpha+\beta}{2}$	$\frac{\alpha+\beta}{2}$
Gauss node	L1	L2	L3	L4	L1'	L2'	L3'	L4'
1'	α	β	β	β	1	0	0	0
2'	β	α	β	β	0	1	0	0
3'	β	β	α	β	0	0	1	0
4'	β	β	β	α	0	0	0	1

$$\alpha = 0.58541020; \beta = 0.13819660$$

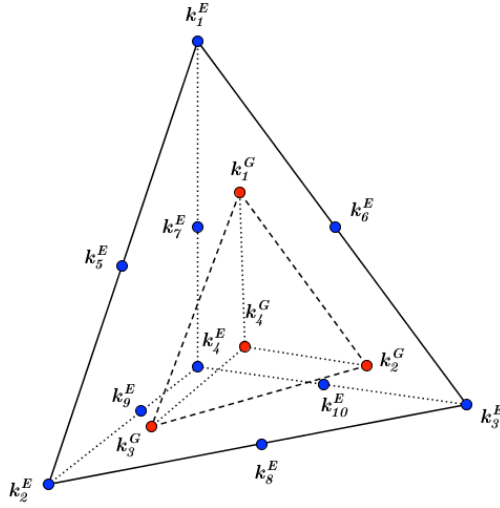


Figure 2.14: Tet10 in element coordinate and Gauss element coordinate.

element stiffness matrix and force vector are also assembled at each degrees of freedom (DOFs). According the work of W. A. Wall [Wall 2014 p.62-64], in FEM, the whole primary field can be seen as a continuous field, in which two neighboring element share one or more nodes. Now we take a simple 2D model as an example, which is meshed with two Tri3 element as depicted in Figure 2.15. We assume that the stiffness matrix k and force vector f for each single element have been calculated beforehand. The stiffness matrix of elements is given as:

$$k^{(1)} = \begin{pmatrix} k_{11}^{(1)} & k_{12}^{(1)} & k_{13}^{(1)} & k_{14}^{(1)} & k_{15}^{(1)} & k_{16}^{(1)} \\ k_{21}^{(1)} & k_{22}^{(1)} & k_{23}^{(1)} & k_{24}^{(1)} & k_{25}^{(1)} & k_{26}^{(1)} \\ k_{31}^{(1)} & k_{32}^{(1)} & k_{33}^{(1)} & k_{34}^{(1)} & k_{35}^{(1)} & k_{36}^{(1)} \\ k_{41}^{(1)} & k_{42}^{(1)} & k_{43}^{(1)} & k_{44}^{(1)} & k_{45}^{(1)} & k_{46}^{(1)} \\ k_{51}^{(1)} & k_{52}^{(1)} & k_{53}^{(1)} & k_{54}^{(1)} & k_{55}^{(1)} & k_{56}^{(1)} \\ k_{61}^{(1)} & k_{62}^{(1)} & k_{63}^{(1)} & k_{64}^{(1)} & k_{65}^{(1)} & k_{66}^{(1)} \end{pmatrix} \quad (2.87)$$

$$k^{(2)} = \begin{pmatrix} k_{11}^{(2)} & k_{12}^{(2)} & k_{13}^{(2)} & k_{14}^{(2)} & k_{15}^{(2)} & k_{16}^{(2)} \\ k_{21}^{(2)} & k_{22}^{(2)} & k_{23}^{(2)} & k_{24}^{(2)} & k_{25}^{(2)} & k_{26}^{(2)} \\ k_{31}^{(2)} & k_{32}^{(2)} & k_{33}^{(2)} & k_{34}^{(2)} & k_{35}^{(2)} & k_{36}^{(2)} \\ k_{41}^{(2)} & k_{42}^{(2)} & k_{43}^{(2)} & k_{44}^{(2)} & k_{45}^{(2)} & k_{46}^{(2)} \\ k_{51}^{(2)} & k_{52}^{(2)} & k_{53}^{(2)} & k_{54}^{(2)} & k_{55}^{(2)} & k_{56}^{(2)} \\ k_{61}^{(2)} & k_{62}^{(2)} & k_{63}^{(2)} & k_{64}^{(2)} & k_{65}^{(2)} & k_{66}^{(2)} \end{pmatrix} \quad (2.88)$$

Now we can assemble both stiffness matrix contribution, namely from Equation 2.87 and from Equation 2.88, at the same degree of freedom. The procedure of assembly is represented as follows:

$$K = \begin{pmatrix} k_{11}^{(1)} & k_{12}^{(1)} & k_{15}^{(1)} & k_{16}^{(1)} & k_{13}^{(1)} & k_{14}^{(1)} & 0 & 0 \\ k_{21}^{(1)} & k_{22}^{(1)} & k_{25}^{(1)} & k_{26}^{(1)} & k_{23}^{(1)} & k_{24}^{(1)} & 0 & 0 \\ k_{51}^{(1)} & k_{52}^{(1)} & k_{55}^{(1)} & k_{56}^{(1)} & k_{53}^{(1)} & k_{54}^{(1)} & 0 & 0 \\ k_{61}^{(1)} & k_{62}^{(1)} & k_{65}^{(1)} & k_{66}^{(1)} & k_{63}^{(1)} & k_{64}^{(1)} & 0 & 0 \\ k_{31}^{(1)} & k_{32}^{(1)} & k_{35}^{(1)} & k_{36}^{(1)} & k_{33}^{(1)} & k_{34}^{(1)} & 0 & 0 \\ k_{41}^{(1)} & k_{42}^{(1)} & k_{45}^{(1)} & k_{46}^{(1)} & k_{43}^{(1)} & k_{44}^{(1)} & 0 & 0 \\ 0 & 0 & 0 & 0 & 0 & 0 & 0 & 0 \\ 0 & 0 & 0 & 0 & 0 & 0 & 0 & 0 \end{pmatrix} + \begin{pmatrix} 0 & 0 & 0 & 0 & 0 & 0 & 0 & 0 \\ 0 & 0 & 0 & 0 & 0 & 0 & 0 & 0 \\ 0 & 0 & k_{11}^{(2)} & k_{12}^{(2)} & k_{13}^{(2)} & k_{14}^{(2)} & k_{15}^{(2)} & k_{16}^{(2)} \\ 0 & 0 & k_{21}^{(2)} & k_{22}^{(2)} & k_{23}^{(2)} & k_{24}^{(2)} & k_{25}^{(2)} & k_{26}^{(2)} \\ 0 & 0 & k_{31}^{(2)} & k_{32}^{(2)} & k_{33}^{(2)} & k_{34}^{(2)} & k_{35}^{(2)} & k_{36}^{(2)} \\ 0 & 0 & k_{41}^{(2)} & k_{42}^{(2)} & k_{43}^{(2)} & k_{44}^{(2)} & k_{45}^{(2)} & k_{46}^{(2)} \\ 0 & 0 & k_{51}^{(2)} & k_{52}^{(2)} & k_{53}^{(2)} & k_{54}^{(2)} & k_{55}^{(2)} & k_{56}^{(2)} \\ 0 & 0 & k_{61}^{(2)} & k_{62}^{(2)} & k_{63}^{(2)} & k_{64}^{(2)} & k_{65}^{(2)} & k_{66}^{(2)} \end{pmatrix}$$

$$\begin{aligned}
 &= \left(\begin{array}{cccccccc}
 k_{11}^{(1)} & k_{12}^{(1)} & k_{15}^{(1)} & k_{16}^{(1)} & k_{13}^{(1)} & k_{14}^{(1)} & 0 & 0 \\
 k_{21}^{(1)} & k_{22}^{(1)} & k_{25}^{(1)} & k_{26}^{(1)} & k_{23}^{(1)} & k_{24}^{(1)} & 0 & 0 \\
 k_{51}^{(1)} & k_{52}^{(1)} & k_{55}^{(1)} + k_{11}^{(2)} & k_{56}^{(1)} + k_{12}^{(2)} & k_{53}^{(1)} + k_{13}^{(2)} & k_{54}^{(1)} + k_{14}^{(2)} & k_{15}^{(2)} & k_{16}^{(2)} \\
 k_{61}^{(1)} & k_{62}^{(1)} & k_{65}^{(1)} + k_{21}^{(2)} & k_{66}^{(1)} + k_{22}^{(2)} & k_{63}^{(1)} + k_{23}^{(2)} & k_{64}^{(1)} + k_{24}^{(2)} & k_{25}^{(2)} & k_{26}^{(2)} \\
 k_{31}^{(1)} & k_{32}^{(1)} & k_{35}^{(1)} + k_{31}^{(2)} & k_{36}^{(1)} + k_{32}^{(2)} & k_{33}^{(1)} + k_{33}^{(2)} & k_{34}^{(1)} + k_{34}^{(2)} & k_{35}^{(2)} & k_{36}^{(2)} \\
 k_{41}^{(1)} & k_{42}^{(1)} & k_{45}^{(1)} + k_{41}^{(2)} & k_{46}^{(1)} + k_{42}^{(2)} & k_{43}^{(1)} + k_{43}^{(2)} & k_{44}^{(1)} + k_{44}^{(2)} & k_{45}^{(2)} & k_{46}^{(2)} \\
 0 & 0 & k_{51}^{(2)} & k_{52}^{(2)} & k_{53}^{(2)} & k_{54}^{(2)} & k_{55}^{(2)} & k_{56}^{(2)} \\
 0 & 0 & k_{61}^{(2)} & k_{62}^{(2)} & k_{63}^{(2)} & k_{64}^{(2)} & k_{65}^{(2)} & k_{66}^{(2)}
 \end{array} \right) \quad (2.89)
 \end{aligned}$$

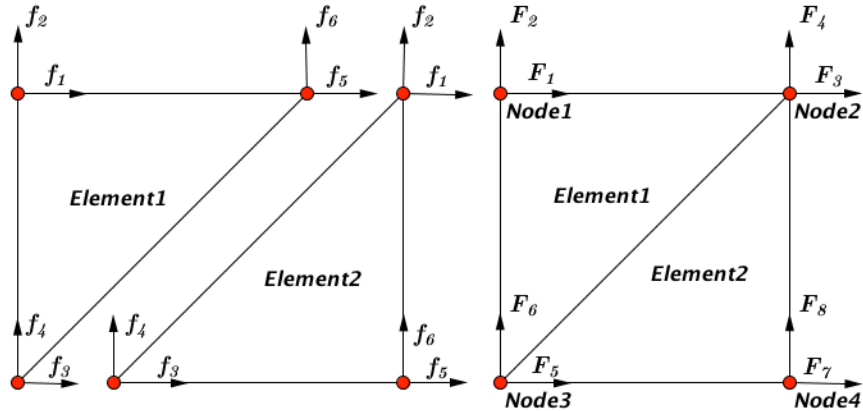


Figure 2.15: Two Tri6 elements in global and local perspective.

The same approach is also applied to force vector, because it also share the contribution at

each degree of freedom. The procedure of assembly are expressed as:

$$F = \begin{pmatrix} f_1^{(1)} \\ f_2^{(1)} \\ f_5^{(1)} \\ f_6^{(1)} \\ f_3^{(1)} \\ f_4^{(1)} \\ 0 \\ 0 \end{pmatrix} + \begin{pmatrix} 0 \\ 0 \\ f_1^{(2)} \\ f_2^{(2)} \\ f_3^{(2)} \\ f_4^{(2)} \\ f_5^{(2)} \\ f_6^{(2)} \end{pmatrix} = \begin{pmatrix} f_1^{(1)} \\ f_2^{(1)} \\ f_5^{(1)} + f_1^{(2)} \\ f_6^{(1)} + f_2^{(2)} \\ f_3^{(1)} + f_3^{(2)} \\ f_4^{(1)} + f_4^{(2)} \\ f_5^{(2)} \\ f_6^{(2)} \end{pmatrix} \quad (2.90)$$

For strain and stress, we need to assemble the contributions at each node. According to the work of Carlos A. Felippa [Felippa 2004 section 28 p.6], an extra procedure after assembling strain or stress is calculating the average value by dividing the number of elements that share the same node, because the value of strain and stress are discontinuous between neighboring elements. The rule for averaging strain or stress can be formed as:

$$\epsilon = \sum_{i=1}^n \frac{\epsilon_{i,raw}}{n} \quad \sigma = \sum_{i=1}^n \frac{\sigma_{i,raw}}{n} \quad (2.91)$$

$$\epsilon_{raw} = \begin{pmatrix} \epsilon_{1xx}^{(1)} & \epsilon_{1yy}^{(1)} & \epsilon_{1zz}^{(1)} & 2\epsilon_{1yz}^{(1)} & 2\epsilon_{1xz}^{(1)} & 2\epsilon_{1xy}^{(1)} \\ \epsilon_{2xx}^{(1)} & \epsilon_{2yy}^{(1)} & \epsilon_{2zz}^{(1)} & 2\epsilon_{2yz}^{(1)} & 2\epsilon_{2xz}^{(1)} & 2\epsilon_{2xy}^{(1)} \\ \epsilon_{5xx}^{(1)} & \epsilon_{5yy}^{(1)} & \epsilon_{5zz}^{(1)} & 2\epsilon_{5yz}^{(1)} & 2\epsilon_{5xz}^{(1)} & 2\epsilon_{5xy}^{(1)} \\ \epsilon_{6xx}^{(1)} & \epsilon_{6yy}^{(1)} & \epsilon_{6zz}^{(1)} & 2\epsilon_{6yz}^{(1)} & 2\epsilon_{6xz}^{(1)} & 2\epsilon_{6xy}^{(1)} \\ \epsilon_{3xx}^{(1)} & \epsilon_{3yy}^{(1)} & \epsilon_{3zz}^{(1)} & 2\epsilon_{3yz}^{(1)} & 2\epsilon_{3xz}^{(1)} & 2\epsilon_{3xy}^{(1)} \\ \epsilon_{4xx}^{(1)} & \epsilon_{4yy}^{(1)} & \epsilon_{4zz}^{(1)} & 2\epsilon_{4yz}^{(1)} & 2\epsilon_{4xz}^{(1)} & 2\epsilon_{4xy}^{(1)} \\ 0 & 0 & 0 & 0 & 0 & 0 \\ 0 & 0 & 0 & 0 & 0 & 0 \end{pmatrix} + \begin{pmatrix} 0 & 0 & 0 & 0 & 0 & 0 \\ 0 & 0 & 0 & 0 & 0 & 0 \\ \epsilon_{1xx}^{(2)} & \epsilon_{1yy}^{(2)} & \epsilon_{1zz}^{(2)} & 2\epsilon_{1yz}^{(2)} & 2\epsilon_{1xz}^{(2)} & 2\epsilon_{1xy}^{(2)} \\ \epsilon_{2xx}^{(2)} & \epsilon_{2yy}^{(2)} & \epsilon_{2zz}^{(2)} & 2\epsilon_{2yz}^{(2)} & 2\epsilon_{2xz}^{(2)} & 2\epsilon_{2xy}^{(2)} \\ \epsilon_{3xx}^{(2)} & \epsilon_{3yy}^{(2)} & \epsilon_{3zz}^{(2)} & 2\epsilon_{3yz}^{(2)} & 2\epsilon_{3xz}^{(2)} & 2\epsilon_{3xy}^{(2)} \\ \epsilon_{4xx}^{(2)} & \epsilon_{4yy}^{(2)} & \epsilon_{4zz}^{(2)} & 2\epsilon_{4yz}^{(2)} & 2\epsilon_{4xz}^{(2)} & 2\epsilon_{4xy}^{(2)} \\ \epsilon_{5xx}^{(2)} & \epsilon_{5yy}^{(2)} & \epsilon_{5zz}^{(2)} & 2\epsilon_{5yz}^{(2)} & 2\epsilon_{5xz}^{(2)} & 2\epsilon_{5xy}^{(2)} \\ \epsilon_{6xx}^{(2)} & \epsilon_{6yy}^{(2)} & \epsilon_{6zz}^{(2)} & 2\epsilon_{6yz}^{(2)} & 2\epsilon_{6xz}^{(2)} & 2\epsilon_{6xy}^{(2)} \end{pmatrix}$$

$$\epsilon = \begin{pmatrix} \epsilon_{1xx}^{(1)} & \epsilon_{1yy}^{(1)} & \epsilon_{1zz}^{(1)} & 2\epsilon_{1yz}^{(1)} & 2\epsilon_{1xz}^{(1)} & 2\epsilon_{1xy}^{(1)} \\ \epsilon_{2xx}^{(1)} & \epsilon_{2yy}^{(1)} & \epsilon_{2zz}^{(1)} & 2\epsilon_{2yz}^{(1)} & 2\epsilon_{2xz}^{(1)} & 2\epsilon_{2xy}^{(1)} \\ \frac{\epsilon_{5xx}^{(1)} + \epsilon_{1xx}^{(2)}}{2} & \frac{\epsilon_{5yy}^{(1)} + \epsilon_{1yy}^{(2)}}{2} & \frac{\epsilon_{5zz}^{(1)} + \epsilon_{1zz}^{(2)}}{2} & \frac{2\epsilon_{5yz}^{(1)} + 2\epsilon_{1yz}^{(2)}}{2} & \frac{2\epsilon_{5xz}^{(1)} + 2\epsilon_{1xz}^{(2)}}{2} & \frac{2\epsilon_{5xy}^{(1)} + 2\epsilon_{1xy}^{(2)}}{2} \\ \frac{\epsilon_{6xx}^{(1)} + \epsilon_{2xx}^{(2)}}{2} & \frac{\epsilon_{6yy}^{(1)} + \epsilon_{2yy}^{(2)}}{2} & \frac{\epsilon_{6zz}^{(1)} + \epsilon_{2zz}^{(2)}}{2} & \frac{2\epsilon_{6yz}^{(1)} + 2\epsilon_{2yz}^{(2)}}{2} & \frac{2\epsilon_{6xz}^{(1)} + 2\epsilon_{2xz}^{(2)}}{2} & \frac{2\epsilon_{6xy}^{(1)} + 2\epsilon_{2xy}^{(2)}}{2} \\ \frac{\epsilon_{3xx}^{(1)} + \epsilon_{3xx}^{(2)}}{2} & \frac{\epsilon_{3yy}^{(1)} + \epsilon_{3yy}^{(2)}}{2} & \frac{\epsilon_{3zz}^{(1)} + \epsilon_{3zz}^{(2)}}{2} & \frac{2\epsilon_{3yz}^{(1)} + 2\epsilon_{3yz}^{(2)}}{2} & \frac{2\epsilon_{3xz}^{(1)} + 2\epsilon_{3xz}^{(2)}}{2} & \frac{2\epsilon_{3xy}^{(1)} + 2\epsilon_{3xy}^{(2)}}{2} \\ \frac{\epsilon_{4xx}^{(1)} + \epsilon_{4xx}^{(2)}}{2} & \frac{\epsilon_{4yy}^{(1)} + \epsilon_{4yy}^{(2)}}{2} & \frac{\epsilon_{4zz}^{(1)} + \epsilon_{4zz}^{(2)}}{2} & \frac{2\epsilon_{4yz}^{(1)} + 2\epsilon_{4yz}^{(2)}}{2} & \frac{2\epsilon_{4xz}^{(1)} + 2\epsilon_{4xz}^{(2)}}{2} & \frac{2\epsilon_{4xy}^{(1)} + 2\epsilon_{4xy}^{(2)}}{2} \\ \epsilon_{5xx}^{(2)} & \epsilon_{5yy}^{(2)} & \epsilon_{5zz}^{(2)} & 2\epsilon_{5yz}^{(2)} & 2\epsilon_{5xz}^{(2)} & 2\epsilon_{5xy}^{(2)} \\ \epsilon_{6xx}^{(2)} & \epsilon_{6yy}^{(2)} & \epsilon_{6zz}^{(2)} & 2\epsilon_{6yz}^{(2)} & 2\epsilon_{6xz}^{(2)} & 2\epsilon_{6xy}^{(2)} \end{pmatrix} \quad (2.92)$$

$$\sigma_{raw} = \begin{pmatrix} \sigma_{1xx}^{(1)} & \sigma_{1yy}^{(1)} & \sigma_{1zz}^{(1)} & \sigma_{1yz}^{(1)} & \sigma_{1xz}^{(1)} & \sigma_{1xy}^{(1)} \\ \sigma_{2xx}^{(1)} & \sigma_{2yy}^{(1)} & \sigma_{2zz}^{(1)} & \sigma_{2yz}^{(1)} & \sigma_{2xz}^{(1)} & f_{2xy}^{(1)} \\ \sigma_{5xx}^{(1)} & \sigma_{5yy}^{(1)} & \sigma_{5zz}^{(1)} & \sigma_{5yz}^{(1)} & \sigma_{5xz}^{(1)} & \sigma_{5xy}^{(1)} \\ \sigma_{6xx}^{(1)} & \sigma_{6yy}^{(1)} & \sigma_{6zz}^{(1)} & \sigma_{6yz}^{(1)} & \sigma_{6xz}^{(1)} & \sigma_{6xy}^{(1)} \\ \sigma_{3xx}^{(1)} & \sigma_{3yy}^{(1)} & \sigma_{3zz}^{(1)} & \sigma_{3yz}^{(1)} & \sigma_{3xz}^{(1)} & \sigma_{3xy}^{(1)} \\ \sigma_{4xx}^{(1)} & \sigma_{4yy}^{(1)} & \sigma_{4zz}^{(1)} & \sigma_{4yz}^{(1)} & \sigma_{4xz}^{(1)} & \sigma_{4xy}^{(1)} \\ 0 & 0 & 0 & 0 & 0 & 0 \\ 0 & 0 & 0 & 0 & 0 & 0 \end{pmatrix} + \begin{pmatrix} 0 & 0 & 0 & 0 & 0 & 0 \\ 0 & 0 & 0 & 0 & 0 & 0 \\ \sigma_{1xx}^{(2)} & \sigma_{1yy}^{(2)} & \sigma_{1zz}^{(2)} & \sigma_{1yz}^{(2)} & \sigma_{1xz}^{(2)} & \sigma_{1xy}^{(2)} \\ \sigma_{2xx}^{(2)} & \sigma_{2yy}^{(2)} & \sigma_{2zz}^{(2)} & \sigma_{2yz}^{(2)} & \sigma_{2xz}^{(2)} & \sigma_{2xy}^{(2)} \\ \sigma_{3xx}^{(2)} & \sigma_{3yy}^{(2)} & \sigma_{3zz}^{(2)} & \sigma_{3yz}^{(2)} & \sigma_{3xz}^{(2)} & \sigma_{3xy}^{(2)} \\ \sigma_{4xx}^{(2)} & \sigma_{4yy}^{(2)} & \sigma_{4zz}^{(2)} & \sigma_{4yz}^{(2)} & \sigma_{4xz}^{(2)} & \sigma_{4xy}^{(2)} \\ \sigma_{5xx}^{(2)} & \sigma_{5yy}^{(2)} & \sigma_{5zz}^{(2)} & \sigma_{5yz}^{(2)} & \sigma_{5xz}^{(2)} & \sigma_{5xy}^{(2)} \\ \sigma_{6xx}^{(2)} & \sigma_{6yy}^{(2)} & \sigma_{6zz}^{(2)} & \sigma_{6yz}^{(2)} & \sigma_{6xz}^{(2)} & \sigma_{6xy}^{(2)} \end{pmatrix}$$

$$\sigma = \begin{pmatrix} \sigma_{1xx}^{(1)} & \sigma_{1yy}^{(1)} & \sigma_{1zz}^{(1)} & \sigma_{1yz}^{(1)} & \sigma_{1xz}^{(1)} & \sigma_{1xy}^{(1)} \\ \sigma_{2xx}^{(1)} & \sigma_{2yy}^{(1)} & \sigma_{2zz}^{(1)} & \sigma_{2yz}^{(1)} & \sigma_{2xz}^{(1)} & f_{2xy}^{(1)} \\ \frac{\sigma_{5xx}^{(1)} + \sigma_{1xx}^{(2)}}{2} & \frac{\sigma_{5yy}^{(1)} + \sigma_{1yy}^{(2)}}{2} & \frac{\sigma_{5zz}^{(1)} + \sigma_{1zz}^{(2)}}{2} & \frac{\sigma_{5yz}^{(1)} + \sigma_{1yz}^{(2)}}{2} & \frac{\sigma_{5xz}^{(1)} + \sigma_{1xz}^{(2)}}{2} & \frac{\sigma_{5xy}^{(1)} + \sigma_{1xy}^{(2)}}{2} \\ \frac{\sigma_{6xx}^{(1)} + \sigma_{2xx}^{(2)}}{2} & \frac{\sigma_{6yy}^{(1)} + \sigma_{2yy}^{(2)}}{2} & \frac{\sigma_{6zz}^{(1)} + \sigma_{2zz}^{(2)}}{2} & \frac{\sigma_{6yz}^{(1)} + \sigma_{2yz}^{(2)}}{2} & \frac{\sigma_{6xz}^{(1)} + \sigma_{2xz}^{(2)}}{2} & \frac{\sigma_{6xy}^{(1)} + \sigma_{2xy}^{(2)}}{2} \\ \frac{\sigma_{3xx}^{(1)} + \sigma_{3xx}^{(2)}}{2} & \frac{\sigma_{3yy}^{(1)} + \sigma_{3yy}^{(2)}}{2} & \frac{\sigma_{3zz}^{(1)} + \sigma_{3zz}^{(2)}}{2} & \frac{\sigma_{3yz}^{(1)} + \sigma_{3yz}^{(2)}}{2} & \frac{\sigma_{3xz}^{(1)} + \sigma_{3xz}^{(2)}}{2} & \frac{\sigma_{3xy}^{(1)} + \sigma_{3xy}^{(2)}}{2} \\ \frac{\sigma_{4xx}^{(1)} + \sigma_{4xx}^{(2)}}{2} & \frac{\sigma_{4yy}^{(1)} + \sigma_{4yy}^{(2)}}{2} & \frac{\sigma_{4zz}^{(1)} + \sigma_{4zz}^{(2)}}{2} & \frac{\sigma_{4yz}^{(1)} + \sigma_{4yz}^{(2)}}{2} & \frac{\sigma_{4xz}^{(1)} + \sigma_{4xz}^{(2)}}{2} & \frac{\sigma_{4xy}^{(1)} + \sigma_{4xy}^{(2)}}{2} \\ \sigma_{5xx}^{(2)} & \sigma_{5yy}^{(2)} & \sigma_{5zz}^{(2)} & \sigma_{5yz}^{(2)} & \sigma_{5xz}^{(2)} & \sigma_{5xy}^{(2)} \\ \sigma_{6xx}^{(2)} & \sigma_{6yy}^{(2)} & \sigma_{6zz}^{(2)} & \sigma_{6yz}^{(2)} & \sigma_{6xz}^{(2)} & \sigma_{6xy}^{(2)} \end{pmatrix} \quad (2.93)$$

Chapter 3

Programming Implementation and Investigation

3.1 Pre-Processing with ANSYS

The purpose of Pre-Processing is to build a numerical model and export data of a meshed geometry as two lists: node list and element list. The two lists are ultimately imported into AMfe Toolbox. ANSYS Parametric Design Language (APDL) code is used to create a meshed geometry in ANSYS. A simple meshed geometry is shown in Figure 3.1. The steps for building model contains a series of related path. An example of such path is:

Geometry ⇒ Element Type ⇒ Material ⇒ Mesh ⇒ Boundary Condition

After building the model, numerical data can be exported as a node list and an element list. The node list contains coordinates of nodes. The element list consists of the attributes of each element and the index of each node that belongs to the element. The element attributes are assigned to the different parts of model by referring to the appropriate entries in the element list. The pointers are simply a set of reference numbers that include the element index (ELEM), material number (MAT), element type number (TYP), real constant set number (REAL), a coordinate system number (ESY) ,and section ID number (SEC) [ANSYS 2011]. According to the example in Figure 3.1, both lists are depicted in Table 3.1 and Table 3.2. The numerical information of both lists are captured using regular expression and stored in AMfe Toolbox. For different kinds of data it is necessary to store in its specific data type. The coordinate of each node and the index of nodes from elements are stored as NumPy array. NumPy is the fundamental package for scientific computing using Python. The advantage of NumPy for storage of node and element information depends on its efficient multi-dimensional container of generic data. According to the documentation of Numpy community [Numpy 2016], "NumPy contains a powerful N-dimensional array object and sophisticated (broadcasting) functions." Moreover, it is possible to integrate Fortran code. General attributes of the element can be stored as an efficient form- Pandas DataFrames. According to the documentation of Wes Mckinney and PyData Development Team [Mckinney 2016], "Pandas is a powerful data analysis toolkit, which provides fast, flexible, and expressive data structures designed to make working with relational or labeled data both easy and intuitive.

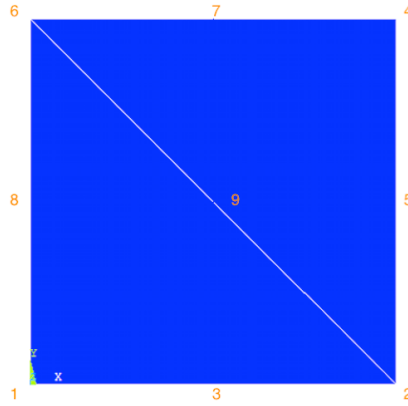


Figure 3.1: A simple meshed geometry

Pandas DataFrames is a two-dimensional size-mutable, potentially heterogeneous tabular data structure with labeled axes (rows and columns). Arithmetic operations align on both row and column labels. This format can be thought of as a dictionary-like container for Series objects." We can calculate the nodal strain and stress from the Pre-Processing data from ANSYS by using the Stress-Recovery-Algorithms. In addition, the solutions of nodal strain and stress from ANSYS and the corresponding solutions from AMfe are comparable, because the Pre-Processing data for both solutions are identical.

3.2 Unit Testing with Python

According to the documentation of Fred L. Drake, Jr. [Fred L. Drake 2016], automated unit testing is the best way to determine whether the element type works well. Unit test is the batteries-included test module in the Python standard library. The motivation for writing a unit testing is to evaluate the quality of each element type and try to find the reasons for failed tests. The element types to be tested are Tri3, Tri6, Quad4, Quad8, Tet4 and Tet10. We test the strain and stress components with all the element types. As is mentioned before, the numerical solution to a mechanical problem is only an approximate solution. There is an error between the analytical solution and FEM solution for sure. Here we do not have an analytical solution to compare with our AMfe solution. The results of components from ANSYS will be compared to the results that are calculated from AMfe Toolbox. Although the solution from ANSYS is not the analytical solution, it could still help us check the quality of element types in AMfe Toolbox. As a comparison, we need to define both the absolute error and the relative error in the test. According to the work of Rao V. Dukkipati [Dukkipati 2010], absolute error is the magnitude of the difference between actual value and approximate value. It can be defined as:

$$e_{abs} = \|X_{actual} - X_{fem}\| \quad (3.1)$$

Table 3.1: Node list exported from ANSYS

NODE	X	Y	Z	THXY	THYZ	THZX
1	0.0000	0.0000	0.0000	0.00	0.00	0.00
2	50.000	0.0000	0.0000	0.00	0.00	0.00
3	25.000	0.0000	0.0000	0.00	0.00	0.00
4	50.000	50.000	0.0000	0.00	0.00	0.00
5	50.000	25.000	0.0000	0.00	0.00	0.00
6	0.0000	50.000	0.0000	0.00	0.00	0.00
7	25.000	50.000	0.0000	0.00	0.00	0.00
8	0.0000	25.000	0.0000	0.00	0.00	0.00
9	25.000	25.000	0.0000	0.00	0.00	0.00

Table 3.2: Element list exported from ANSYS

ELEM	MAT	TYP	REL	ESY	SEC	Node	Node	Node	Node	Node	Node
1	1	1	1	0	1	6	2	4	9	5	7
2	1	1	1	0	1	6	1	2	8	3	9

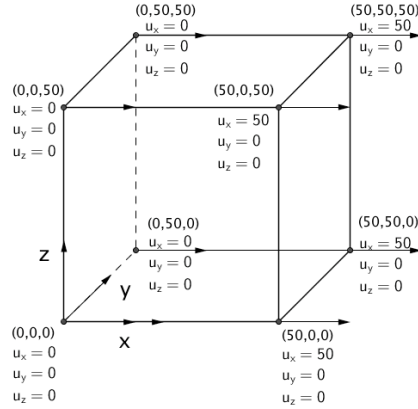


Figure 3.2: A model for test of 3D elements

Relative error is the absolute error relative to the actual value. It can be defined as:

$$e_{rel} = \frac{\|X_{actual} - X_{fem}\|}{X_{actual}} \quad (3.2)$$

As Rao V. Dukkipati [Dukkipati 2010] has noted, "it is noteworthy that errors of approximation or rounding and truncation are introduced by numerical methods or algorithms and calculating with finite precision. Truncation error represents the error that occurs when some series is truncated to a fewer number of terms. Such error is virtually an algorithmic error. Roundoff error occurs because of the computing tool's inability to handle certain numbers." It is hard to set one tolerance standard for all engineering problems. The tolerance for error can vary in different situations. One thing we can do here is set the tolerance with different values and compare the results of testing between elements. In the engineering field, Von Mises stress is usually regarded as a failure criterion to judge a design. Hence, here we calculate the von Mises stress by meshing with each element type in their corresponding 2D or 3D models. According to the research of P. M. Kurowski [Kurowski 2012], the Von Mises stress can be expressed by the principle stresses as:

$$\sigma_{vm} = \sqrt{\frac{1}{2} \left[(\sigma_1 - \sigma_2)^2 + (\sigma_2 - \sigma_3)^2 + (\sigma_3 - \sigma_1)^2 \right]} \quad (3.3)$$

The 2D and 3D model for unit testing are build in a simple way. We create a rectangle for 2D elements and a cube for 3D elements. We apply only Dirichlet boundary condition on these models. Figure 3.3 and Figure 3.2 illustrate the model for 2D and 3D element, respectively. The complete test of all the element types is shown in Table 3.3 and Table 3.4. It is obvious that both algorithms perform well in Tri3 and Quad4. The other element types fail the unit test. It is necessary to investigate into what is wrong with the other element types.

Table 3.3: Unit testing of the result using Direct-Evaluation-Algorithms

Tolerance Parameter	Tri3	Tri6	Quad4	Quad8	Tet4	Tet10
$e_{abs} = 10^{-10}; e_{rel} = 10^{-4}$	Fail	Fail	Fail	Fail	Fail	Fail
$e_{abs} = 10^{-10}; e_{rel} = 5 \times 10^{-4}$	Pass	Fail	Fail	Fail	Fail	Fail
$e_{abs} = 10^{-10}; e_{rel} = 10^{-3}$	Pass	Fail	Pass	Fail	Fail	Fail

3.3 The Patch Test

After testing the quality of each element type, we find out that the element types Tri6, Quad8, Tet4, and Tet10 are problematic and need to be fixed. In order to fix these problems, we need to know if the finite element program has the correct algorithmic procedure. This is generally not easy to verify when the modelling is too complex. The patch test is a useful technique in checking the performance of element type that is being tested. The basic idea of the patch test is to apply special boundary conditions so as to maintain a constant strain and a constant stress field. This is to simplify a complex problem to a simple one, to which we already know the correct numerical solutions.

According to the theory of Carlos A. Felippa [Felippa 2004 section 15 p.9-11], the procedures of the displacement patch test are as follows: create a simple geometry that consists of one or several elements; pick a patch and apply the displacement at exterior nodes and the prescribed displacement field will be set as $u_x = x, u_y = 0$. The reason the displacement field only applies to exterior nodes is that displacements are related to the background continuum. The last step is to verify whether the patch has a constant strain field. The mechanism behind the displacement patch test is setting the strain at every exterior node as 1, which can be calculated by:

$$\frac{du}{dx} = 1 \quad (3.4)$$

As we know,

$$\sum N_i = 1 \quad (3.5)$$

and,

$$\epsilon = \sum N_i \cdot \epsilon_i \quad (3.6)$$

Here we have $\epsilon_i = 0$ and $\sum N_i = 1$, hence the strain field is constant and equal 1.

Now we take Tri3 as an example in implementing the displacement patch test. We create a simple rectangle that consists of two Tri3 elements in ANSYS, and the prescribed displacement field is depicted in Figure 3.3. Strain field from ANSYS can be viewed in Figure 3.4. As is expected,

Table 3.4: Unit testing of the extrapolate result using Stress-Recovery-Algorithms

Tolerance Parameter	Tri3	Tri6	Quad4	Quad8	Tet4	Tet10
$e_{abs} = 10^{-10}; e_{rel} = 10^{-4}$	Fail	Fail	Fail	Fail	Fail	Fail
$e_{abs} = 10^{-10}; e_{rel} = 5 \times 10^{-4}$	Pass	Fail	Fail	Fail	Fail	Fail
$e_{abs} = 10^{-10}; e_{rel} = 10^{-3}$	Pass	Fail	Pass	Fail	Fail	Fail

$\epsilon_{xx} = 1$. Thus, we have successfully built the model for a patch test. Now it is time to check whether AMfe Toolbox has the same constant strain field or not. We export the node, element, and displacement data from ANSYS and import all of them into AMfe Toolbox. After computing strain and stress in AMfe, the contour plot of strain in ParaView is shown as the picture on right-hand side of Figure 3.4. The plot from AMfe Toolbox illustrates the same result of $\epsilon_{xx} = 1$. This proves that the displacement patch test has been passed. Other element types, namely Tri6, Quad4, Quad8, Tet4, and Tet10, each have a constant field. However, the results of the patch test using element Tri6, Quad8, Tet4, and Tet10 are still problematic because all of these elements have the value of 1.5 as the constant strain, as is demonstrated by the problematic result from Tet4 in Figure 3.5. It is necessary to investigate why all these elements have the same strain with the value of 1.5. By debugging the AMfe Code we can find that the strain values at Gauss points are all 1.5. This proves that the Stress-Recovery-Algorithms is correct. The problem exists in the calculation of the strain at Gauss points. Moreover, all of these element types except Tri3 and Quad4 have the same problem.

3.4 Convergence Analysis

We can either decrease the element size or increase the polynomial degrees of the shape function to approach an relatively exact approximation. This process is denoted as convergence. A convergence analysis provides a function to reduce the relative error of the solution with increasing number of degrees of freedom [Wall 2014]. An example of convergence analysis is illustrated in Figure 3.6. On the one hand, because of the technical restriction, we can only export the node, element, and displacement lists from ANSYS and set all of them as input into AMfe Toolbox for solving strain and stress. As of now, we did not reverse the process and solve the displacement by using prescribed Neumann boundary condition and Dirichlet boundary condition as input. However, it is still a feasible plan for future research. On the other hand, we can analyse this problem using another software, Gmsh, as Pre-Processing tool. The procedures of our convergence analysis for investigating 2D elements are as follows: first, we create a 2D geometry in ANSYS and generate a fine meshing with element types Quad4, Quad8, Tri3, and Tri6, respectively. Then we pick one node to view the displacement. In this case, we do not have the analytical solution,

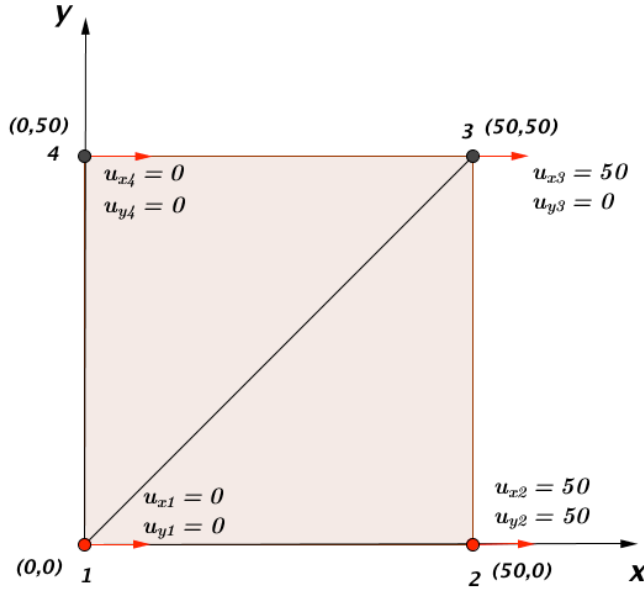


Figure 3.3: A model for test of 2D elements

thus the displacement result in this fine meshing will be regarded as a referential solution. In next step, we create an identical modelling in Gmsh and refine the meshing of all the 2D element types by decreasing the size of the elements. Then, we can record the displacement results of both AMfe and ANSYS from meshing with different degrees of freedom (DOFs), and plot the corresponding ratios of AMfe results to ANSYS results. The 3D element types, Tet4 and Tet10, can also be analysed using this approach. An example of 2D model meshing with Tri3 is shown in Figure 3.7 and an example of 3D model meshing with Tet4 is shown in Figure 3.8. The displacement for each of the 2D element types has been recorded in Table 3.5 and Table 3.6. The displacement for 3D element types are represented in Table 3.7. The same nodal displacements from a fine meshing in ANSYS are:

$$2D : Ux = -0.0015045; Uy = 0.011738$$

$$3D : Ux = 9.47; Uy = 0; Uz = 0$$

The convergence plots of 2D element types are depicted in Figure 3.9 and Figure 3.10. Figure 3.11 shows the convergence performance of 3D element types. All the element types show a good convergence to the exact solution. The higher order element types (Tri6 and Tet10) have a relatively higher convergence rate than that of the lower order element types (Tri3 and Tet4). This characteristic is not that discernible in quadrilateral element types (Quad4 and Quad8).

It is also important to check the convergence of Von Mises stress. Thus we refine the meshing in a 2D or 3D modelling using all the element types in ANSYS, and then export the data of node, element, and displacement from ANSYS and import them into AMfe Toolbox. The next step is

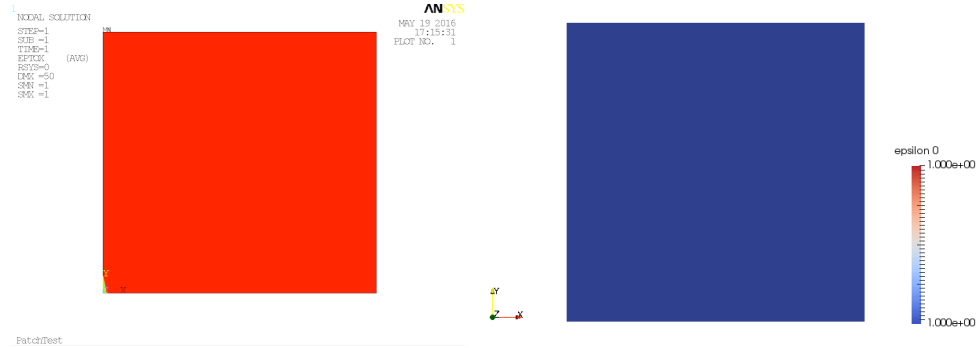


Figure 3.4: left: Contour plot of ϵ_{xx} from ANSYS (SMN: minimal value; SMX: maximal value); right: Contour plot of ϵ_{xx} calculated in AMfe, demonstrate in ParaView

to run the code to get the computing results for our convergence study. $\sigma_{xy}, \sigma_{yy}, \sigma_{zz}$ are for 2D convergence analysis and $\sigma_{xy}, \sigma_{yy}, \sigma_{zz}, \sigma_{xy}, \sigma_{yz}, \sigma_{xz}$ are for 3D convergence analysis. Then we can use these values to calculate the Von Mises stress:

$$\sigma_v = \sqrt{\frac{1}{2} \left[(\sigma_{11} - \sigma_{22})^2 + (\sigma_{22} - \sigma_{33})^2 + (\sigma_{33} - \sigma_{11})^2 + 6(\sigma_{12}^2 + \sigma_{23}^2 + \sigma_{31}^2) \right]} \quad (3.7)$$

For a general plane stress case with restrictions $\sigma_3 = 0$ and $\sigma_{31} = \sigma_{23} = 0$, we can simplify the Von Mises equation as:

$$\sigma_v = \sqrt{\sigma_{11}^2 - \sigma_{11}\sigma_{22} + \sigma_{22}^2 + 3\sigma_{12}^2} \quad (3.8)$$

The 2D model is built as is shown in Figure 3.12 and the 3D model is built as is shown in Figure 3.13. Table 3.8 shows the test data of convergence analysis for all element types. Figure 3.14 illustrates the relation between the DOFs of mesh and the Von Mises stress of the observer point, which is denoted C in 2D model and is denoted D in 3D model. The three plots in Figure 3.14 show that all the element types converge to the exact solution and the element types with higher order (Tri6, Quad8, and Tet10) converge faster than the ones with lower order (Tri3, Quad4, and Tet4) do. When we compare the two 2D element Tri3 and Quad4, we can find the Quad4 has a higher convergence rate than Tri3.

3.5 Complex Model Test

The patch test is only applicable to the simple models. It is meaningful to know how these element types behave in a complex model. Now we create a relatively complex model meshing with each element type and calculate the nodal stress in AMfe by using Direct-Evaluation-Algorithms and Stress-Recovery-Algorithms. The main objective of the complex model test is to compare the strain and stress contour plots of each element type in ANSYS and in AMfe Toolbox by using algorithms. Furthermore, the comparison between the two algorithms is also significant for our research. The results from AMfe Toolbox are displayed in ParaView as a Post-Processing tool.

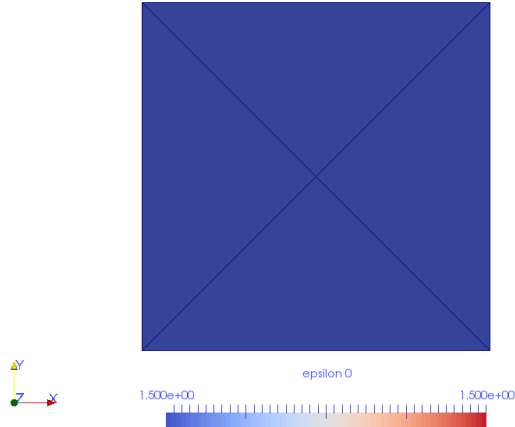


Figure 3.5: Patch Test of Tet4

It is worth noting that the order of the components for tensors follows this mapping rule: 0-xx; 1-yy; 2-zz; 3-yz; 4-yx; 5-xz; 6-zx; 7-xy; 8-xy. For a clear comparison and good contrast, we import an identical color map for ANSYS and ParaView. However, a clear chromatic aberration still exists between the contour plots from ANSYS and ParaView. Figure 3.10 is an example displaying the color difference. This issue may be fixed when we using an advanced version of ANSYS, because ANSYS 12.0, which we used in this paper, can only offer a 7-bit color in color map.

Figure 3.16 to Figure 3.21 illustrate the contour plot of strain and stress in all directions. The

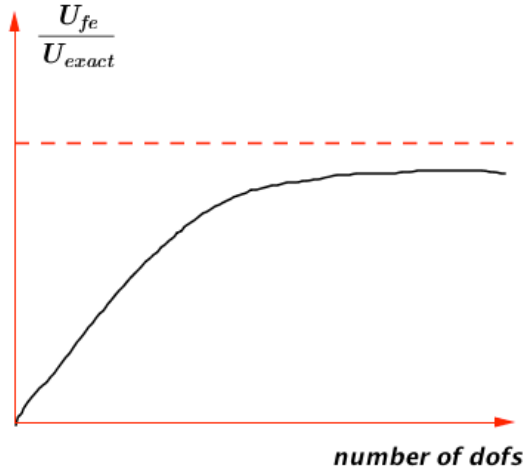


Figure 3.6: Convergence analysis

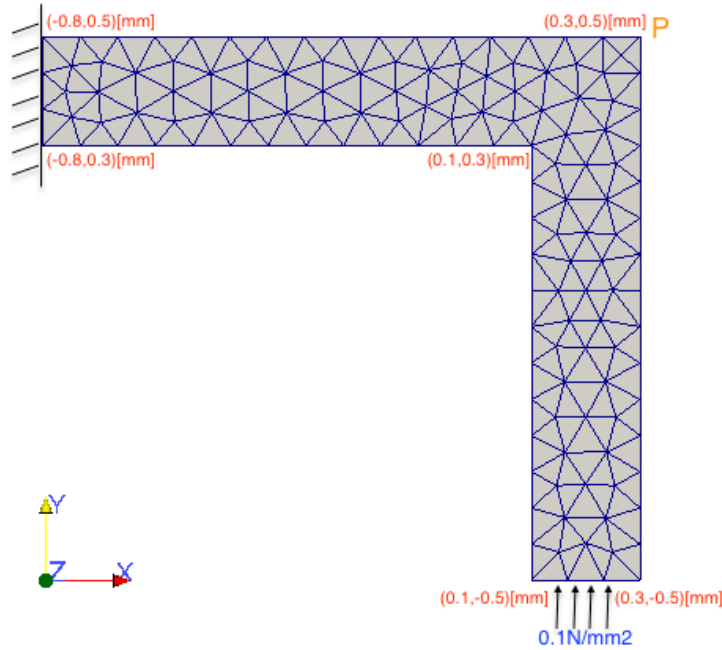


Figure 3.7: 2D model meshing with Tri3 for displacement convergence analysis; P as observer point

contour plots from AMfe are meshed with element type Tri3 and the contour plots from ANSYS are meshed with element PLANE42 (triangular option). According to the documentation of ANSYS [APDL], "PLANE42 is used for 2D modeling of solid structures. The element can be used either as a plane element (plane stress or plane strain) or as an axisymmetric element. The element is defined by four nodes having two degrees of freedom at each node: translations in the nodal x and y directions." By comparing the plots from AMfe and ANSYS, we can find that there is no difference between the two algorithms in AMfe. The solutions of all components from AMfe are very similar to the corresponding solutions from ANSYS.

Figure 3.22 to Figure 3.27 illustrate the contour plot of strain and stress in all direction. The contour plots from AMfe are meshed with element type Tri6 and the contour plots from ANSYS are meshed with element PLANE2. According to the documentation of ANSYS [APDL], "PLANE2 is a 6-node triangular element. The element is defined by six nodes having two degrees of freedom at each node: translations in the nodal x and y directions." The plots show that the AMfe solutions from Stress-Recovery-Algorithms are relatively closer to the ANSYS solutions than that of Direct-Evaluation-Algorithms, which has higher extreme values of strain and stress than ANSYS solution at corner points and the inner side of circle.

Figure 3.28 to Figure 3.33 illustrate the contour plots of strain and stress in all directions. The contour plots from AMfe are meshed with element type Quad4 and the contour plots from ANSYS are meshed with element PLANE42 (quadrangle option). We can observe from the plots that the AMfe solutions from Stress-Recovery-Algorithms is close to ANSYS solutions.

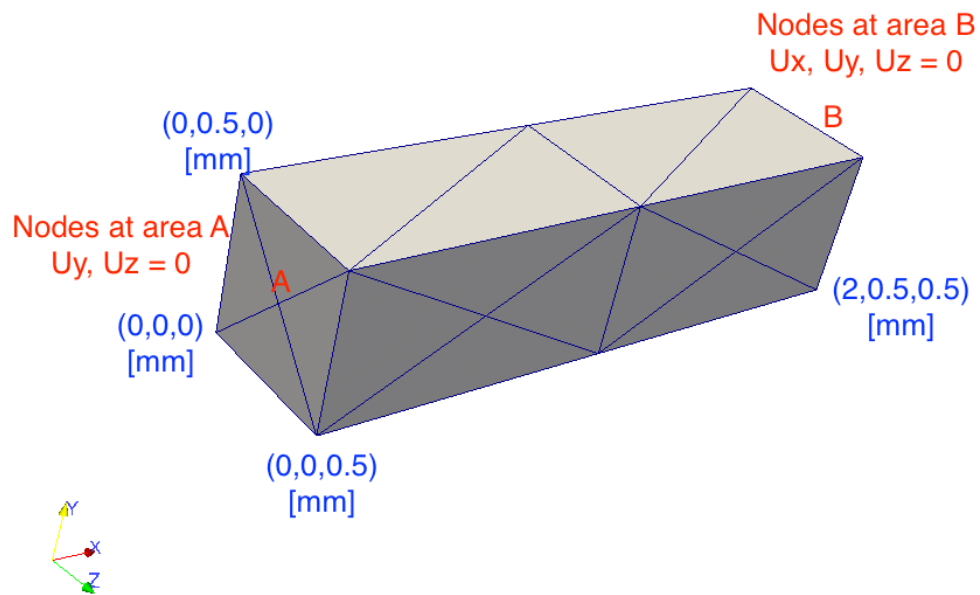


Figure 3.8: 3D model meshing with Tet4 for displacement convergence analysis; P as observer point

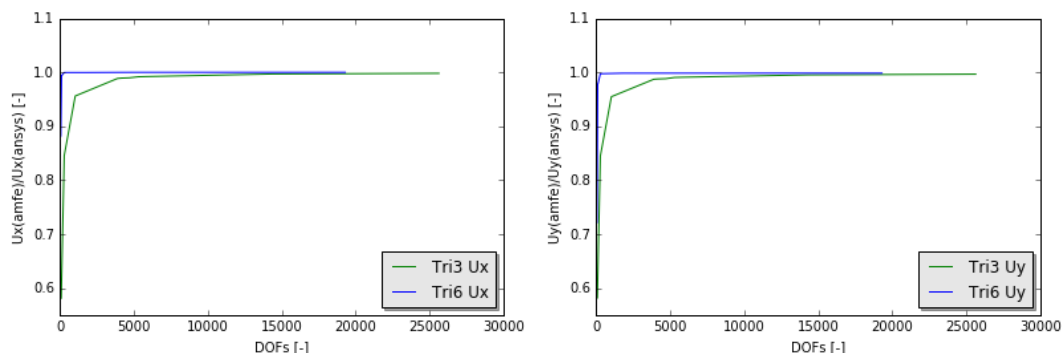


Figure 3.9: Convergence plot of Tri3 and Tri6

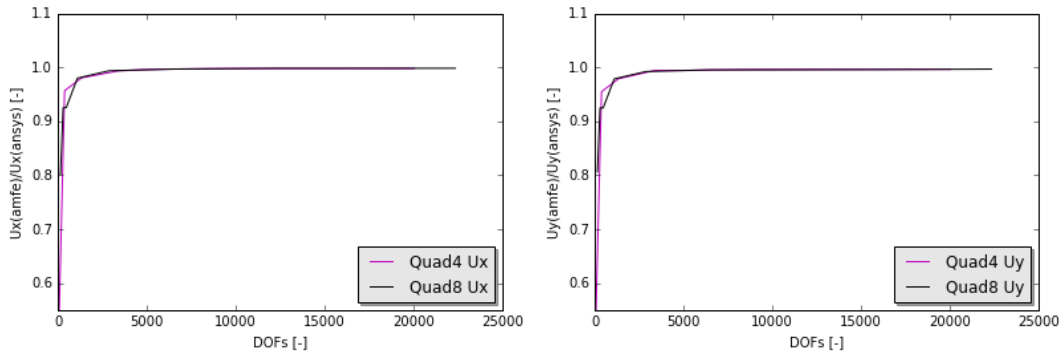


Figure 3.10: Convergence plot of Quad4 and Quad8

The deviation of results from Direct-Evaluation-Algorithms appears at same locations as that of Tri6 and the values of results in the middle range appear closer to the ANSYS than the values at the ends do.

Figure 3.34 to Figure 3.39 illustrate the contour plots of strain and stress in all directions. The contour plots from AMfe are meshed with element type Quad8 and the contour plots from ANSYS are meshed with element PLANE82. According to the documentation of ANSYS [APDL], "Plane82 is a higher order version of the 2D, four node element (PLANE82). It provides more accurate results for mixed (quadrilateral-triangular) automatic meshes and can tolerate irregular shapes without as much loss of accuracy. The 8-node element is defined by eight nodes having two degrees of freedom at each node: translations in nodal x and y directions." Both comparison between the AMfe solution from the two algorithms and the ANSYS solution and the comparison between the solutions from the two algorithms are similar to those comparisons of Quad4.

Figure 3.40 to Figure 3.49 illustrate the contour plots of strain and stress in all directions.

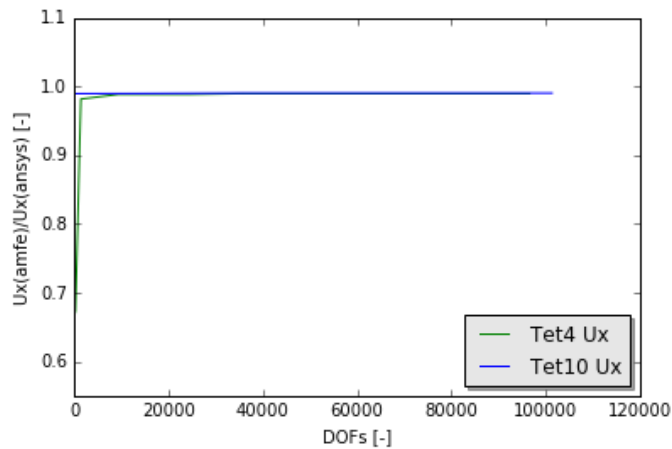


Figure 3.11: Convergence plot of Tet4 and Tet10

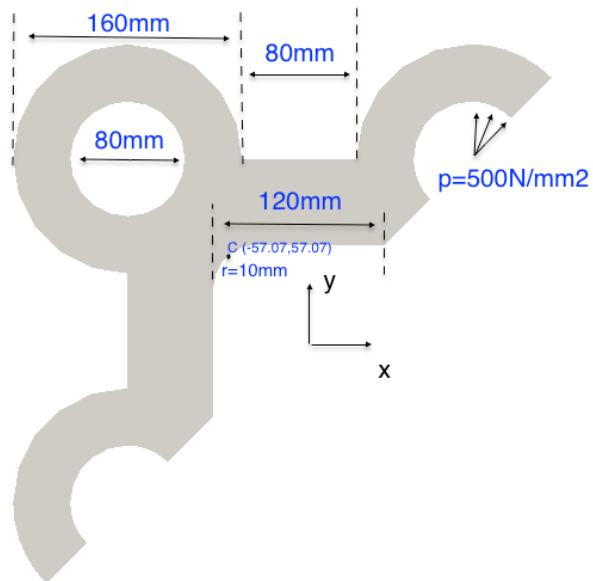


Figure 3.12: Convergence analysis of Von Mises stress in a 2D model

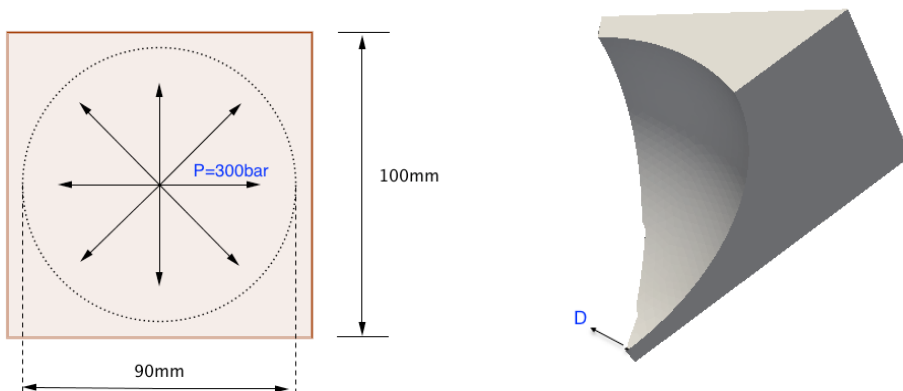


Figure 3.13: Left: Top view of the tank; Right: the 1/16 model of the tank, point D is regarded as the observer point for analysis

Table 3.5: Convergence analysis of displacement for triangular element

DOFs	Tri3-Ux	Tri3-Uy	DOFs	Tri6-Ux	Tri6-Uy
90	-0.000873929	0.0068367	62	-0.00132675	0.00847992
292	-0.00127231	0.00993406	114	-0.00149616	0.011506
1038	-0.00143843	0.0112263	138	-0.00149623	0.011513
3898	-0.00148735	0.0112263	292	-0.001504	0.0117277
4170	-0.00148835	0.0116131	1780	-0.001504	0.0117383
4698	-0.00148919	0.0116189	4830	-0.00150448	0.0117391
5298	-0.00149204	0.0116457	8986	-0.00150449	0.0117392
5842	-0.00149269	0.0116505	12073	-0.00150450	0.0117392
14322	-0.00149982	0.0117028	15609	-0.00150451	0.0117393
25634	-0.00150168	0.0117171	19300	-0.00150453	0.0117393

The contour plots from AMfe are meshed with element type Tet4 and the contour plots from ANSYS are meshed with element SOLID45. According to the documentation of ANSYS [APDL], "SOLID45 is used for the 3D modeling of solid structures. The element is defined by eight nodes having three degrees of freedom at each node: translations in the nodal x , y , and z directions." The plots demonstrate that there is no difference between the two algorithms from AMfe. The two solutions from AMfe have a relative bad performance in shear strain/stress than normal strain/stress.

Figure 3.52 to Figure 3.61 illustrate the contour plot of strain and stress in all direction. The contour plots from AMfe are meshed with element type Tet10 and the contour plot from ANSYS is meshed with element SOLID187 (tetrahedron option). According to the documentation of ANSYS [APDL], "SOLID187 element is a higher order 3D, 10-node element. SOLID187 has a quadratic displacement behavior and is well suited to modeling irregular meshes. The element is defined by 10 nodes having three degrees of freedom at each node: translations in the nodal

Table 3.6: Convergence analysis of displacement for quadrilateral element

DOFs	Quad4-Ux	Quad4-Uy	DOFs	Quad8-Ux	Quad8-Uy
48	-0.00078276	0.00620667	142	-0.00120593	0.00847992
372	-0.0014393	0.0112254	286	-0.00139123	0.0108697
1332	-0.00147509	0.0115086	466	-0.00139228	0.0108725
3374	-0.00149431	0.0116894	1090	-0.00147418	0.0115056
4842	-0.00149817	0.0116894	2870	-0.00149483	0.0116652
6228	-0.00149945	0.0116992	6450	-0.00149948	0.0117018
8386	-0.00150076	0.0117105	10346	-0.00150103	0.0117032
10232	-0.00150123	0.0117123	12342	-0.00150163	0.0117056
15344	-0.00150134	0.0117144	15656	-0.00150166	0.0117079
20044	-0.00150143	0.0117151	22344	-0.00150183	0.0117186

x , y , and z directions." Tet10 has a similar problem as Tet4 and the solutions in shear components appear not good. The plots also show that the solutions from Stress-Recovery-Algorithms performs better than the solutions from Direct-Evaluation-Algorithm.

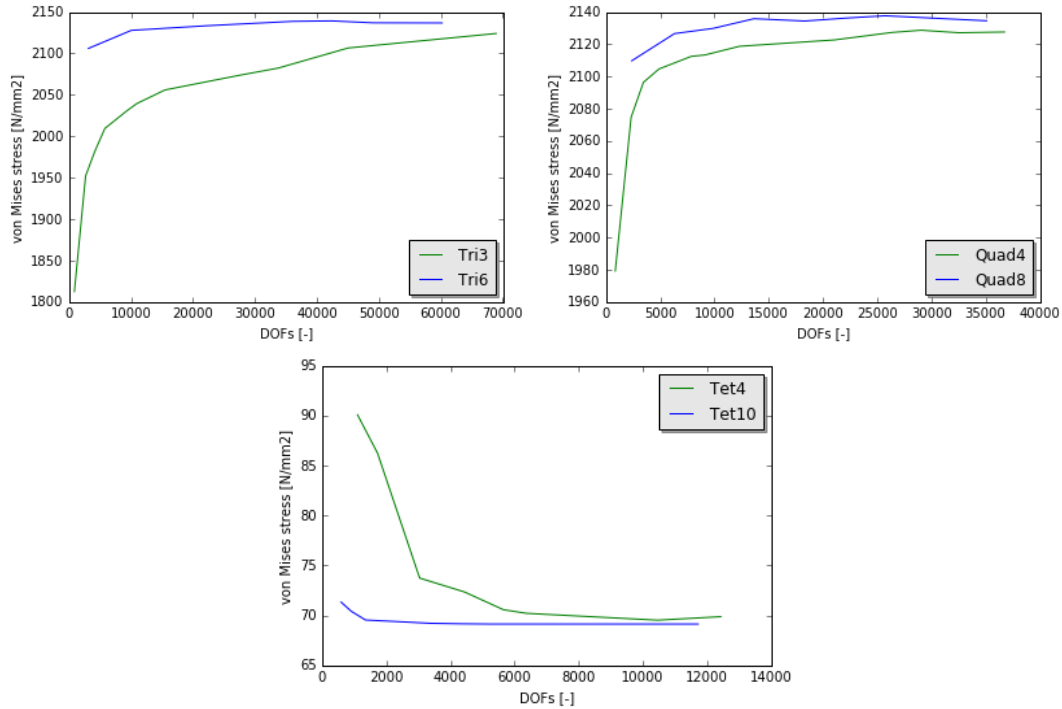


Figure 3.14: Convergence analysis of Von Mises stress, the analytical solutions are $2147.43\text{N}/\text{mm}^2$ for 2D model and $68.94\text{N}/\text{mm}^2$ for 3D model

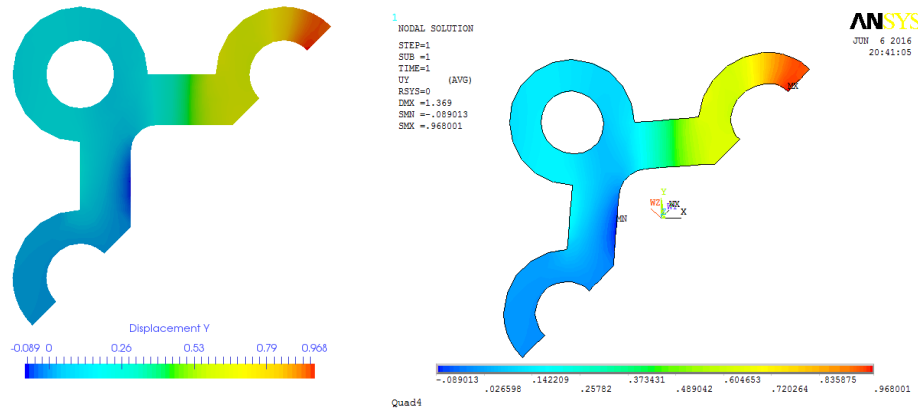


Figure 3.15: Chromatic aberration between ParaView and ANSYS

Table 3.7: Convergence analysis of displacement for tetrahedral element

DOFs	Tet4-Ux	Tet4-Uy	Tet4-Uz	DOFs	Tet10-Ux	Tet10-Uy	Tet10-Uz
54	6.320	0	0	243	9.370	0	0
243	6.372	0	0	579	9.370	0	0
1395	9.295	0	0	13857	9.372	0	0
9315	9.360	0	0	36312	9.378	0	0
24579	9.360	0	0	43521	9.378	0	0
34632	9.370	0	0	57537	9.378	0	0
53307	9.370	0	0	60299	9.378	0	0
64343	9.370	0	0	79683	9.378	0	0
76443	9.370	0	0	84322	9.378	0	0
96567	9.370	0	0	101321	9.378	0	0

Table 3.8: Convergence analysis of Von Mises stress

DOFs	Tri3	DOFs	Tri6	DOFs	Quad4	DOFs	Quad8	DOFs	Tet4	DOFs	Tet1
870	1812.47	3132	2106.11	854	1979.22	2372	2109.74	1101	90.07	588	71.32
2682	1952.20	10058	2127.91	2320	2074.70	6314	2126.62	1725	86.24	906	70.42
4172	1981.88	15892	2130.58	3448	2096.34	9890	2129.87	3039	73.73	1352	69.52
5788	2009.47	22286	2133.51	4882	2104.64	13648	2135.88	4440	72.34	2258	69.32
9354	2030.88	36028	2138.76	7856	2112.48	18340	2134.44	5652	70.57	3396	69.22
10952	2039.58	42344	2139.34	9128	2113.38	22036	2136.23	6366	70.21	4351	69.12
15490	2055.98	49044	2137.02	12310	2118.76	25724	2137.70	10461	69.52	5243	69.12
27332	2073.44	60214	2136.87	21060	2122.70	35096	2134.58	12342	69.87	11721	69.12
33770	2082.39	-	-	26384	2127.35	-	-	-	-	-	-
45032	2106.63	-	-	29056	2128.73	-	-	-	-	-	-
68943	2124.15	-	-	32548	2128.16	-	-	-	-	-	-
-	-	-	-	36750	2128.62	-	-	-	-	-	-

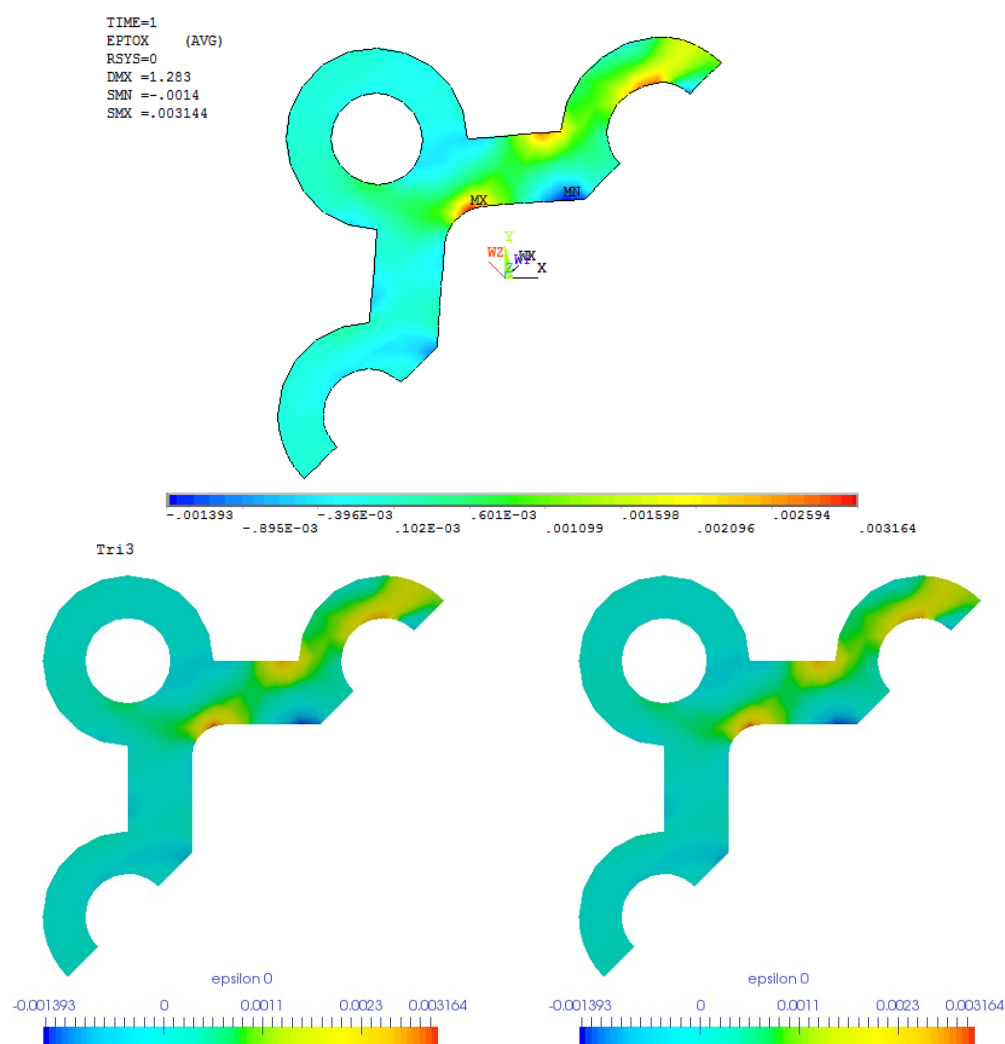


Figure 3.16: Mesh with Tri3, upper: contour plot of ϵ_{xx} in ANSYS; lower left: contour plot of ϵ_{xx} calculated without stress recovery in AMfe; lower right: contour plot of ϵ_{xx} calculated with stress recovery in AMfe

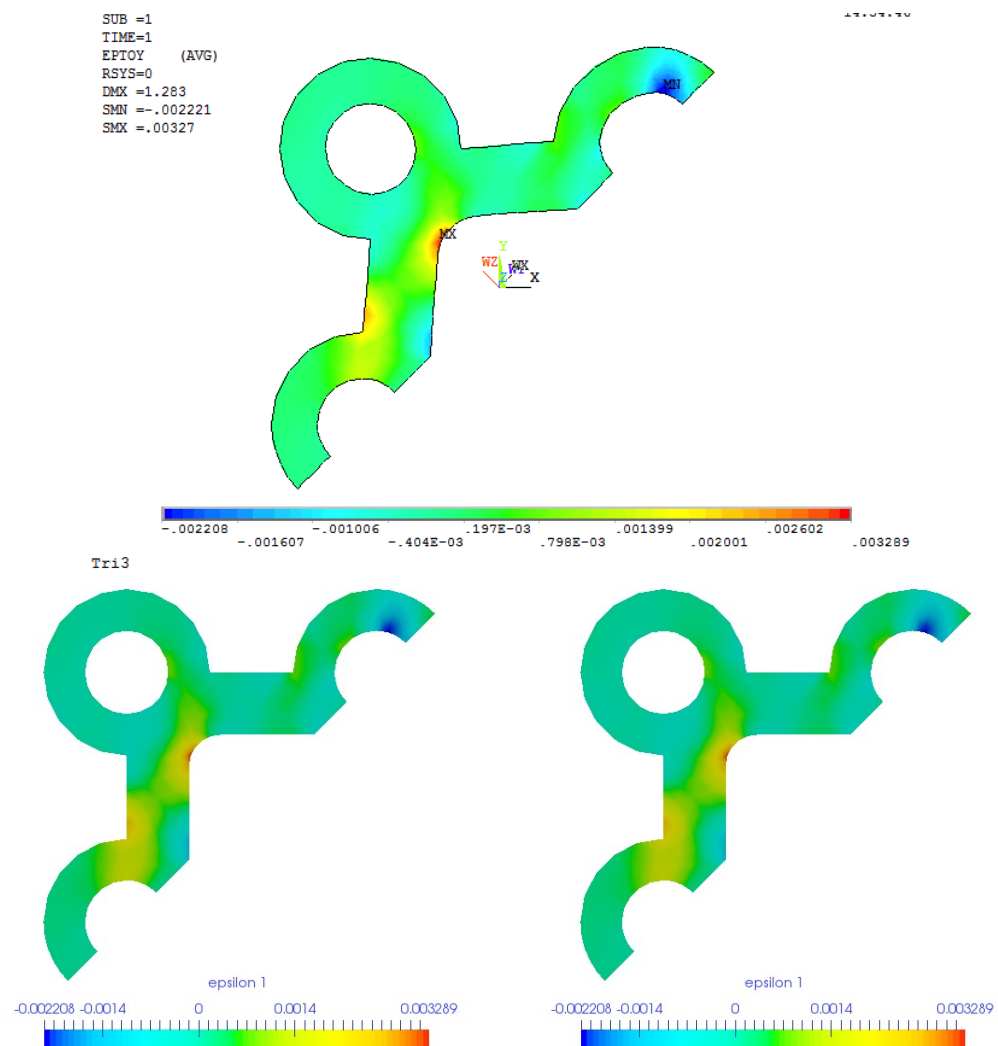


Figure 3.17: Mesh with Tri3, upper: contour plot of ϵ_{yy} in ANSYS; lower left: contour plot of ϵ_{yy} calculated without stress recovery in AMfe; lower right: contour plot of ϵ_{yy} calculated with stress recovery in AMfe

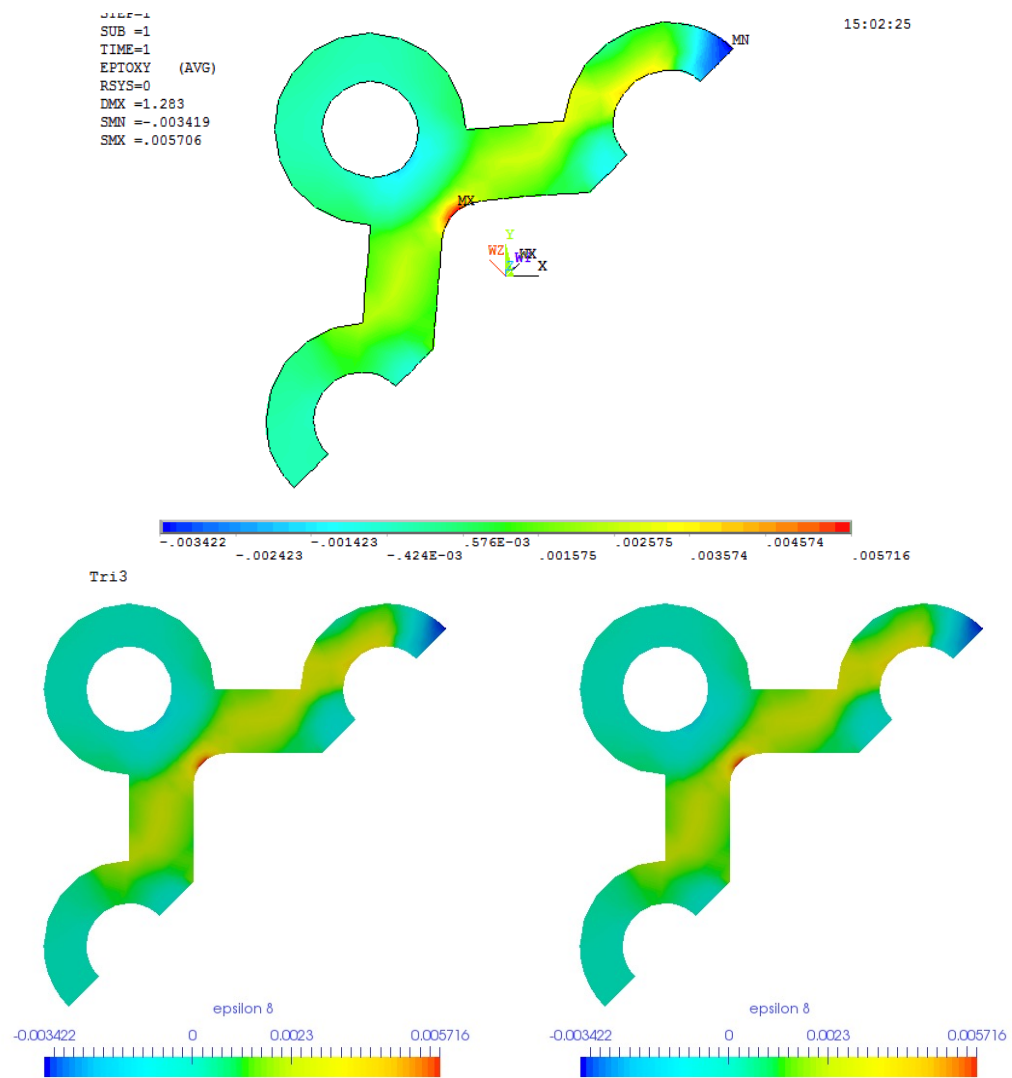


Figure 3.18: Mesh with Tri3, upper: contour plot of ϵ_{xy} in ANSYS; lower left: contour plot of ϵ_{xy} calculated without stress recovery in AMfe; lower right: contour plot of ϵ_{xy} calculated with stress recovery in AMfe

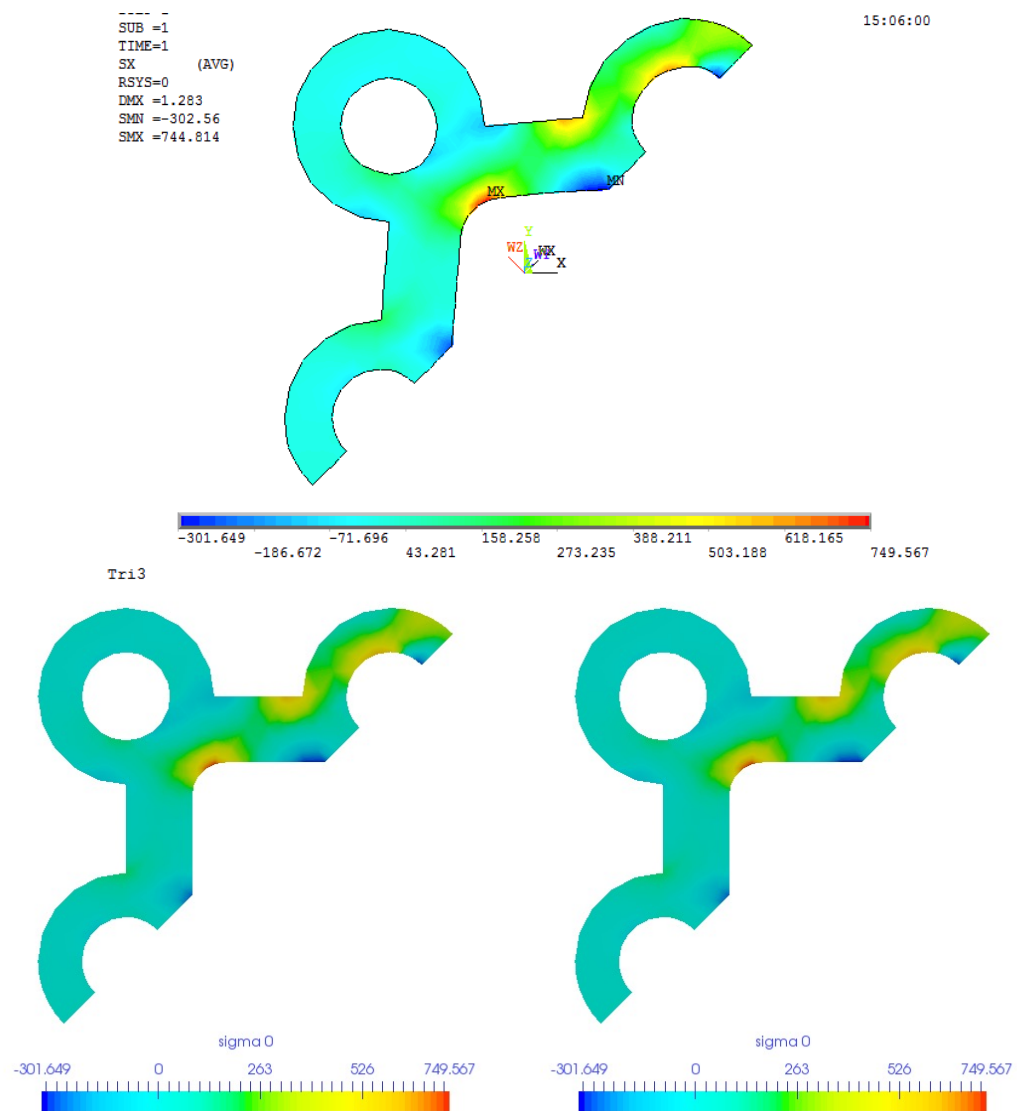


Figure 3.19: Mesh with Tri3, upper: contour plot of σ_{xx} in ANSYS; lower left: contour plot of σ_{xx} calculated without stress recovery in AMfe; lower right: contour plot of σ_{xx} calculated with stress recovery in AMfe

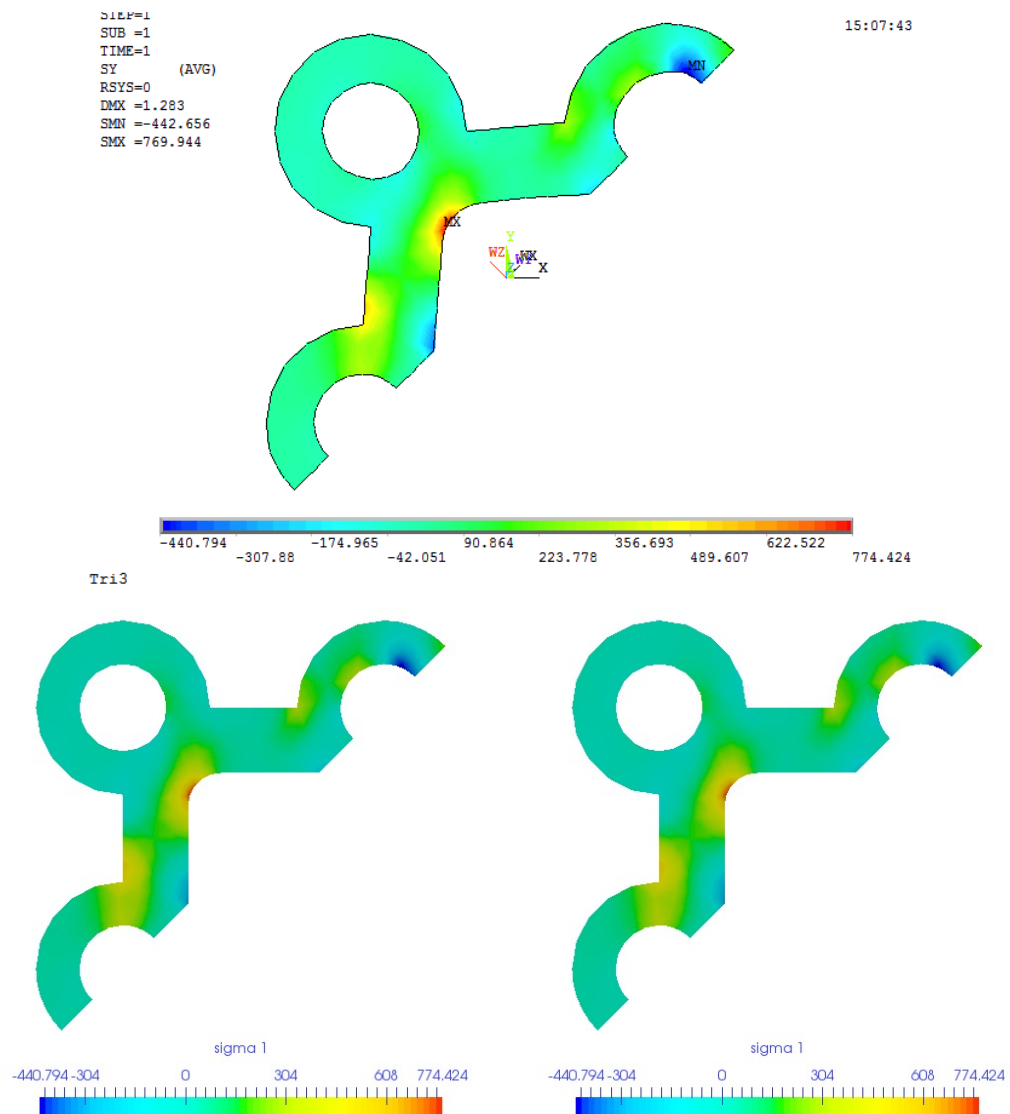


Figure 3.20: Mesh with Tri3, upper: contour plot of σ_{yy} in ANSYS; lower left: contour plot of σ_{yy} calculated without stress recovery in AMfe; lower right: contour plot of σ_{yy} calculated with stress recovery in AMfe

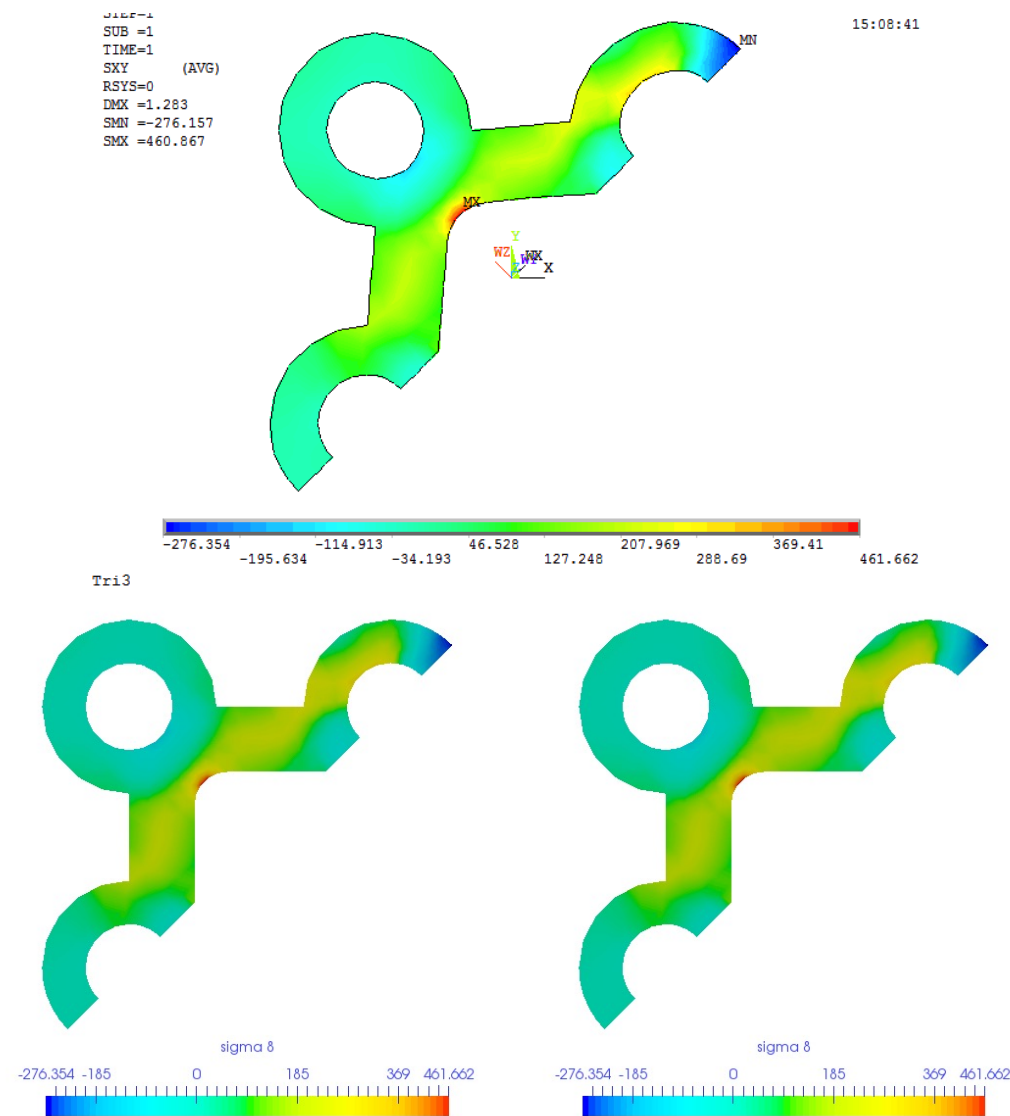


Figure 3.21: Mesh with Tri3, upper: contour plot of σ_{xy} in ANSYS; lower left: contour plot of σ_{xy} calculated without stress recovery in AMfe; lower right: contour plot of σ_{xy} calculated with stress recovery in AMfe

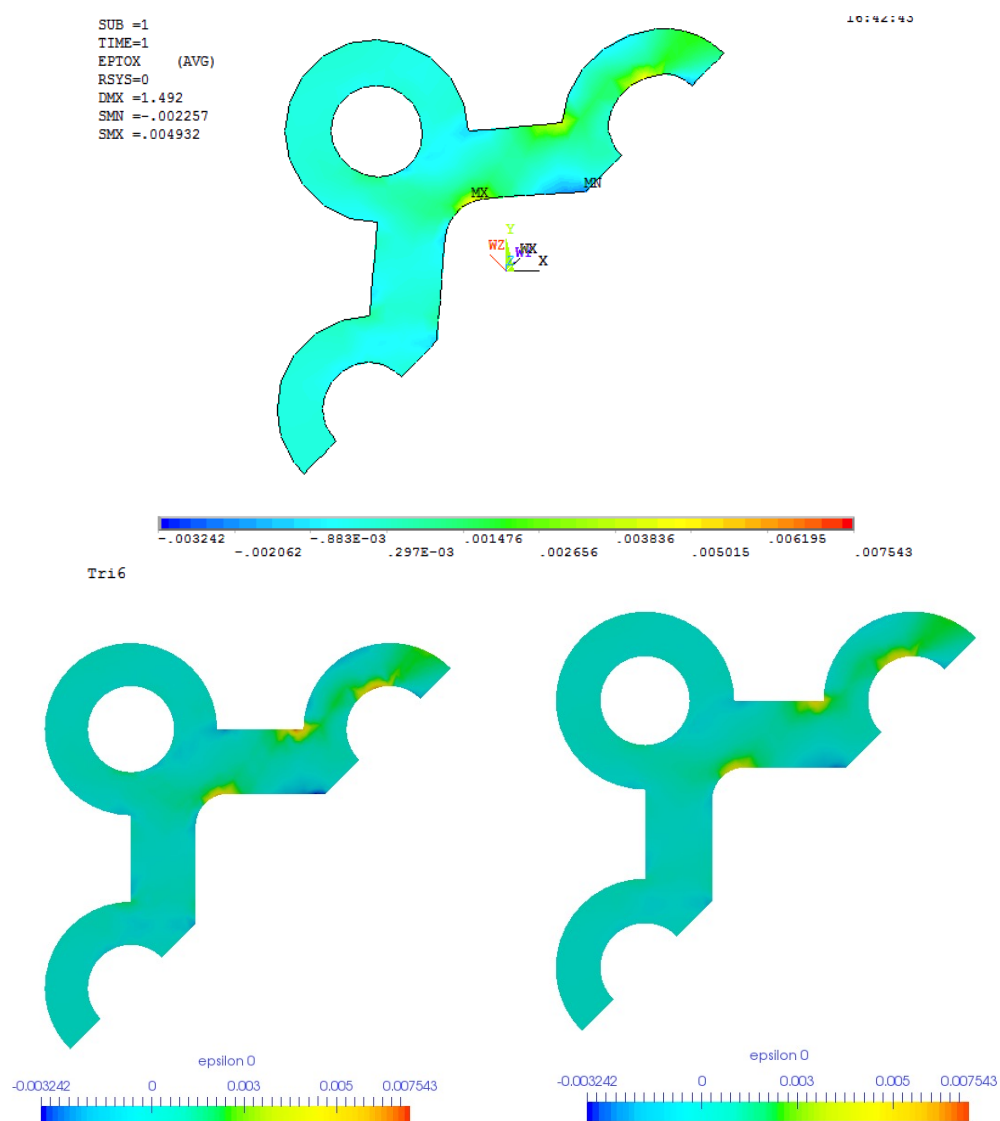


Figure 3.22: Mesh with Tri6, upper: contour plot of ϵ_{xx} in ANSYS; lower left: contour plot of ϵ_{xx} calculated without stress recovery in AMfe; lower right: contour plot of ϵ_{xx} calculated with stress recovery in AMfe

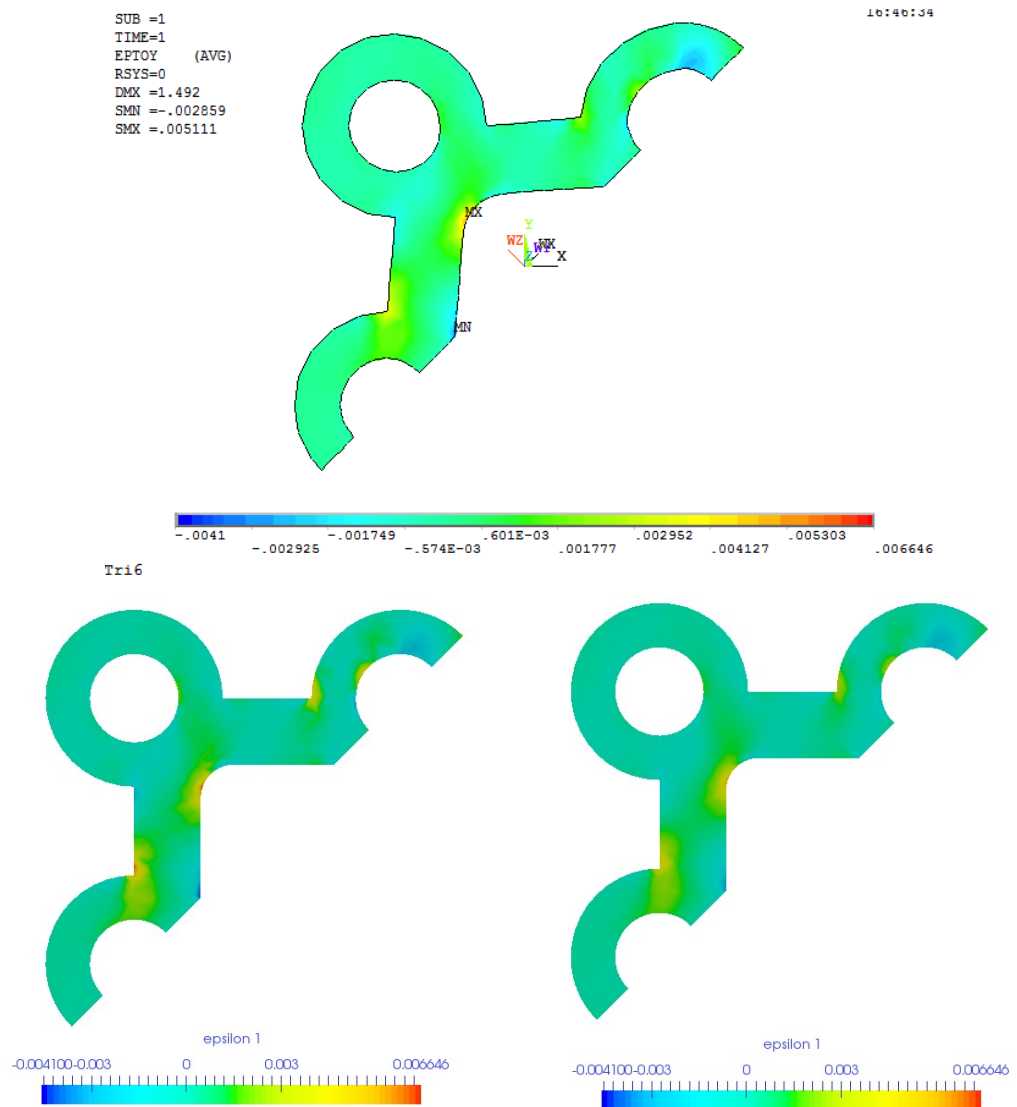


Figure 3.23: Mesh with Tri6, upper: contour plot of ϵ_{yy} in ANSYS; lower left: contour plot of ϵ_{yy} calculated without stress recovery in AMfe; lower right: contour plot of ϵ_{yy} calculated with stress recovery in AMfe

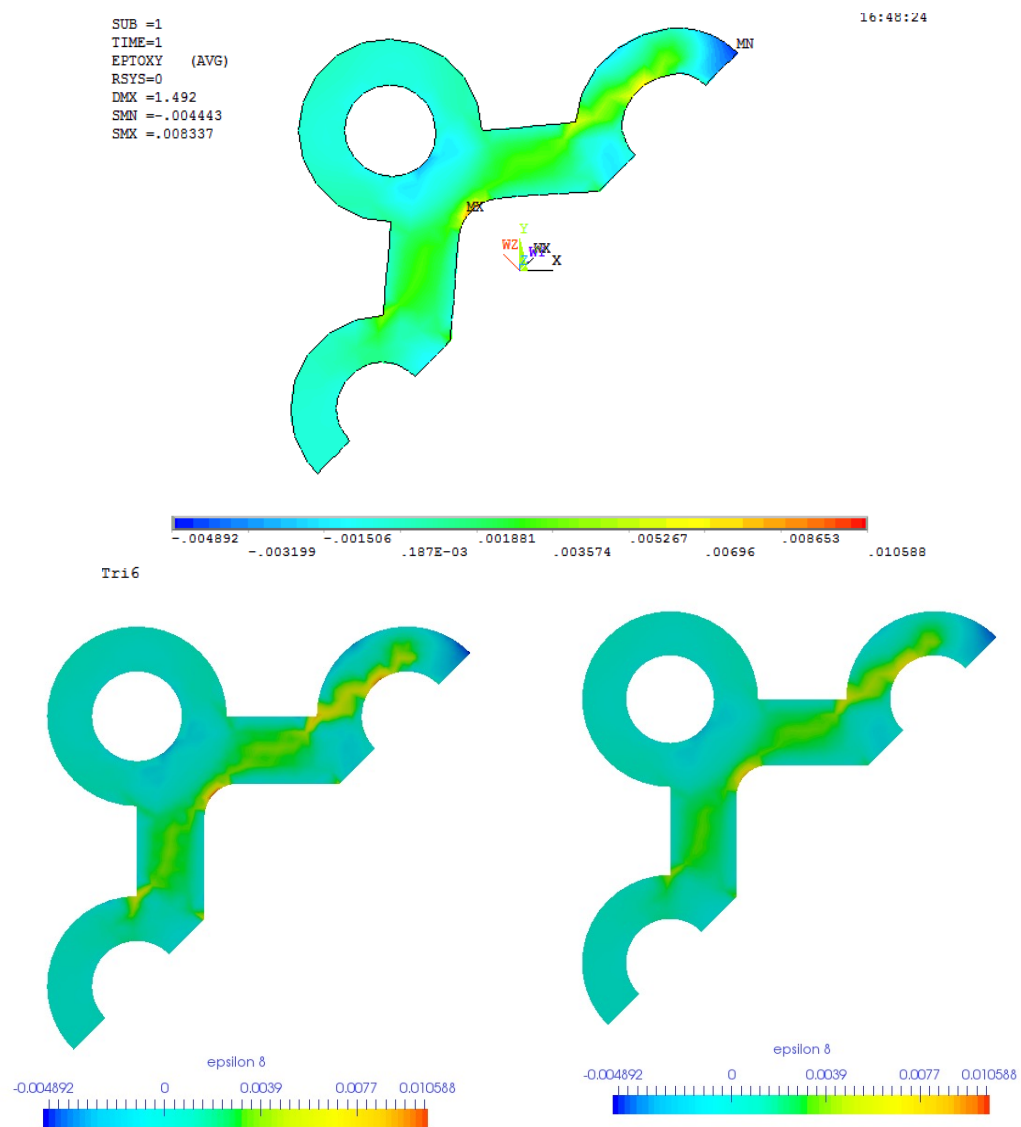


Figure 3.24: Mesh with Tri6, upper: contour plot of ϵ_{xy} in ANSYS; lower left: contour plot of ϵ_{xy} calculated without stress recovery in AMfe; lower right: contour plot of ϵ_{xy} calculated with stress recovery in AMfe

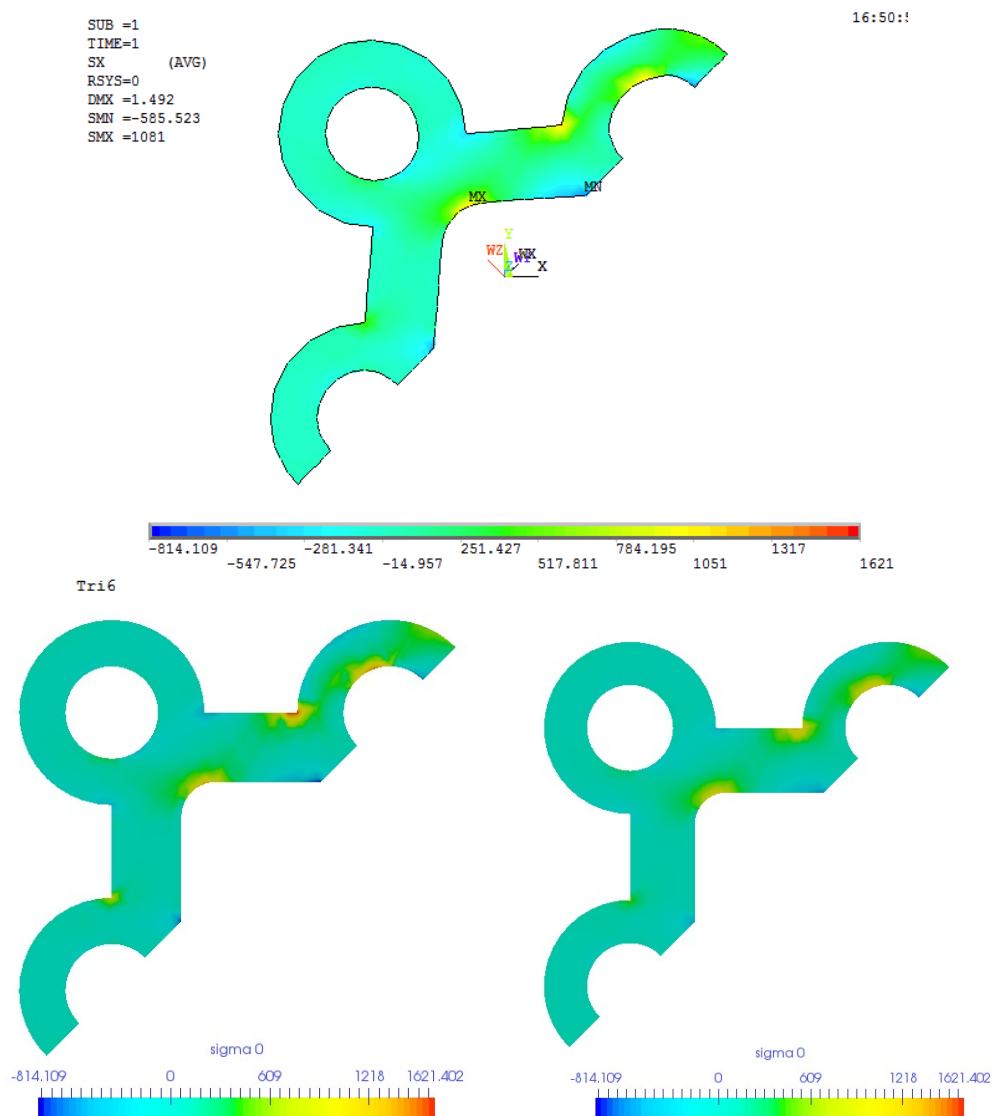


Figure 3.25: Mesh with Tri6, upper: contour plot of σ_{xx} in ANSYS; lower left: contour plot of σ_{xx} calculated without stress recovery in AMfe; lower right: contour plot of σ_{xx} calculated with stress recovery in AMfe

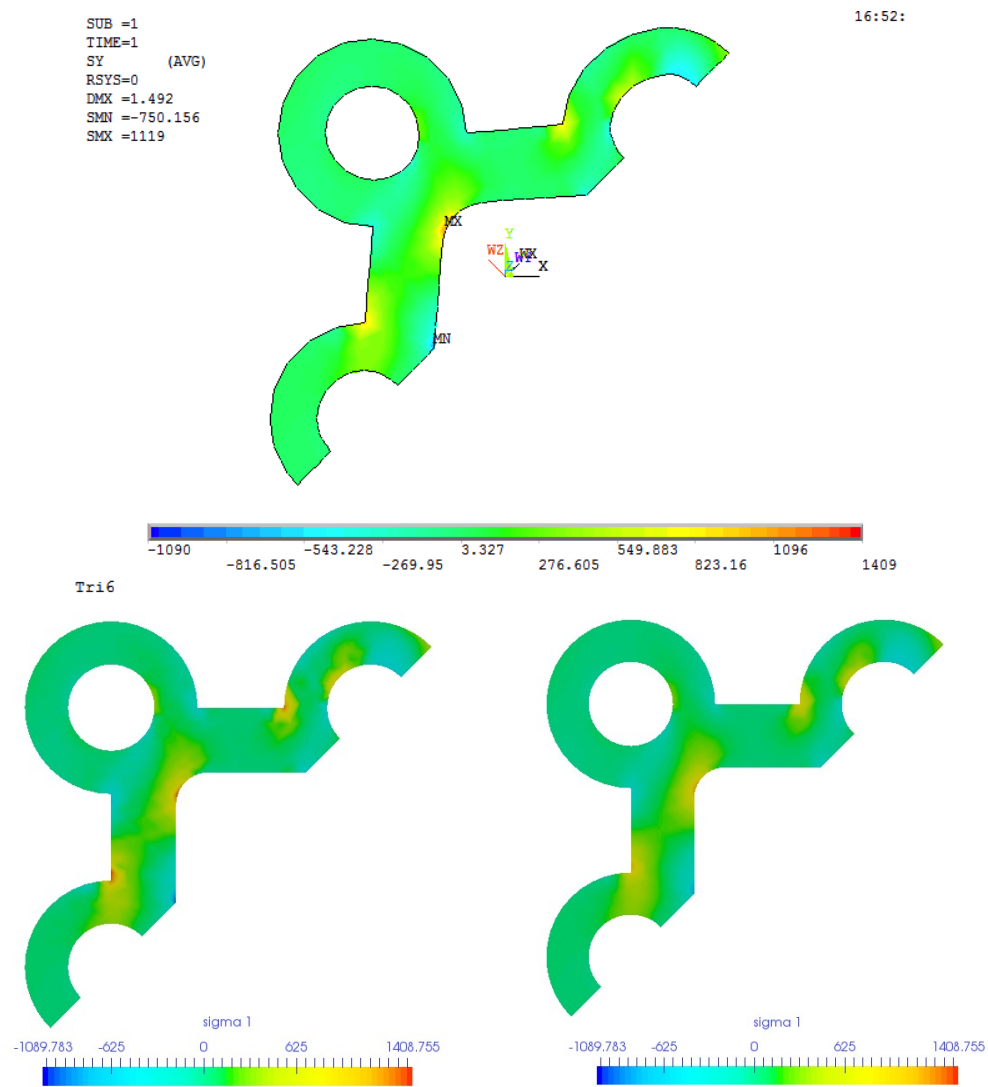


Figure 3.26: Mesh with Tri6, upper: contour plot of σ_{yy} in ANSYS; lower left: contour plot of σ_{yy} calculated without stress recovery in AMfe; lower right: contour plot of σ_{yy} calculated with stress recovery in AMfe

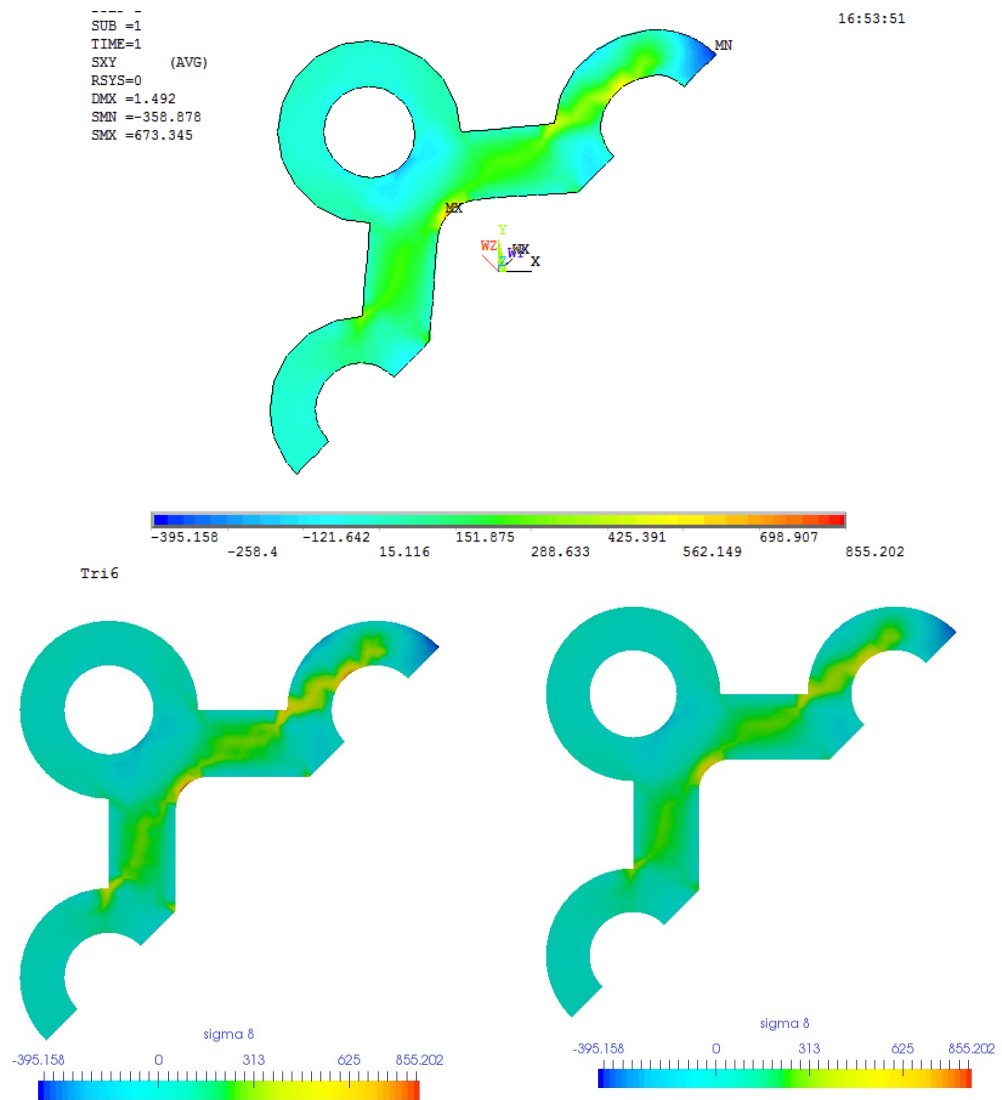


Figure 3.27: Mesh with Tri6, upper: contour plot of σ_{xy} in ANSYS; lower left: contour plot of σ_{xy} calculated without stress recovery in AMfe; lower right: contour plot of σ_{xy} calculated with stress recovery in AMfe

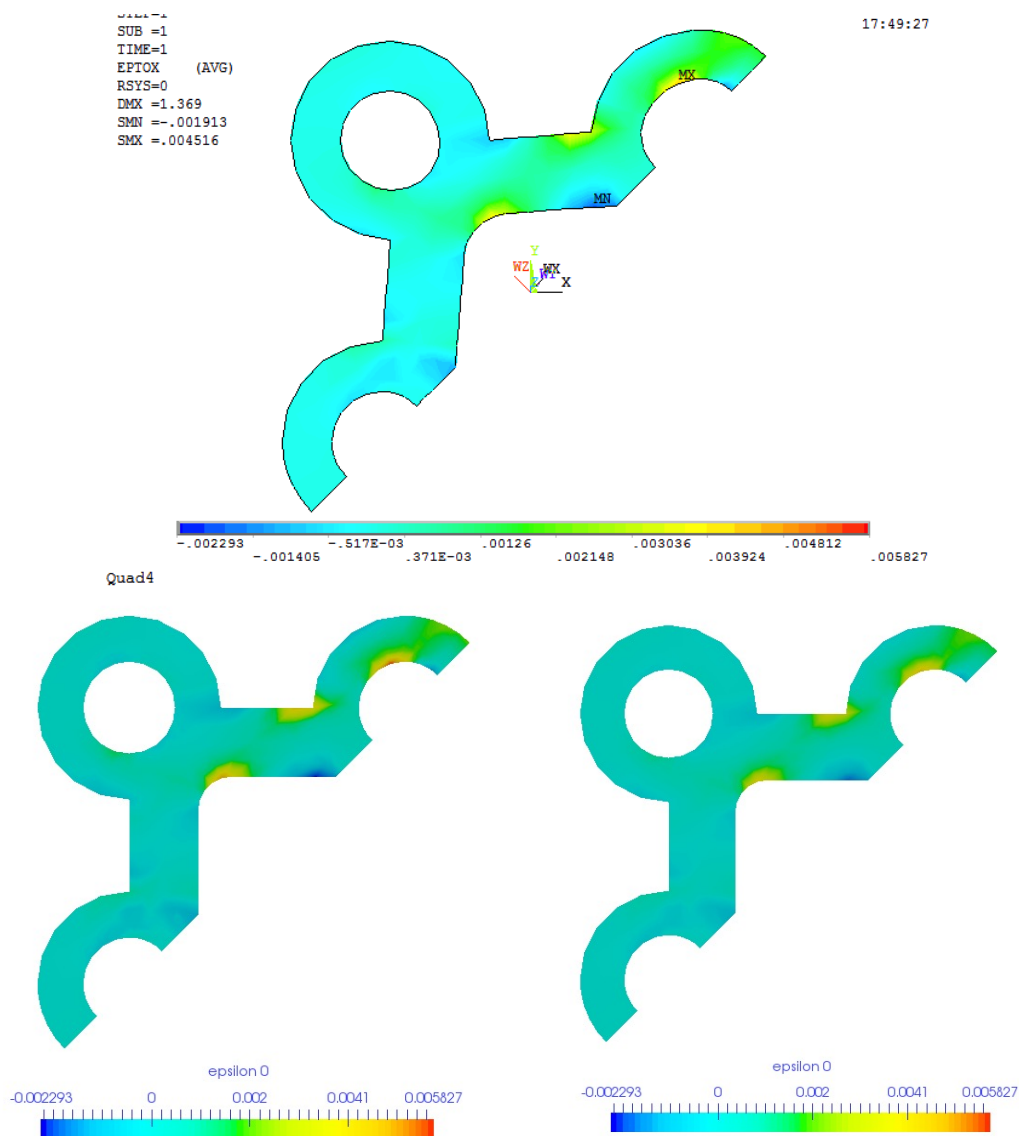


Figure 3.28: Mesh with Quad4, upper: contour plot of ϵ_{xx} in ANSYS; lower left: contour plot of ϵ_{xx} calculated without stress recovery in AMfe; lower right: contour plot of ϵ_{xx} calculated with stress recovery in AMfe

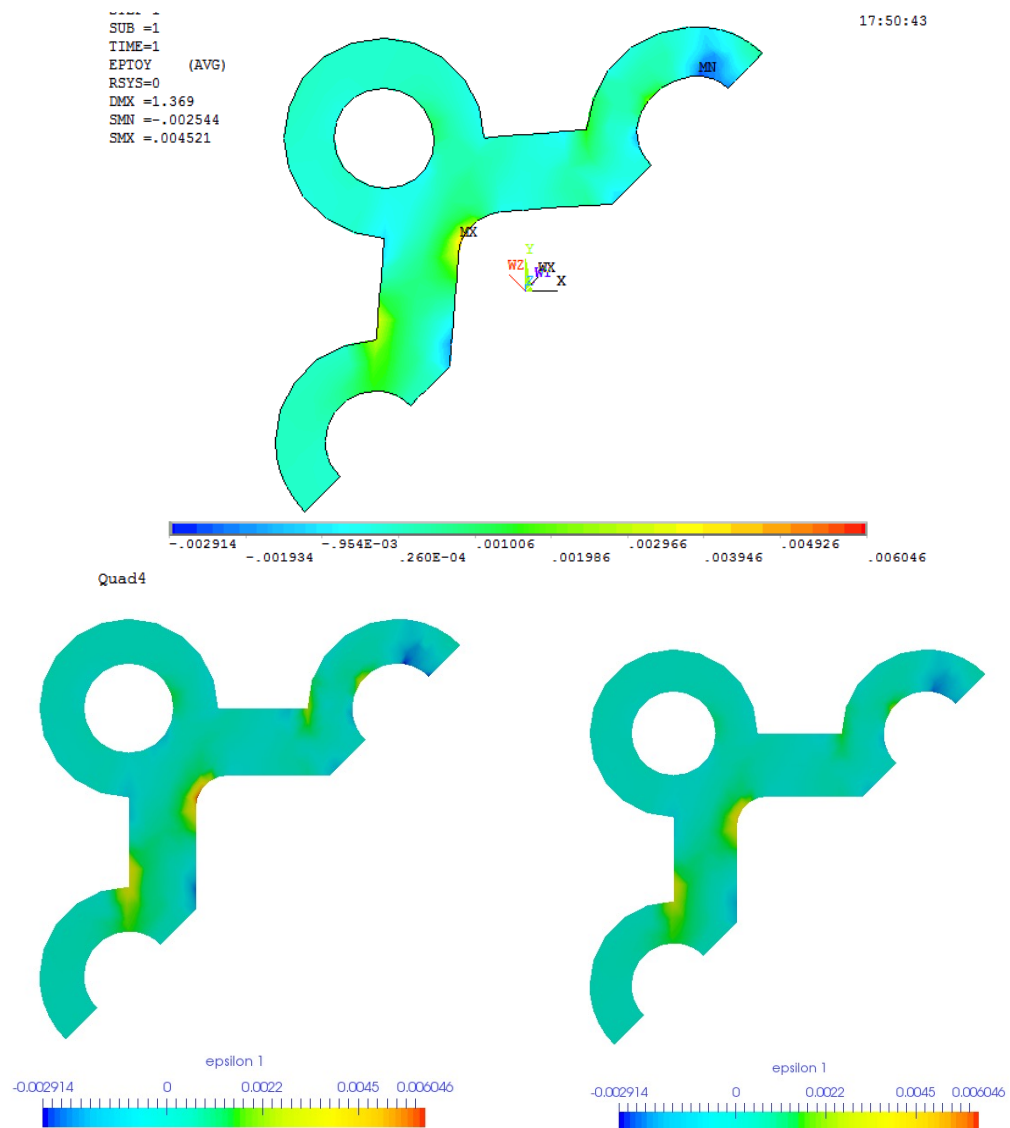


Figure 3.29: Mesh with Quad4, upper: contour plot of ϵ_{yy} in ANSYS; lower left: contour plot of ϵ_{yy} calculated without stress recovery in AMfe; lower right: contour plot of ϵ_{yy} calculated with stress recovery in AMfe

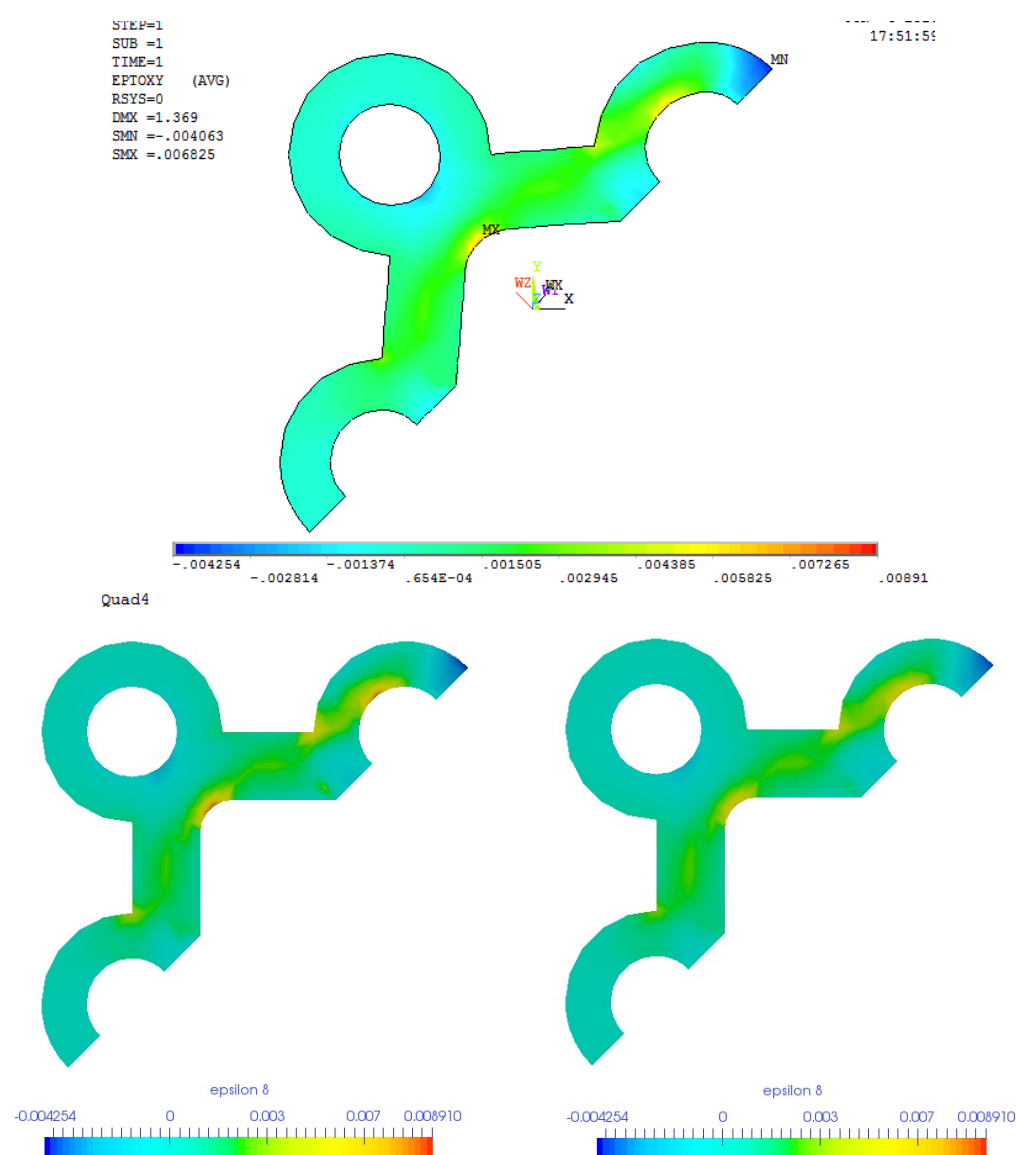


Figure 3.30: Mesh with Quad4, upper: contour plot of ϵ_{xy} in ANSYS; lower left: contour plot of ϵ_{xy} calculated without stress recovery in AMfe; lower right: contour plot of ϵ_{xy} calculated with stress recovery in AMfe

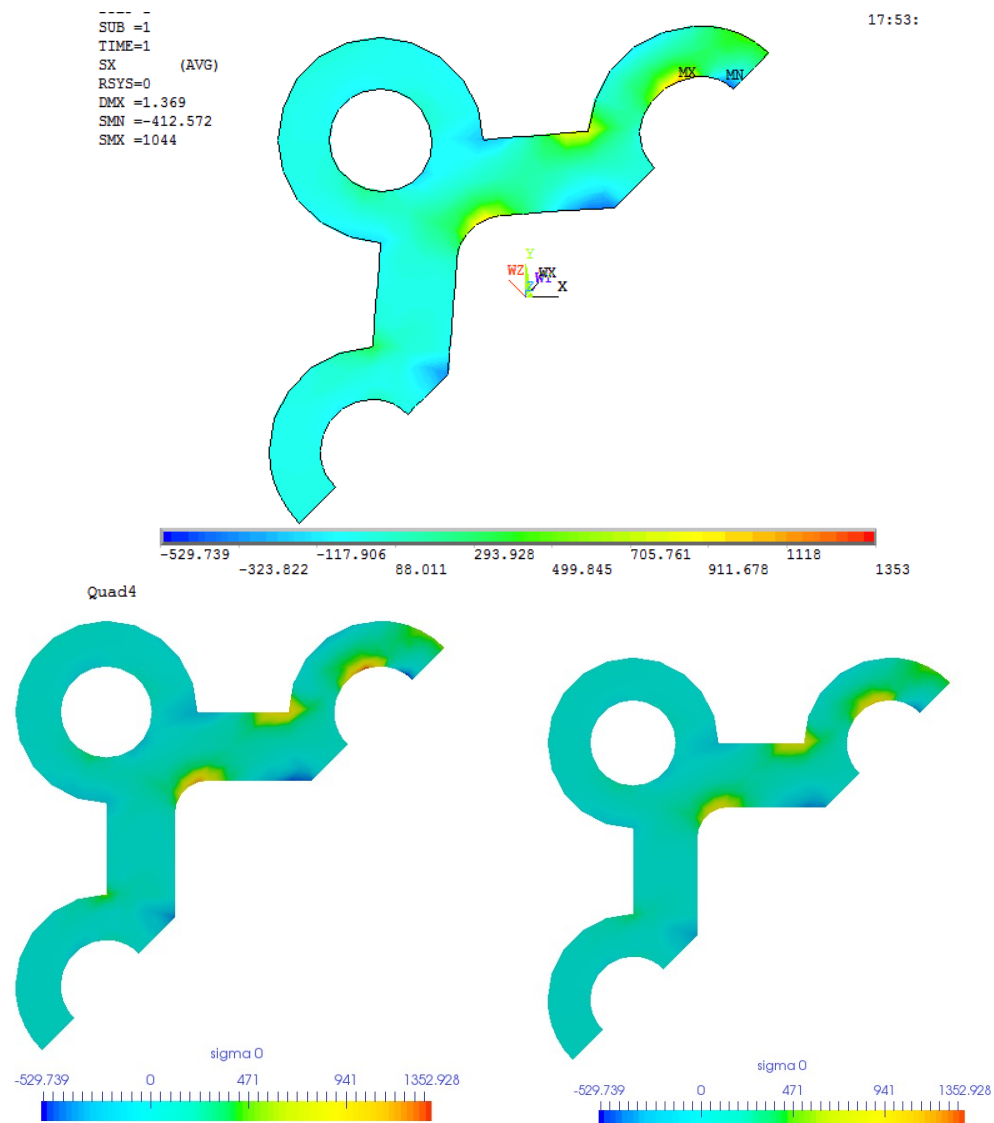


Figure 3.31: Mesh with Quad4, upper: contour plot of σ_{xx} in ANSYS; lower left: contour plot of σ_{xx} calculated without stress recovery in AMfe; lower right: contour plot of σ_{xx} calculated with stress recovery in AMfe

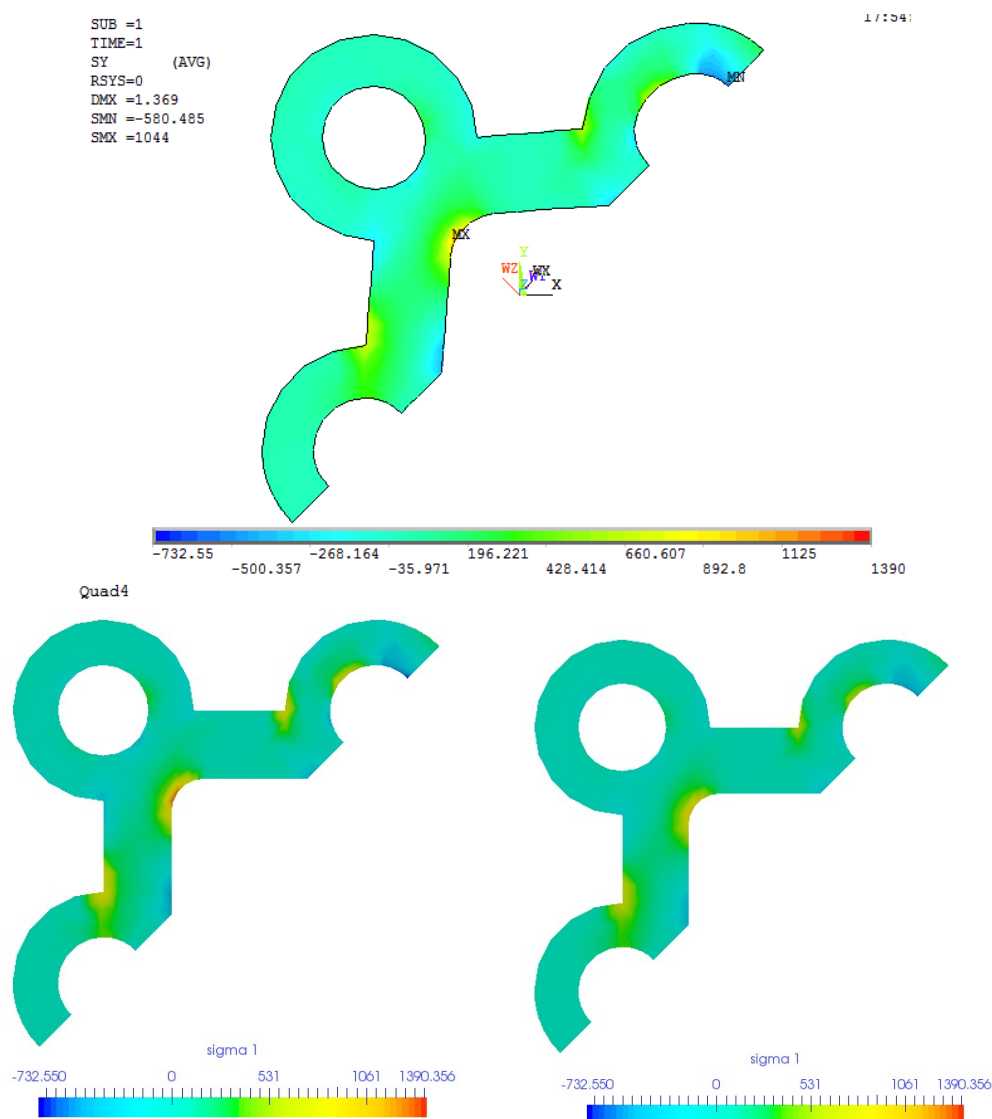


Figure 3.32: Mesh with Quad4, upper: contour plot of σ_{yy} in ANSYS; lower left: contour plot of σ_{yy} calculated without stress recovery in AMfe; lower right: contour plot of σ_{yy} calculated with stress recovery in AMfe

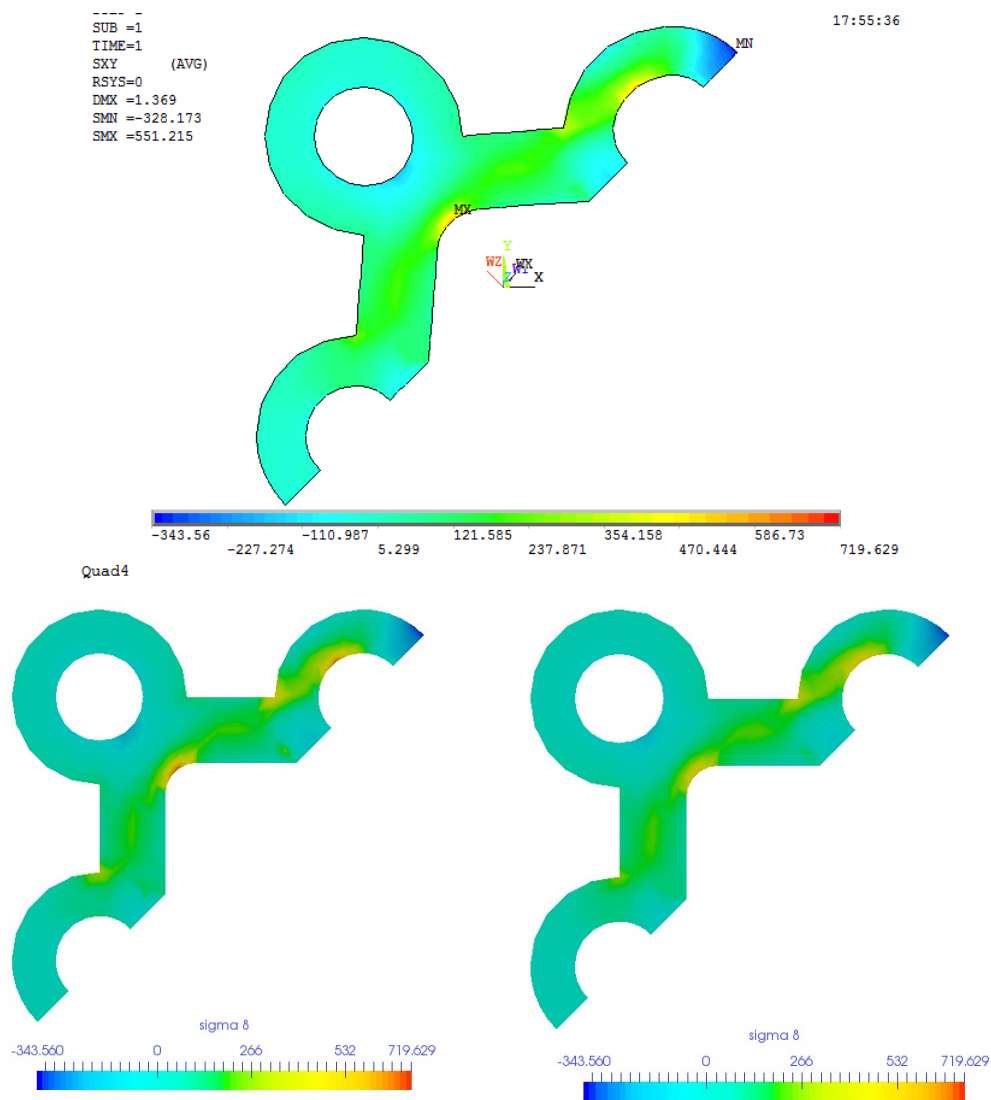


Figure 3.33: Mesh with Quad4, upper: contour plot of σ_{xy} in ANSYS; lower left: contour plot of σ_{xy} calculated without stress recovery in AMfe; lower right: contour plot of σ_{xy} calculated with stress recovery in AMfe

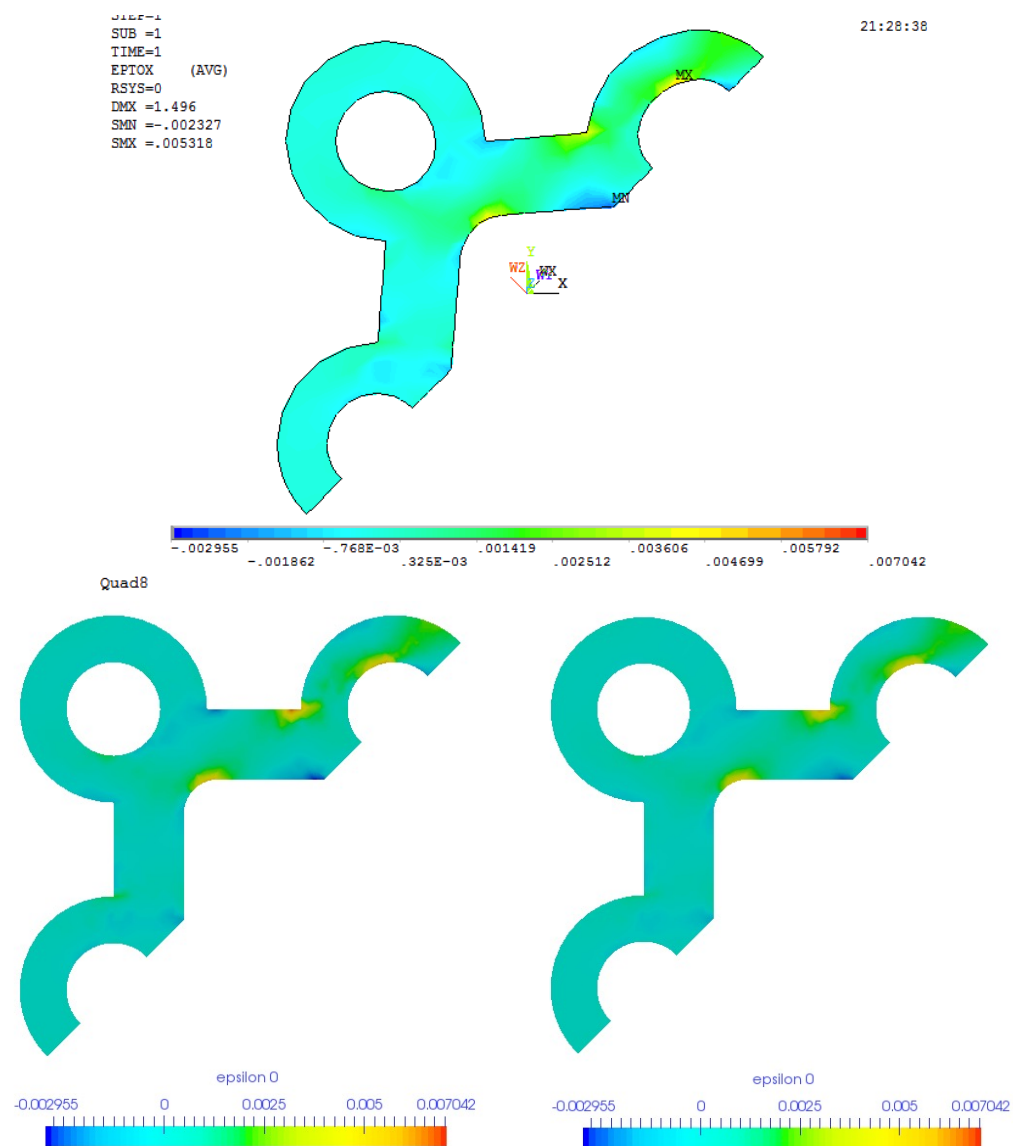


Figure 3.34: Mesh with Quad8, upper: contour plot of ϵ_{xx} in ANSYS; lower left: contour plot of ϵ_{xx} calculated without stress recovery in AMfe; lower right: contour plot of ϵ_{xx} calculated with stress recovery in AMfe

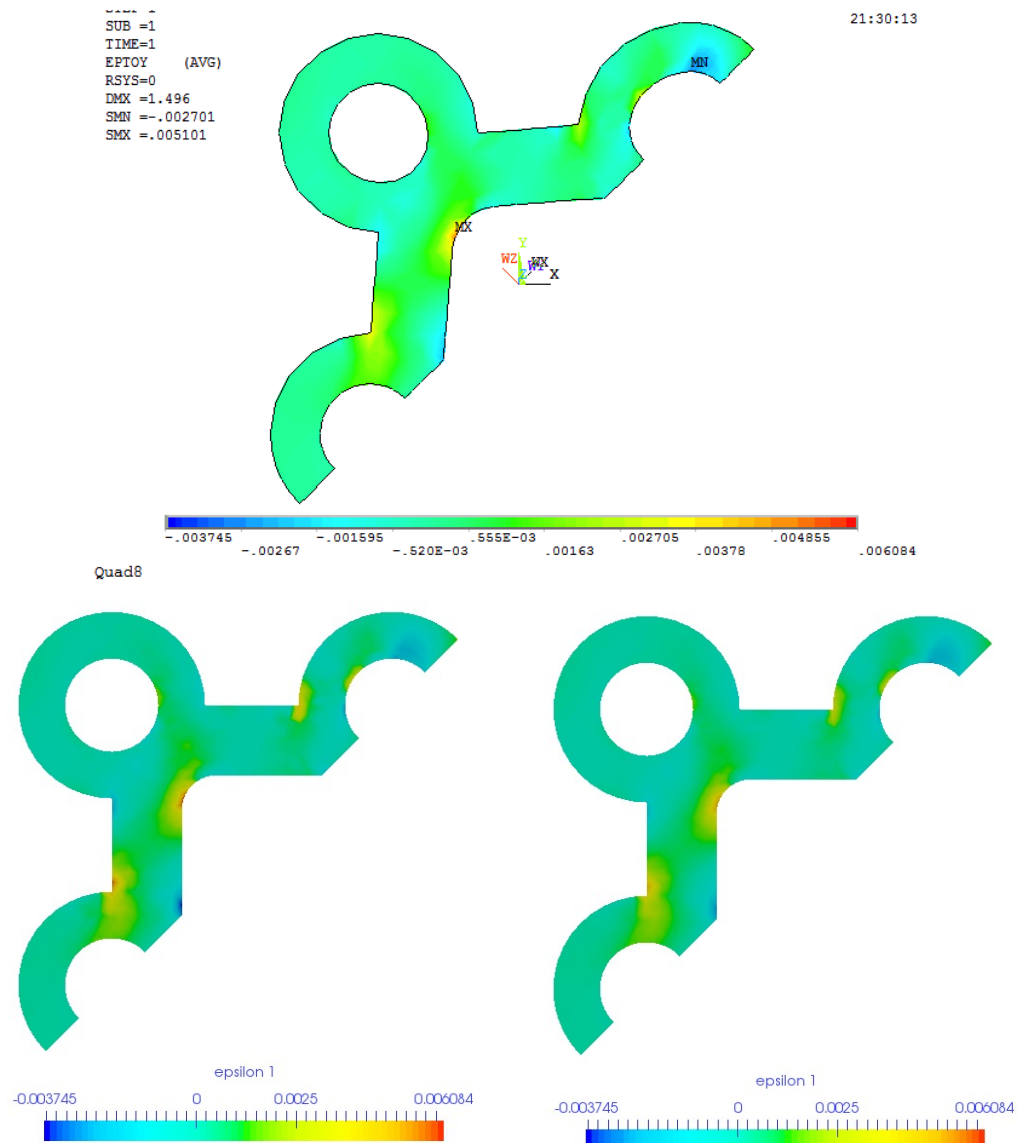


Figure 3.35: Mesh with Quad8, upper: contour plot of ϵ_{yy} in ANSYS; lower left: contour plot of ϵ_{yy} calculated without stress recovery in AMfe; lower right: contour plot of ϵ_{yy} calculated with stress recovery in AMfe

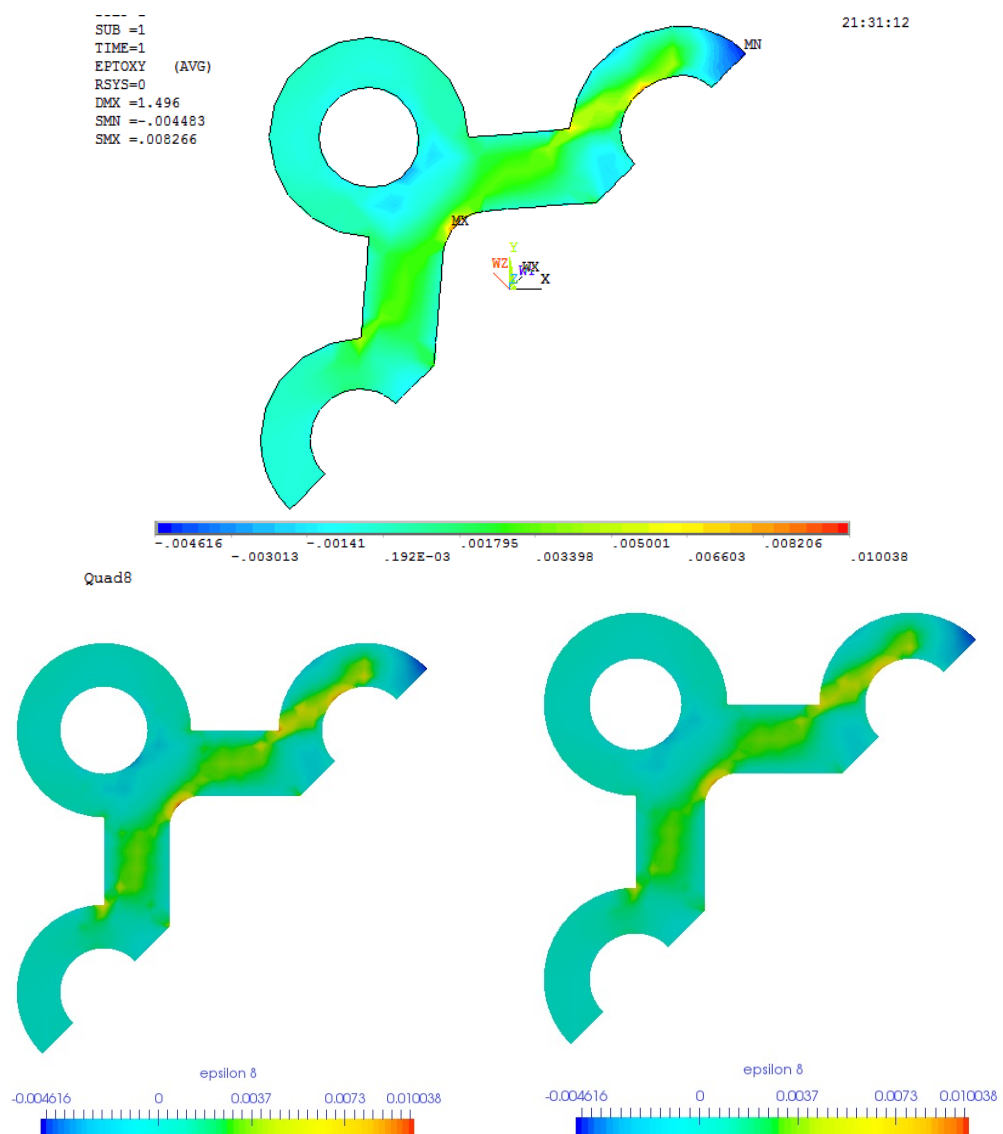


Figure 3.36: Mesh with Quad8, upper: contour plot of ϵ_{xy} in ANSYS; lower left: contour plot of ϵ_{xy} calculated without stress recovery in AMfe; lower right: contour plot of ϵ_{xy} calculated with stress recovery in AMfe

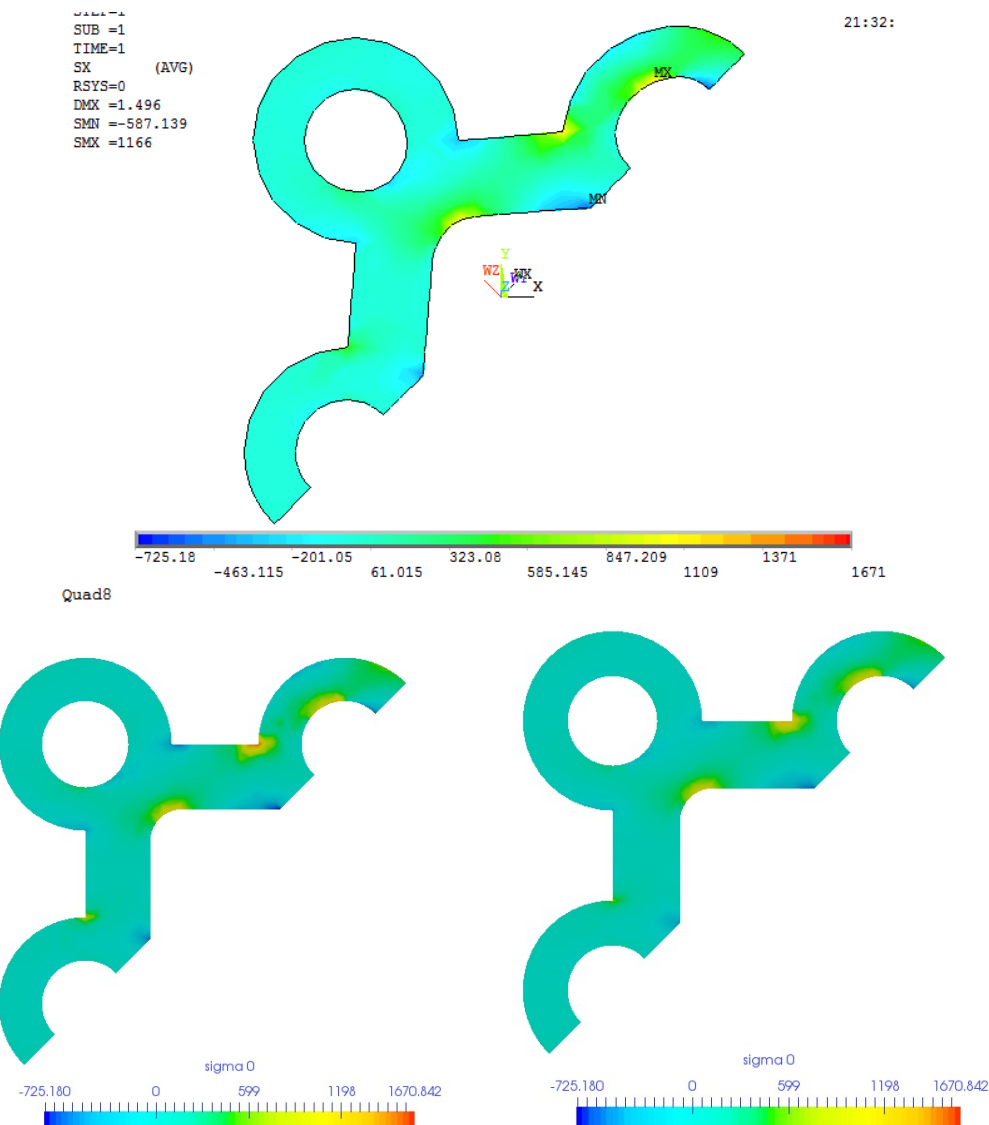


Figure 3.37: Mesh with Quad8, upper: contour plot of σ_{xx} in ANSYS; lower left: contour plot of σ_{xx} calculated without stress recovery in AMfe; lower right: contour plot of σ_{xx} calculated with stress recovery in AMfe

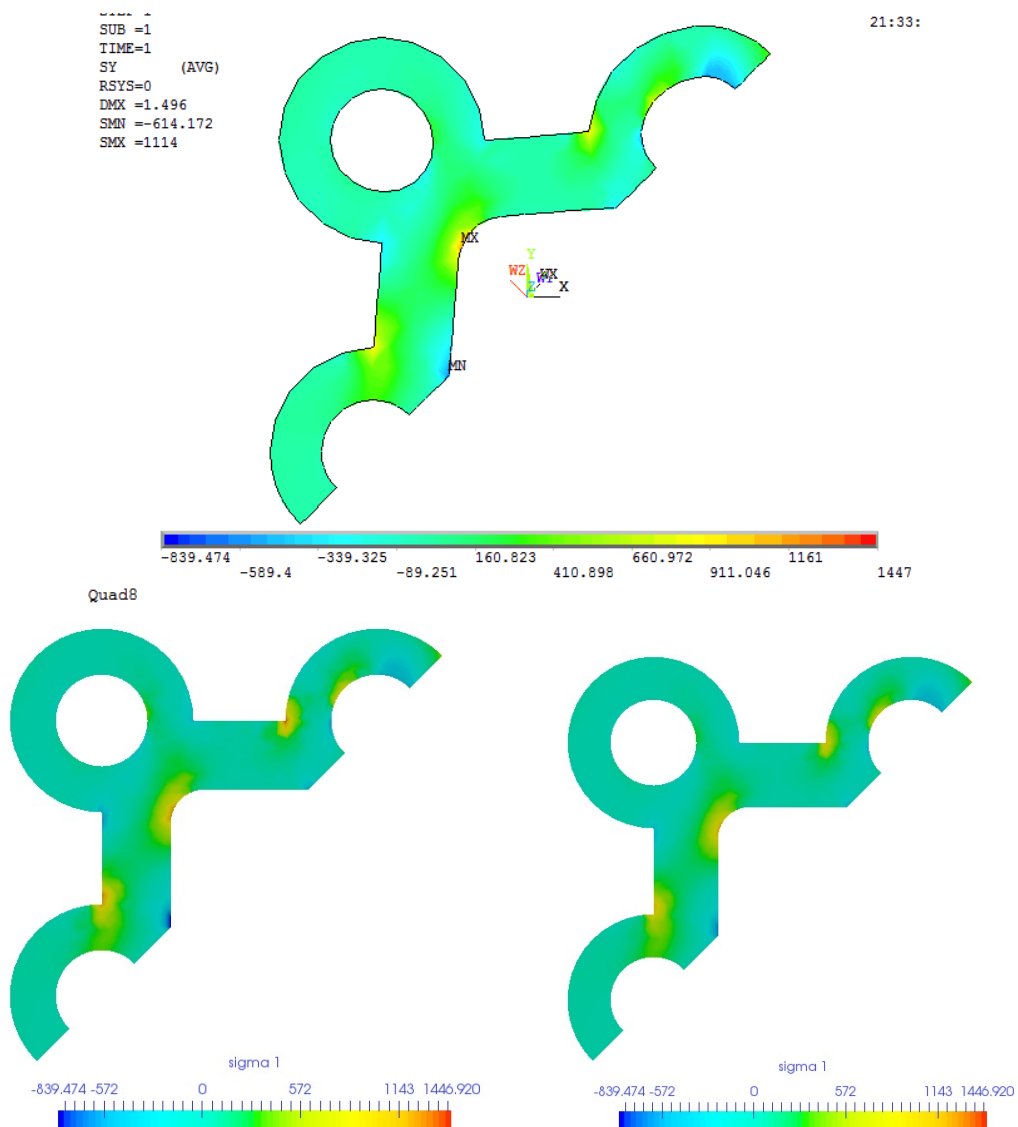


Figure 3.38: Mesh with Quad8, upper: contour plot of σ_{yy} in ANSYS; lower left: contour plot of σ_{yy} calculated without stress recovery in AMfe; lower right: contour plot of σ_{yy} calculated with stress recovery in AMfe

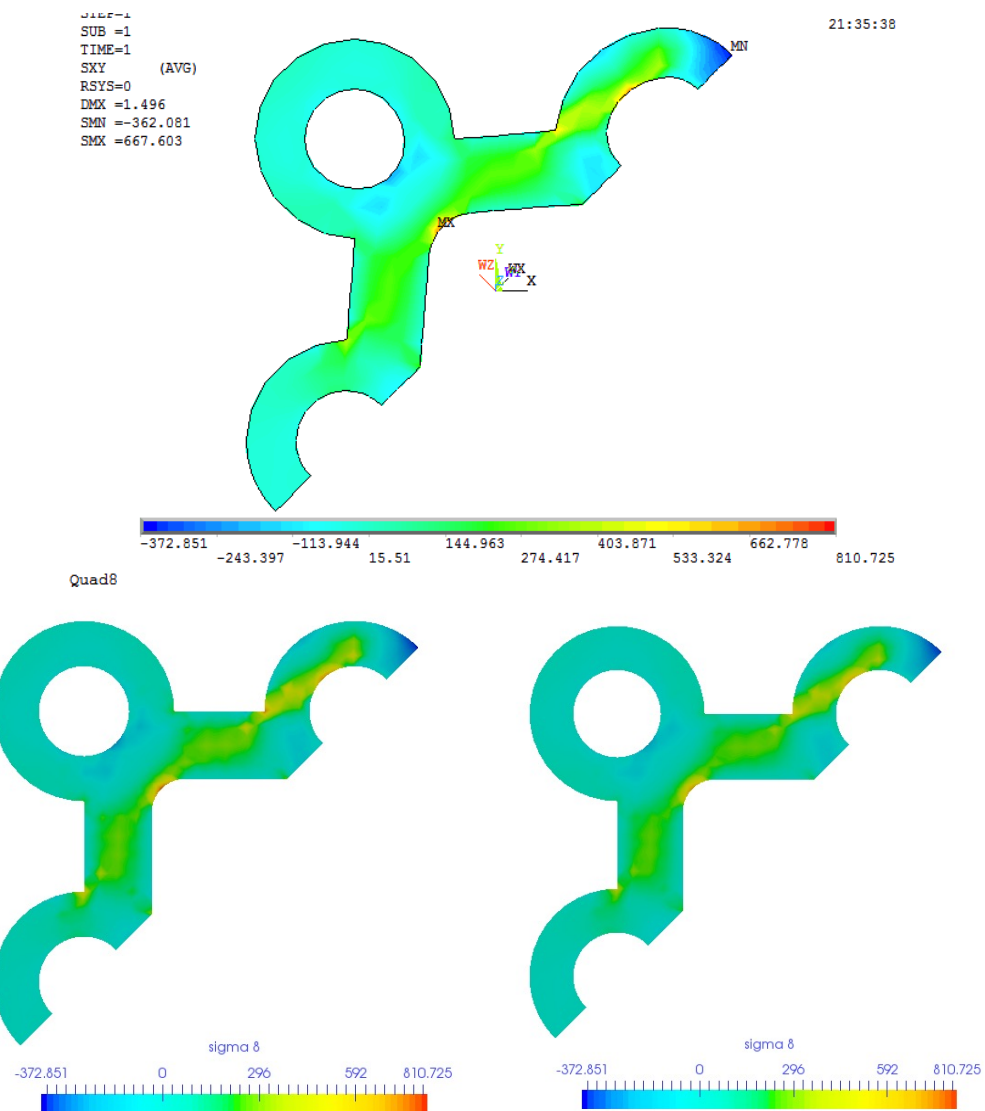


Figure 3.39: Mesh with Quad8, upper: contour plot of σ_{xy} in ANSYS; lower left: contour plot of σ_{xy} calculated without stress recovery in AMfe; lower right: contour plot of σ_{xy} calculated with stress recovery in AMfe

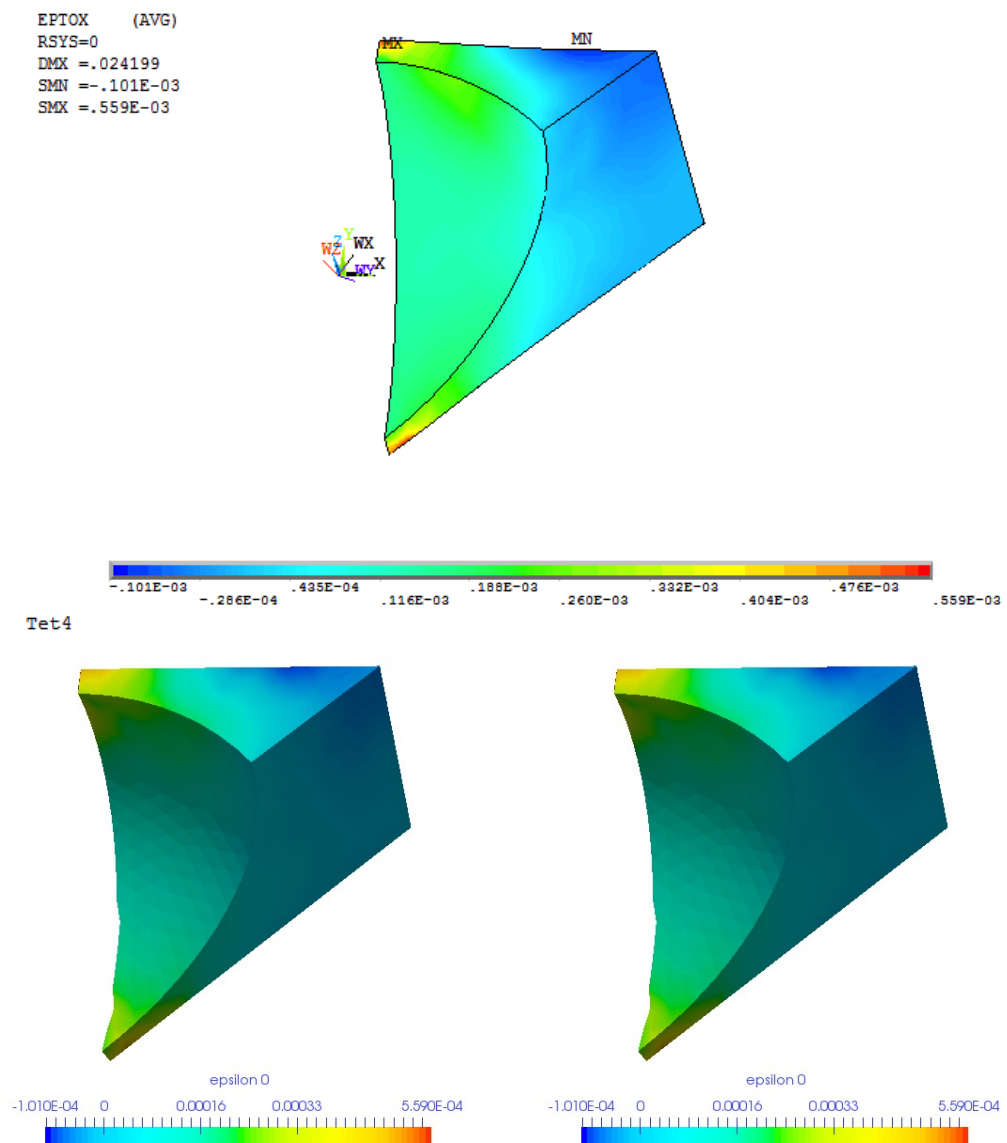


Figure 3.40: Mesh with Tet4, upper: contour plot of ϵ_{xx} in ANSYS; lower left: contour plot of ϵ_{xx} calculated without stress recovery in AMfe; lower right: contour plot of ϵ_{xx} calculated with stress recovery in AMfe

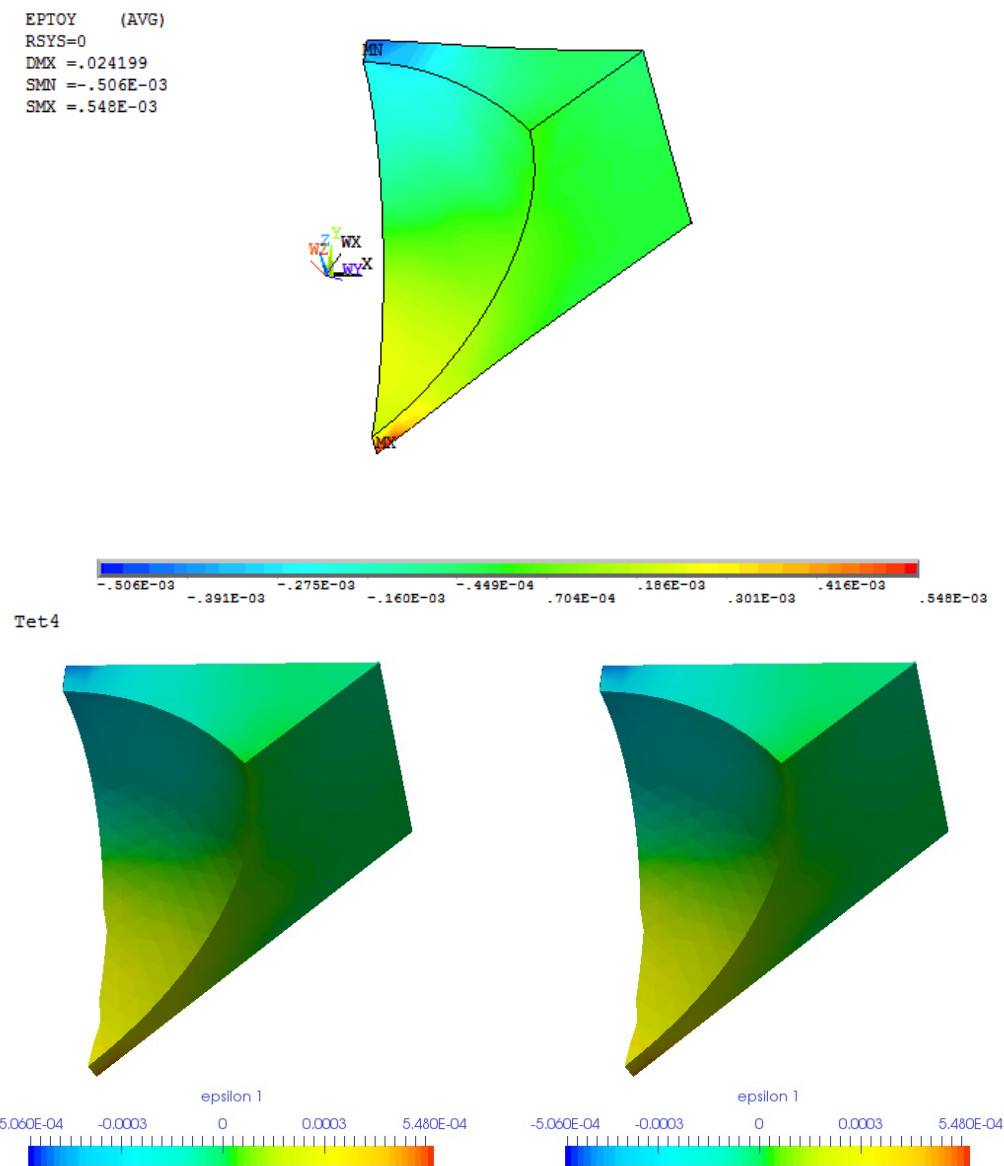


Figure 3.41: Mesh with Tet4, upper: contour plot of ϵ_{yy} in ANSYS; lower left: contour plot of ϵ_{yy} calculated without stress recovery in AMfe; lower right: contour plot of ϵ_{yy} calculated with stress recovery in AMfe

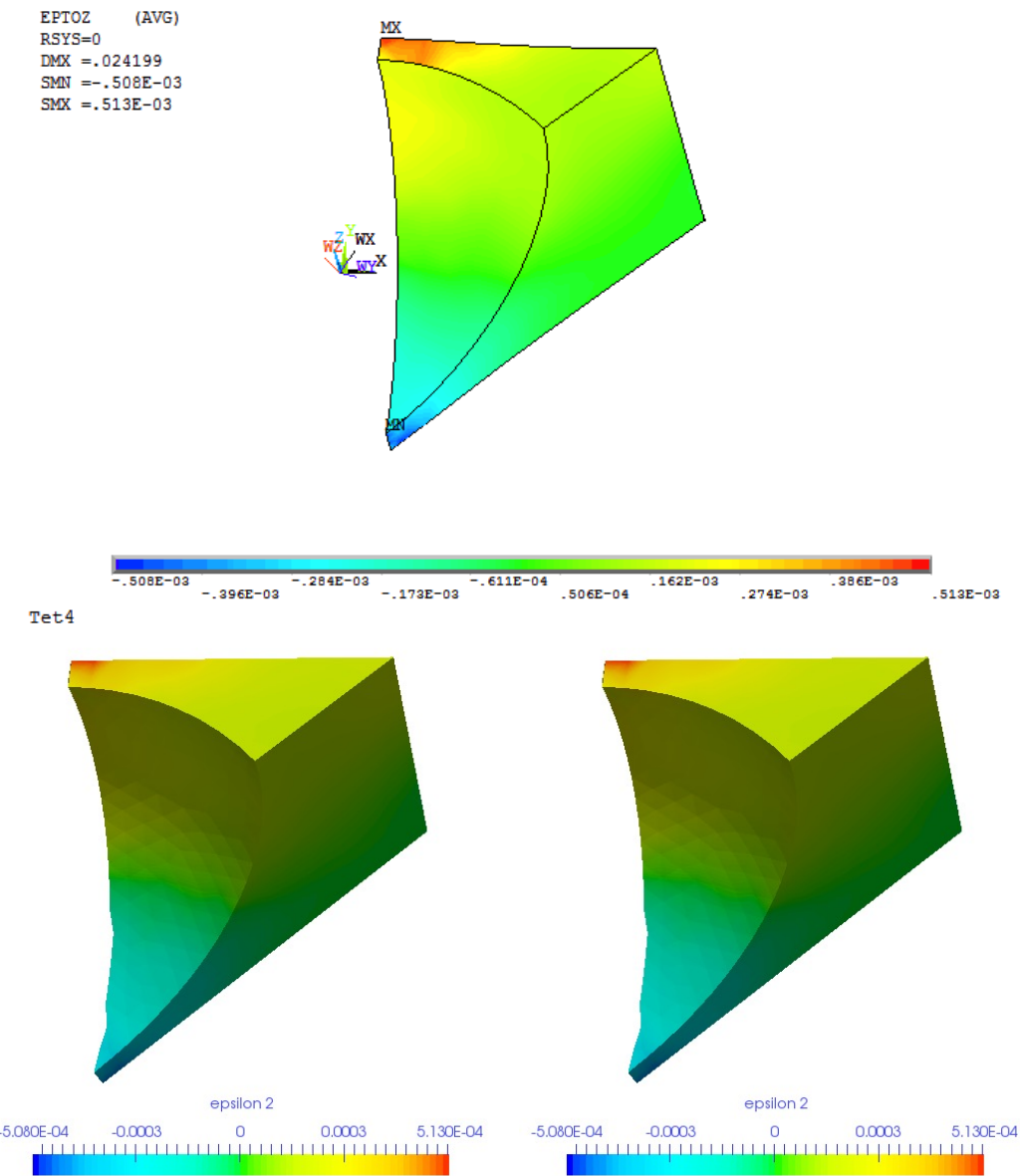


Figure 3.42: Mesh with Tet4, upper: contour plot of ϵ_{zz} in ANSYS; lower left: contour plot of ϵ_{zz} calculated without stress recovery in AMfe; lower right: contour plot of ϵ_{zz} calculated with stress recovery in AMfe

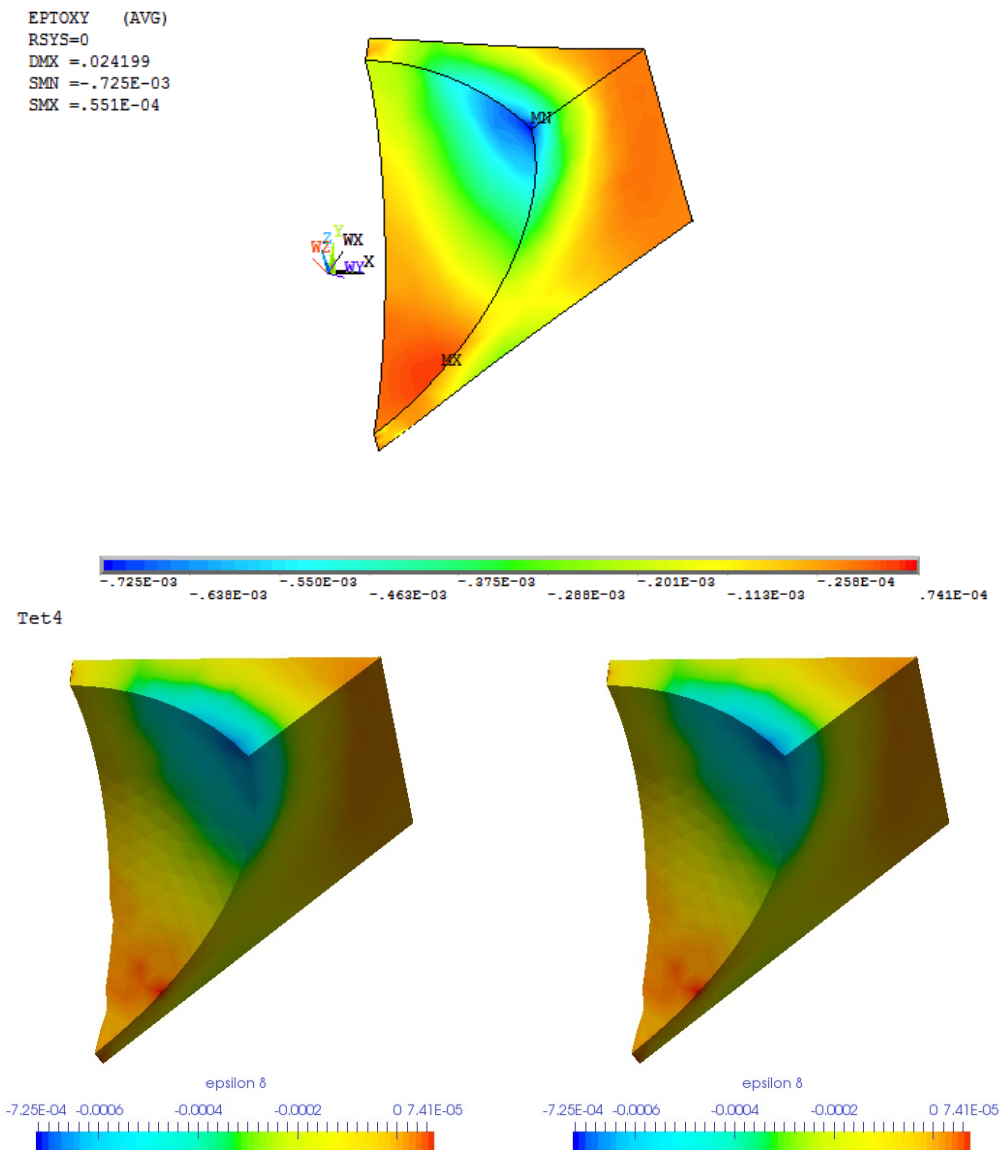


Figure 3.43: Mesh with Tet4, upper: contour plot of ϵ_{xy} in ANSYS; lower left: contour plot of ϵ_{xy} calculated without stress recovery in AMfe; lower right: contour plot of ϵ_{xy} calculated with stress recovery in AMfe

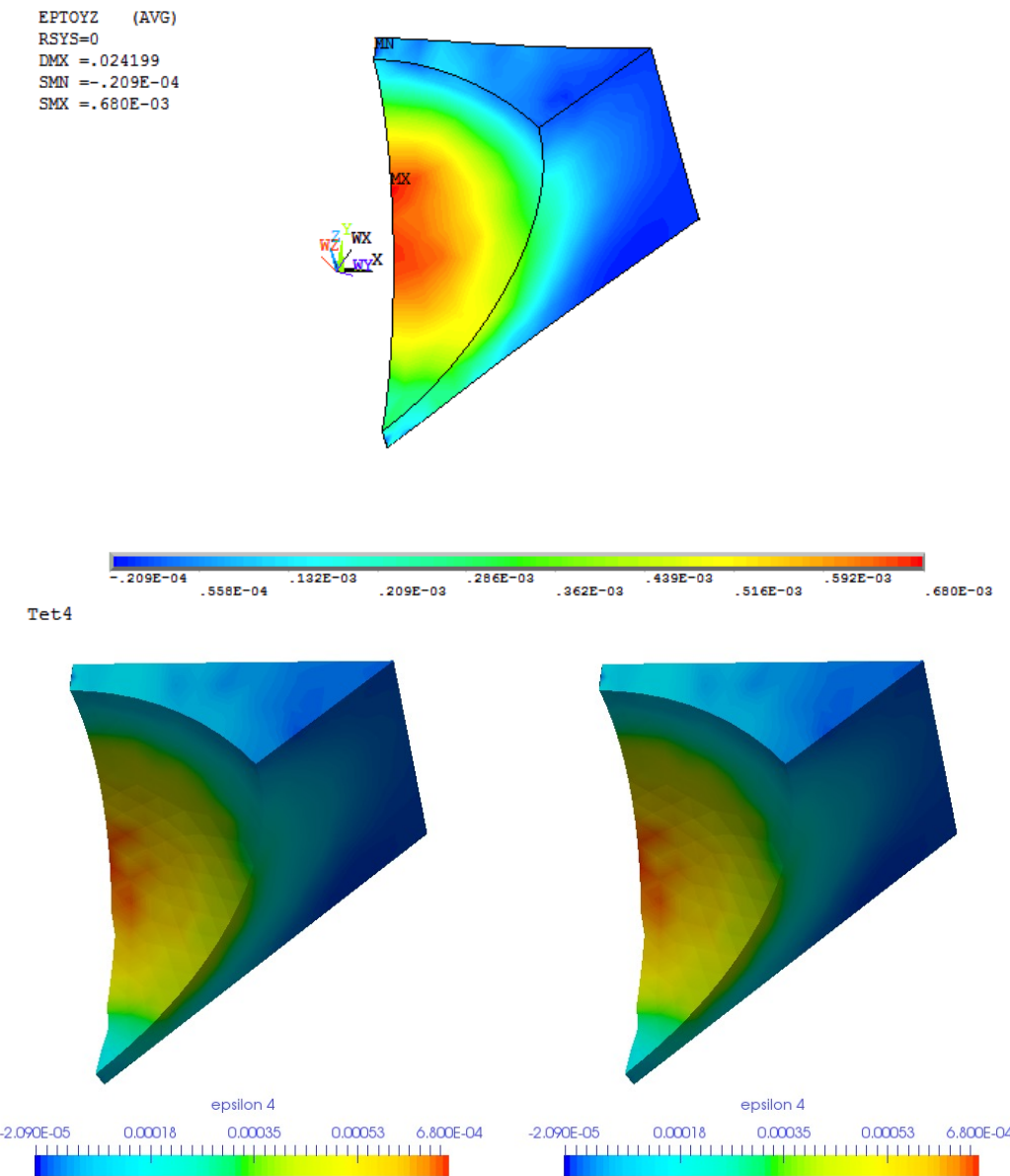


Figure 3.44: Mesh with Tet4, upper: contour plot of ϵ_{yz} in ANSYS; lower left: contour plot of ϵ_{yz} calculated without stress recovery in AMfe; lower right: contour plot of ϵ_{yz} calculated with stress recovery in AMfe

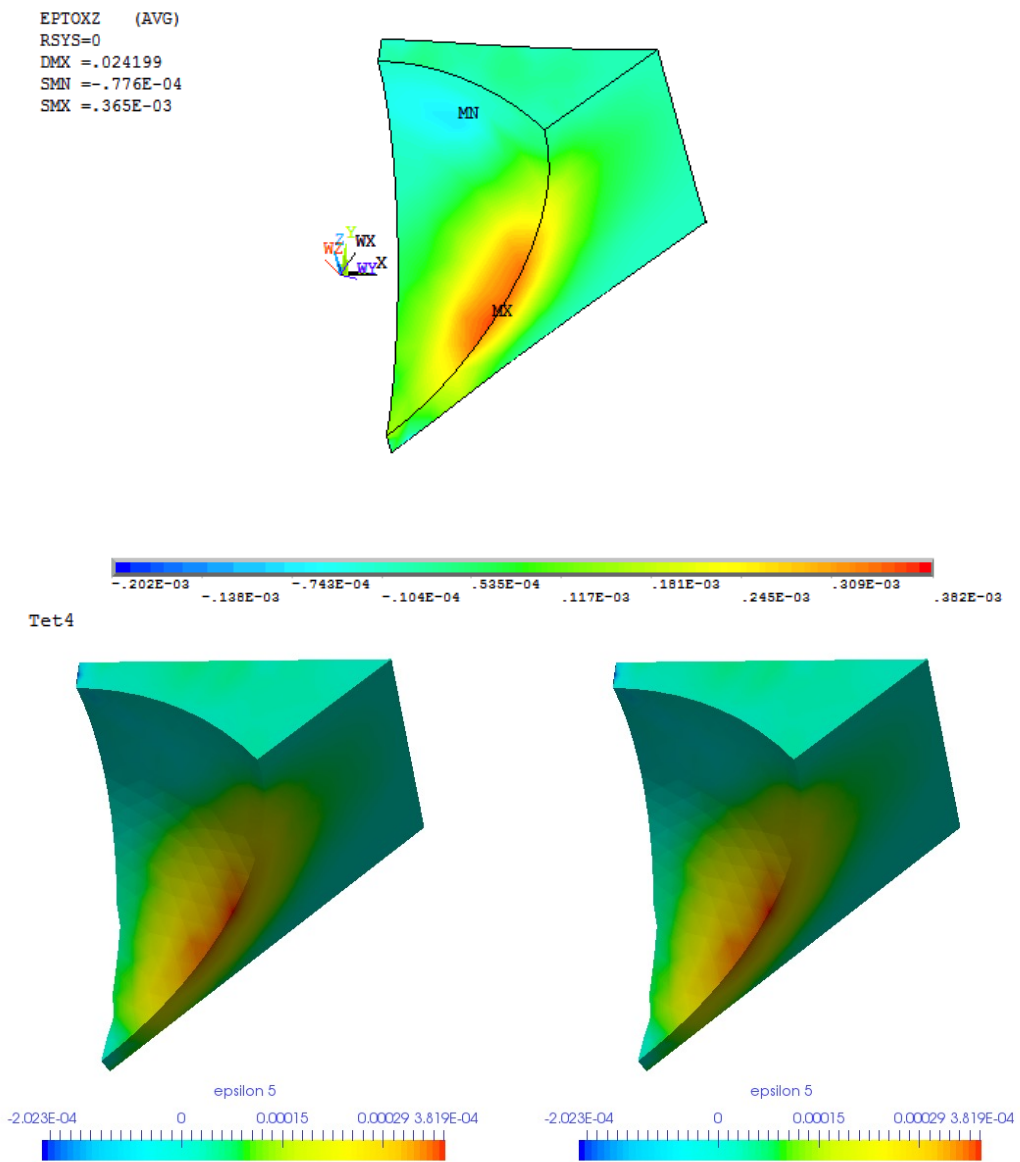


Figure 3.45: Mesh with Tet4, upper: contour plot of ϵ_{xz} in ANSYS; lower left: contour plot of ϵ_{xz} calculated without stress recovery in AMfe; lower right: contour plot of ϵ_{xz} calculated with stress recovery in AMfe

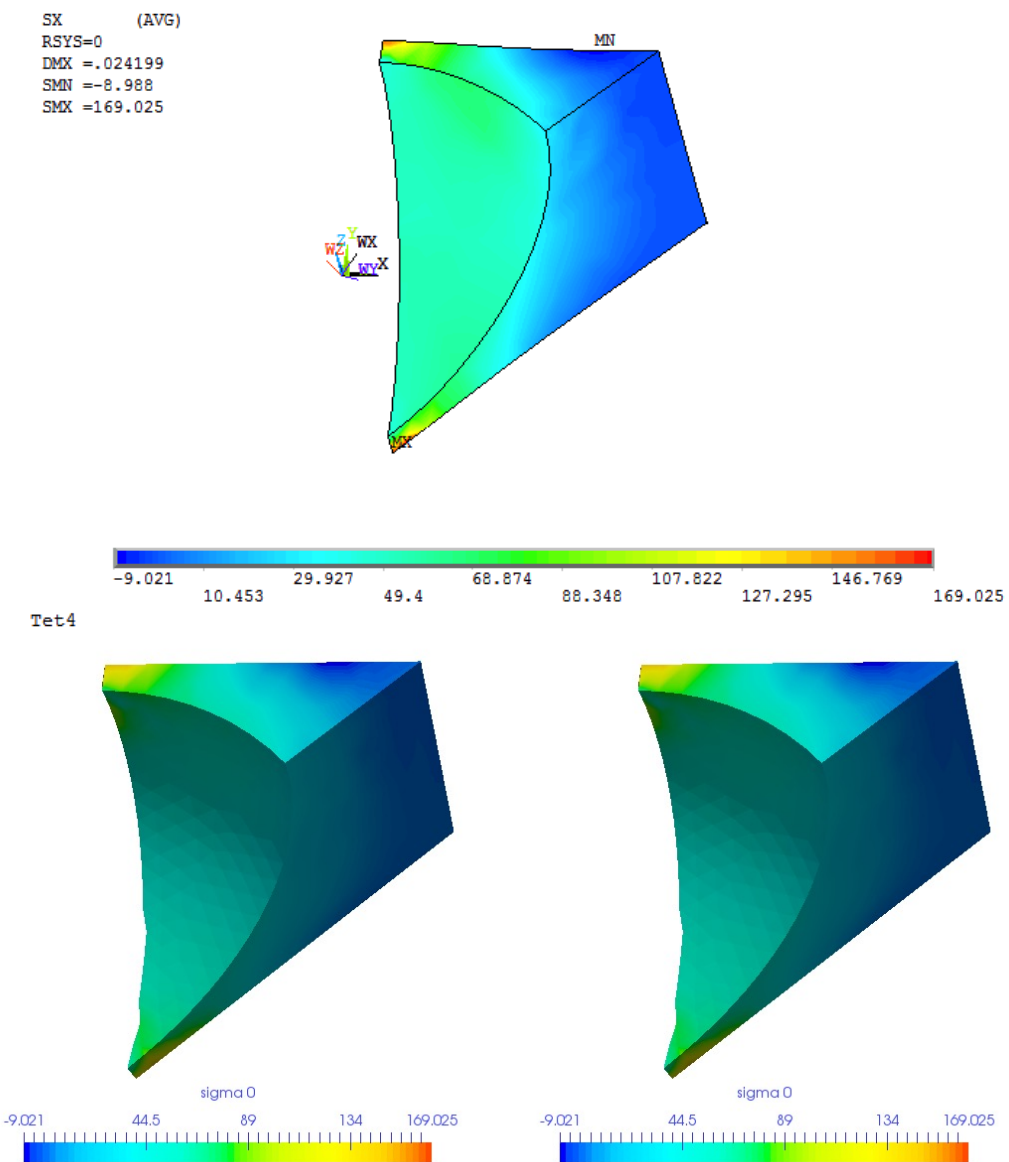


Figure 3.46: Mesh with Tet4, upper: contour plot of σ_{xx} in ANSYS; lower left: contour plot of σ_{xx} calculated without stress recovery in AMfe; lower right: contour plot of σ_{xx} calculated with stress recovery in AMfe

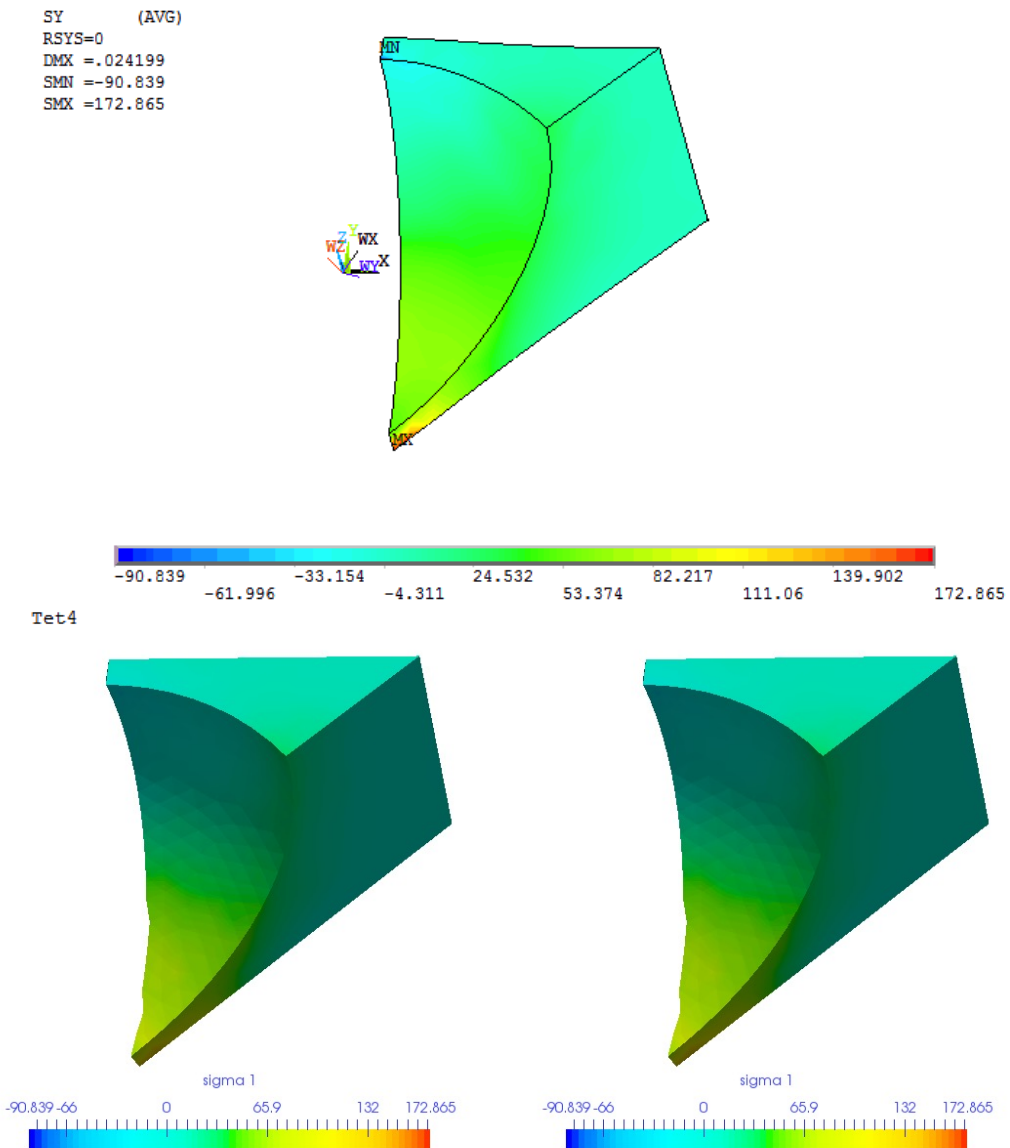


Figure 3.47: Mesh with Tet4, upper: contour plot of σ_{yy} in ANSYS; lower left: contour plot of σ_{yy} calculated without stress recovery in AMfe; lower right: contour plot of σ_{yy} calculated with stress recovery in AMfe

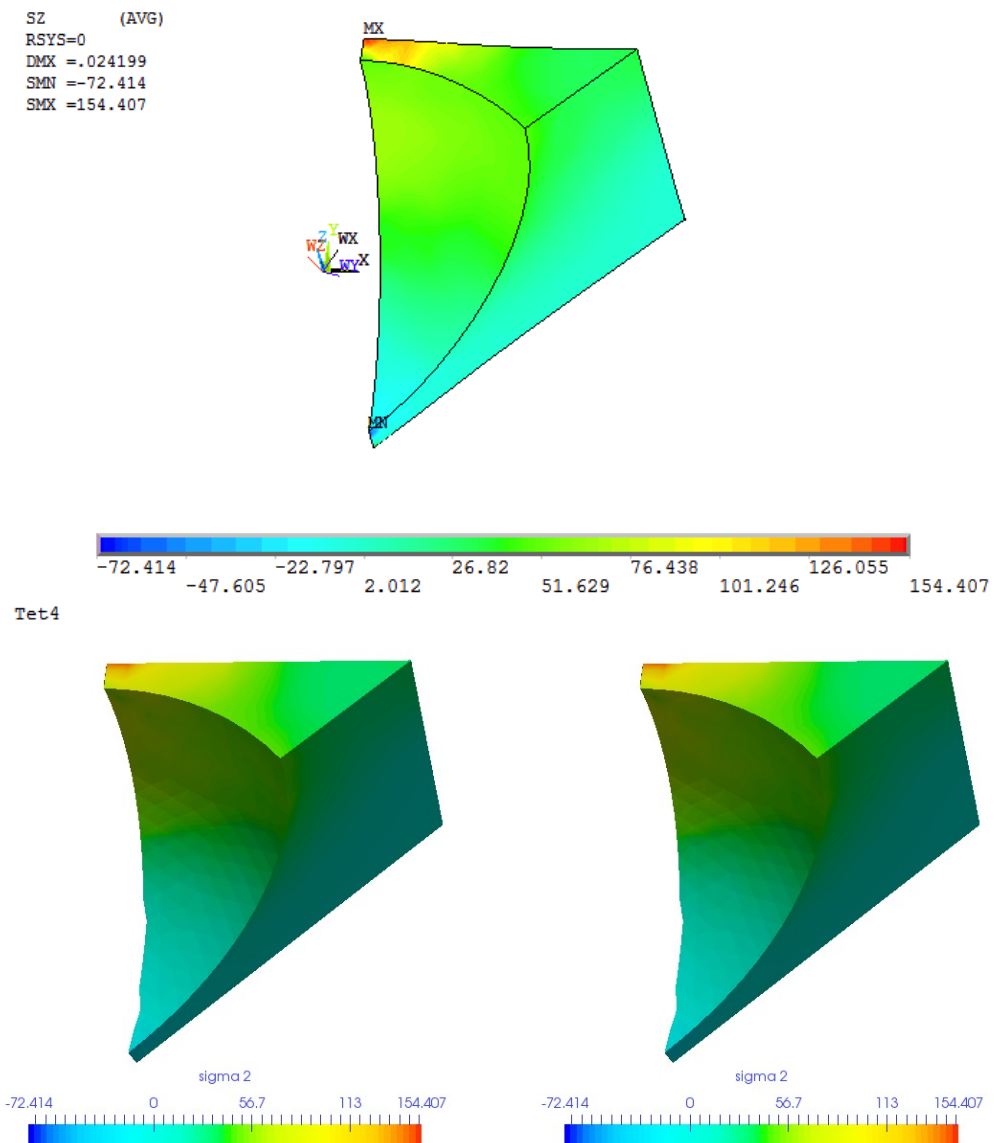


Figure 3.48: Mesh with Tet4, upper: contour plot of σ_{zz} in ANSYS; lower left: contour plot of σ_{zz} calculated without stress recovery in AMfe; lower right: contour plot of σ_{zz} calculated with stress recovery in AMfe

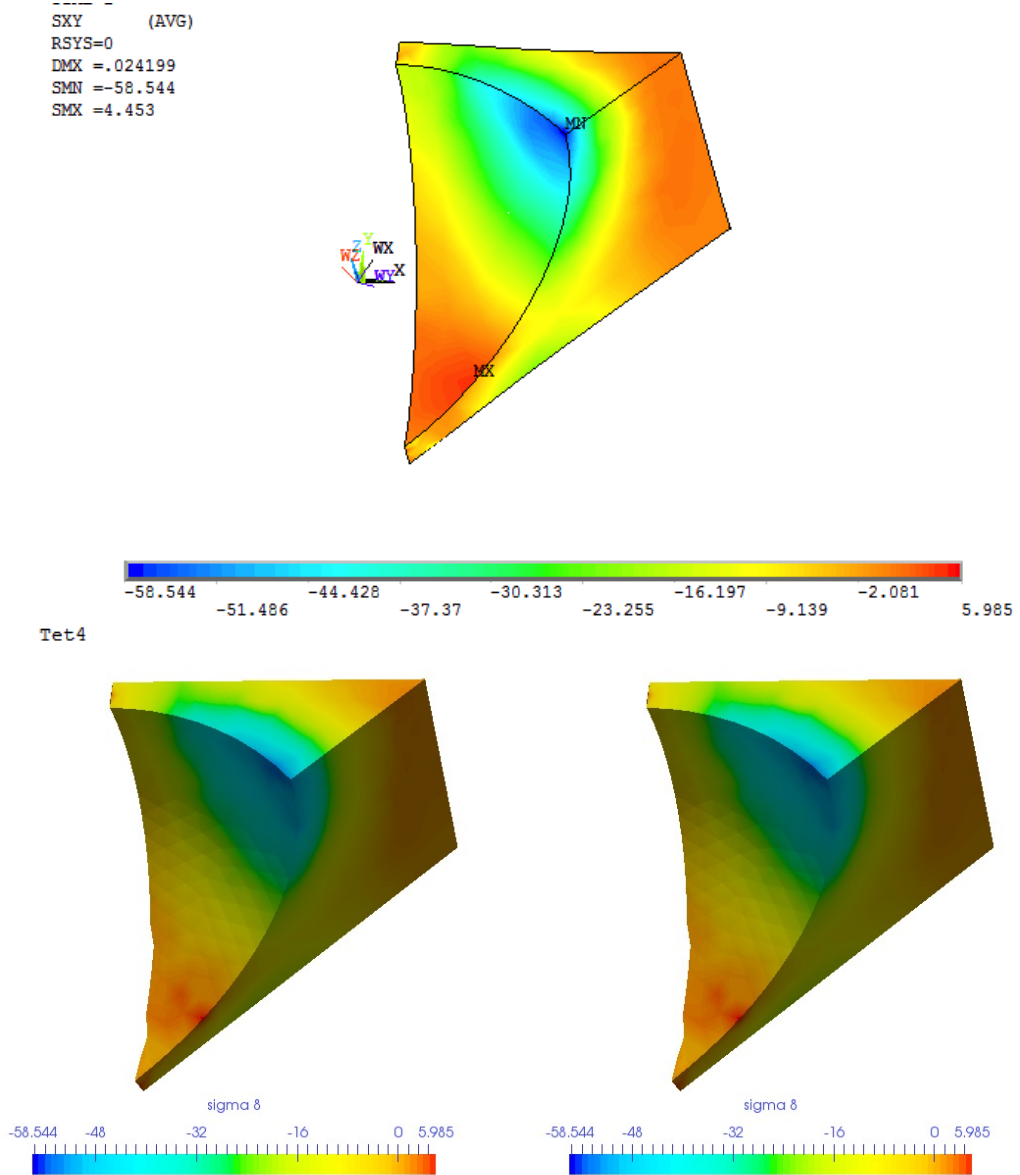


Figure 3.49: Mesh with Tet4, upper: contour plot of σ_{xy} in ANSYS; lower left: contour plot of σ_{xy} calculated without stress recovery in AMfe; lower right: contour plot of σ_{xy} calculated with stress recovery in AMfe

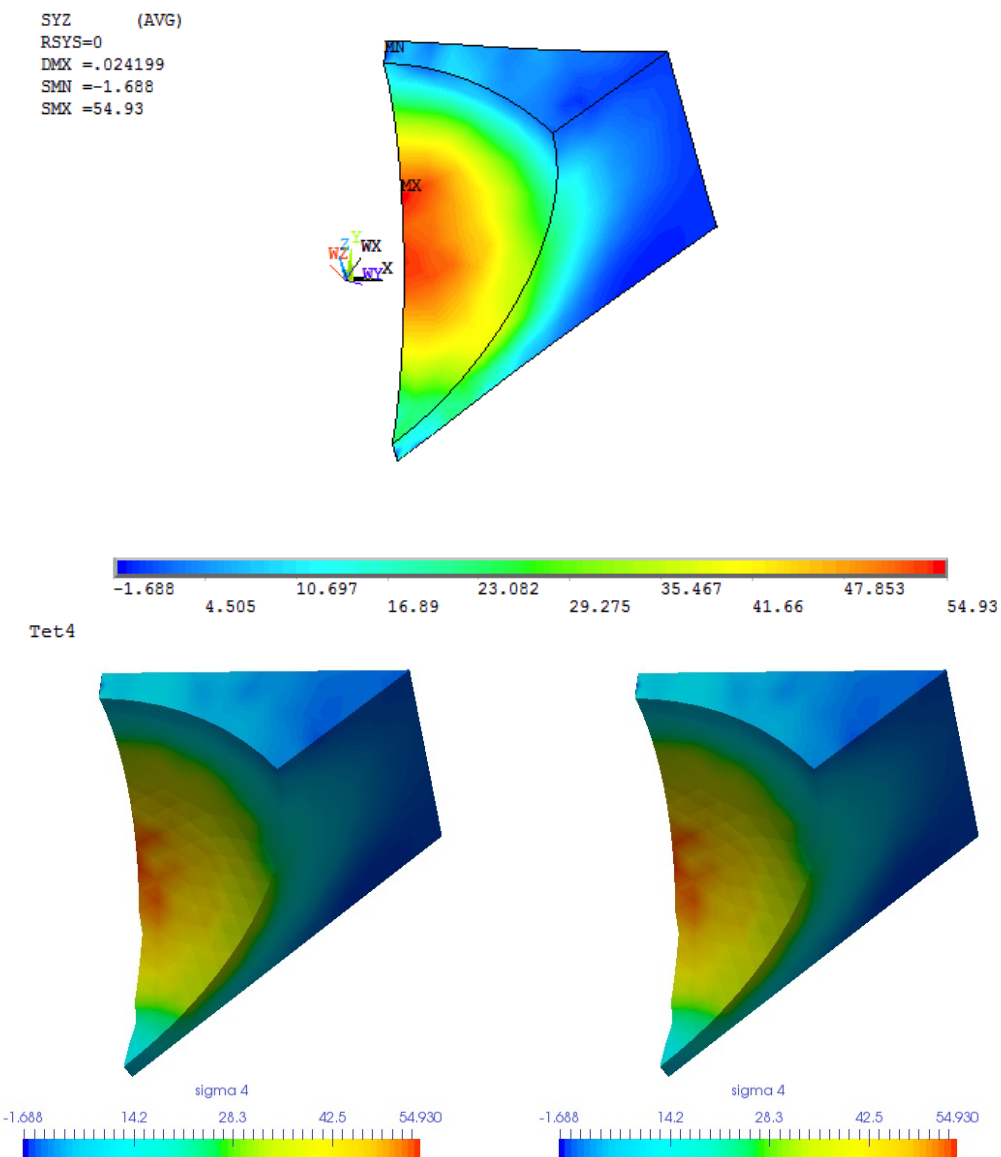


Figure 3.50: Mesh with Tet4, upper: contour plot of σ_{yz} in ANSYS; lower left: contour plot of σ_{yz} calculated without stress recovery in AMfe; lower right: contour plot of σ_{yz} calculated with stress recovery in AMfe

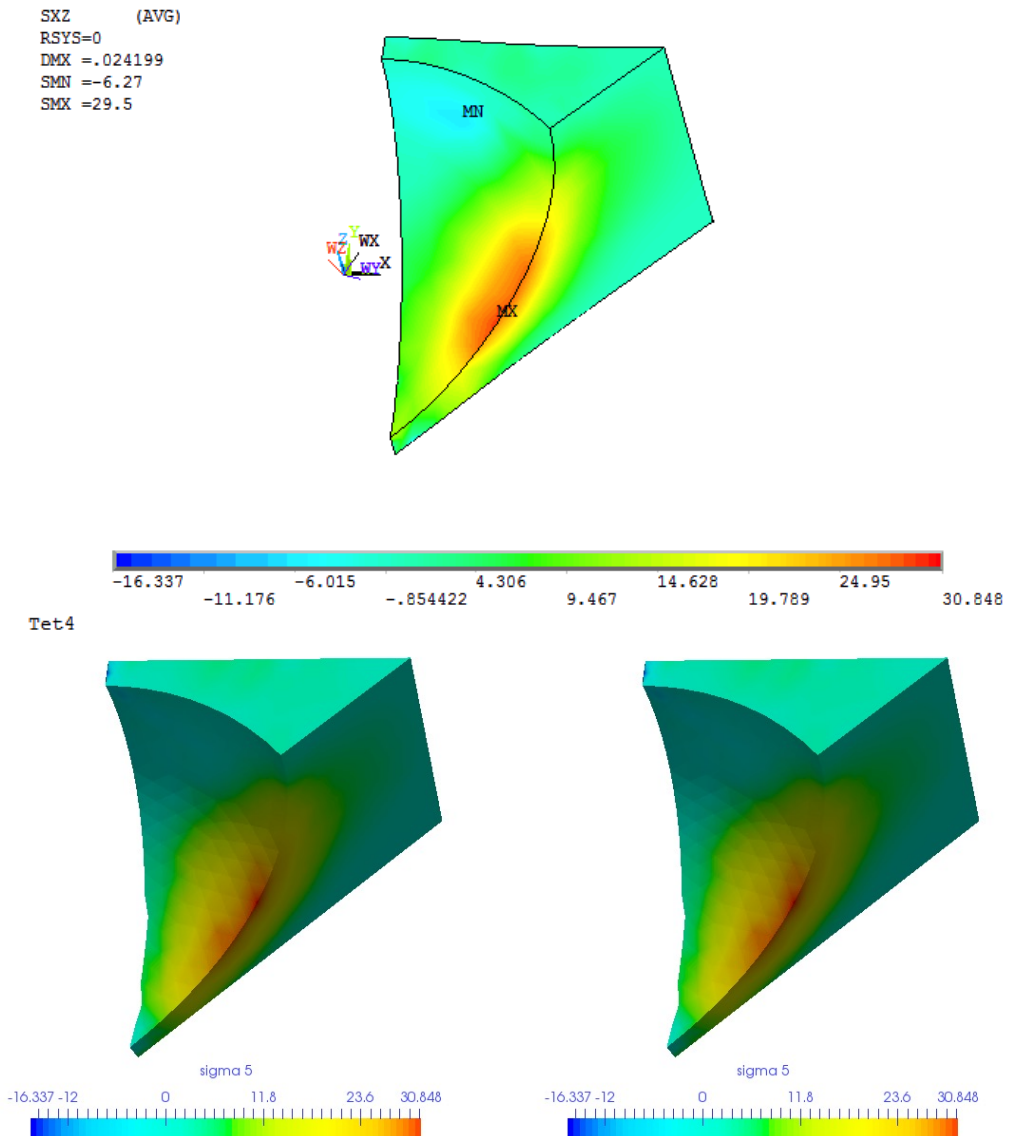


Figure 3.51: Mesh with Tet4, upper: contour plot of σ_{xz} in ANSYS; lower left: contour plot of σ_{xz} calculated without stress recovery in AMfe; lower right: contour plot of σ_{xz} calculated with stress recovery in AMfe

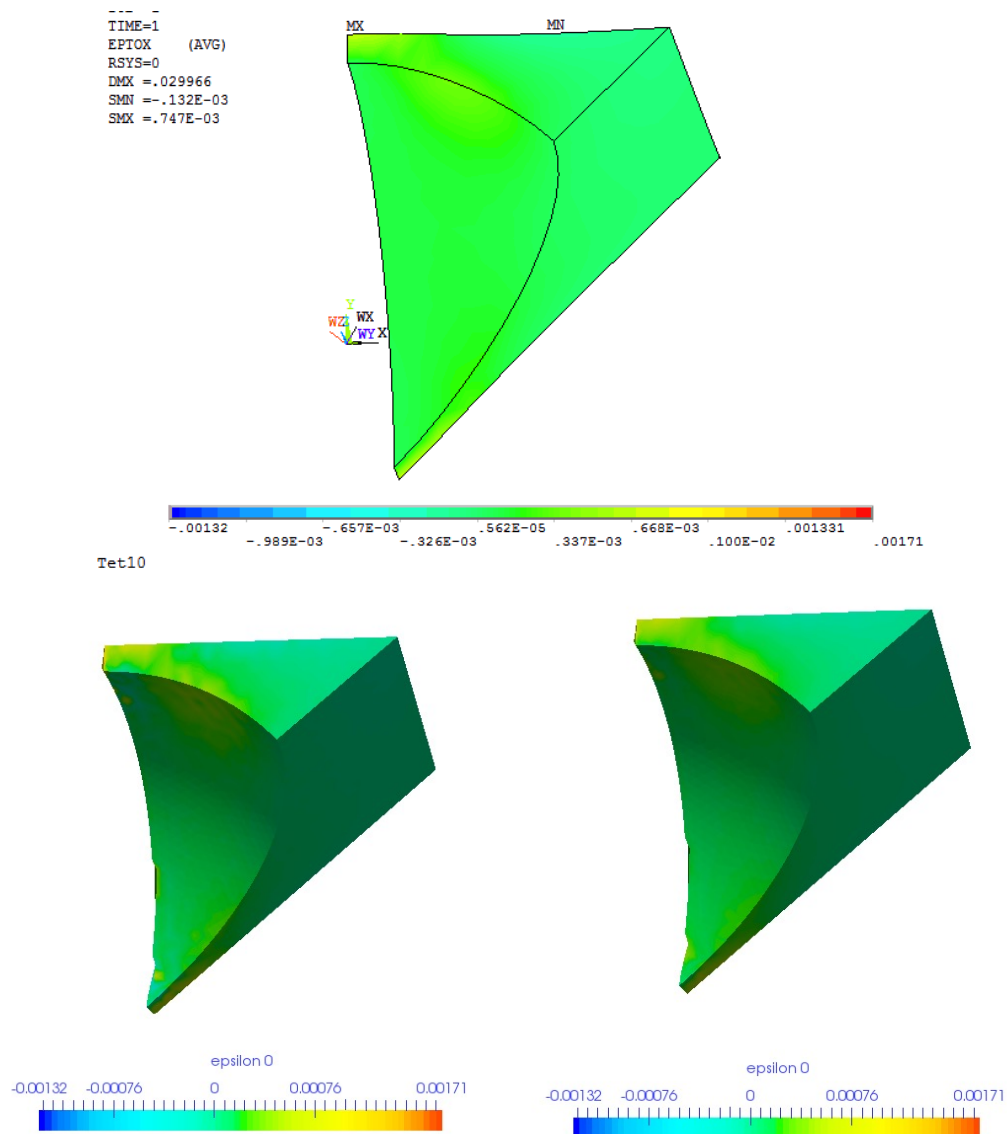


Figure 3.52: Mesh with Tet10, upper: contour plot of ϵ_{xx} in ANSYS; lower left: contour plot of ϵ_{xx} calculated without stress recovery in AMfe; lower right: contour plot of ϵ_{xx} calculated with stress recovery in AMfe

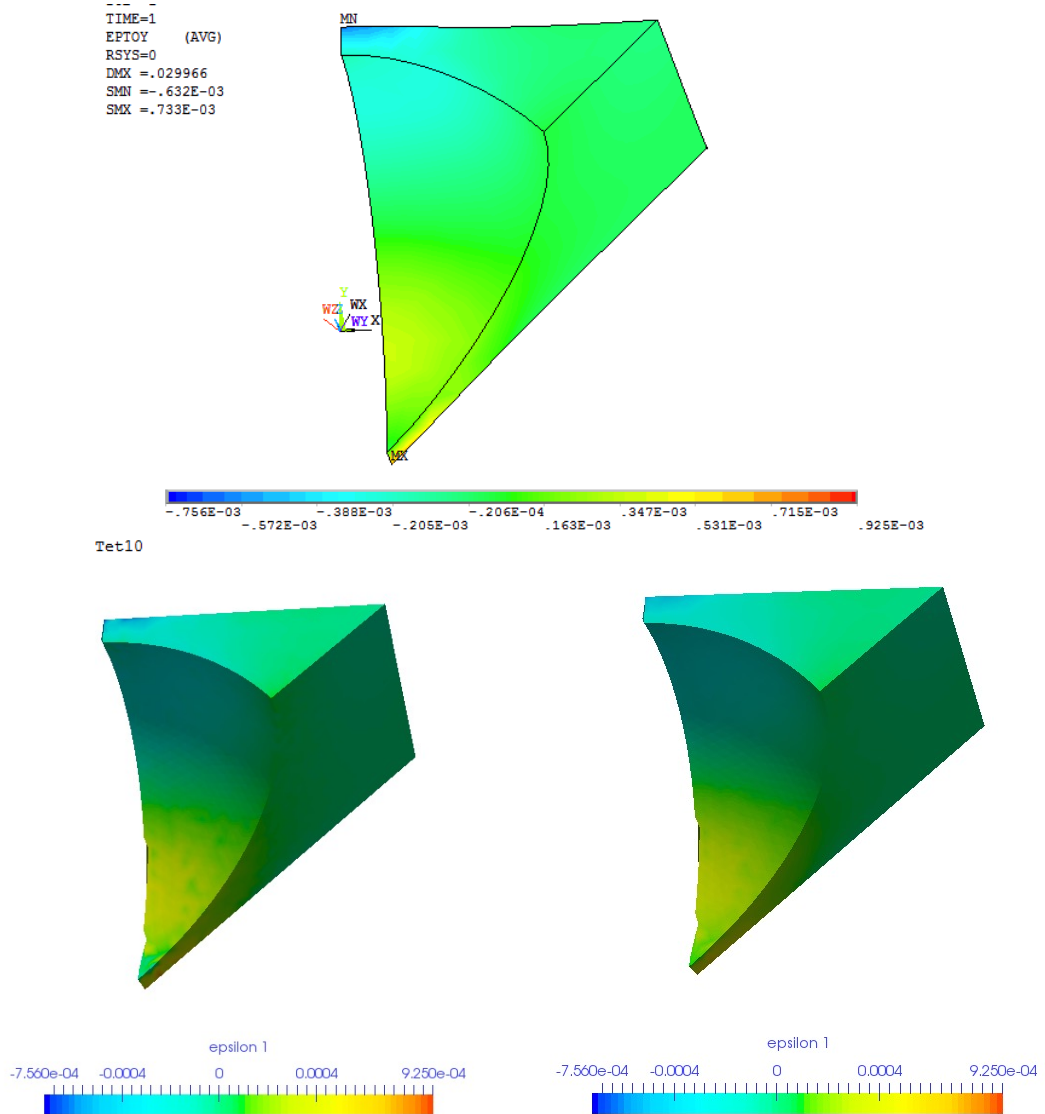


Figure 3.53: Mesh with Tet10, upper: contour plot of ϵ_{yy} in ANSYS; lower left: contour plot of ϵ_{yy} calculated without stress recovery in AMfe; lower right: contour plot of ϵ_{yy} calculated with stress recovery in AMfe

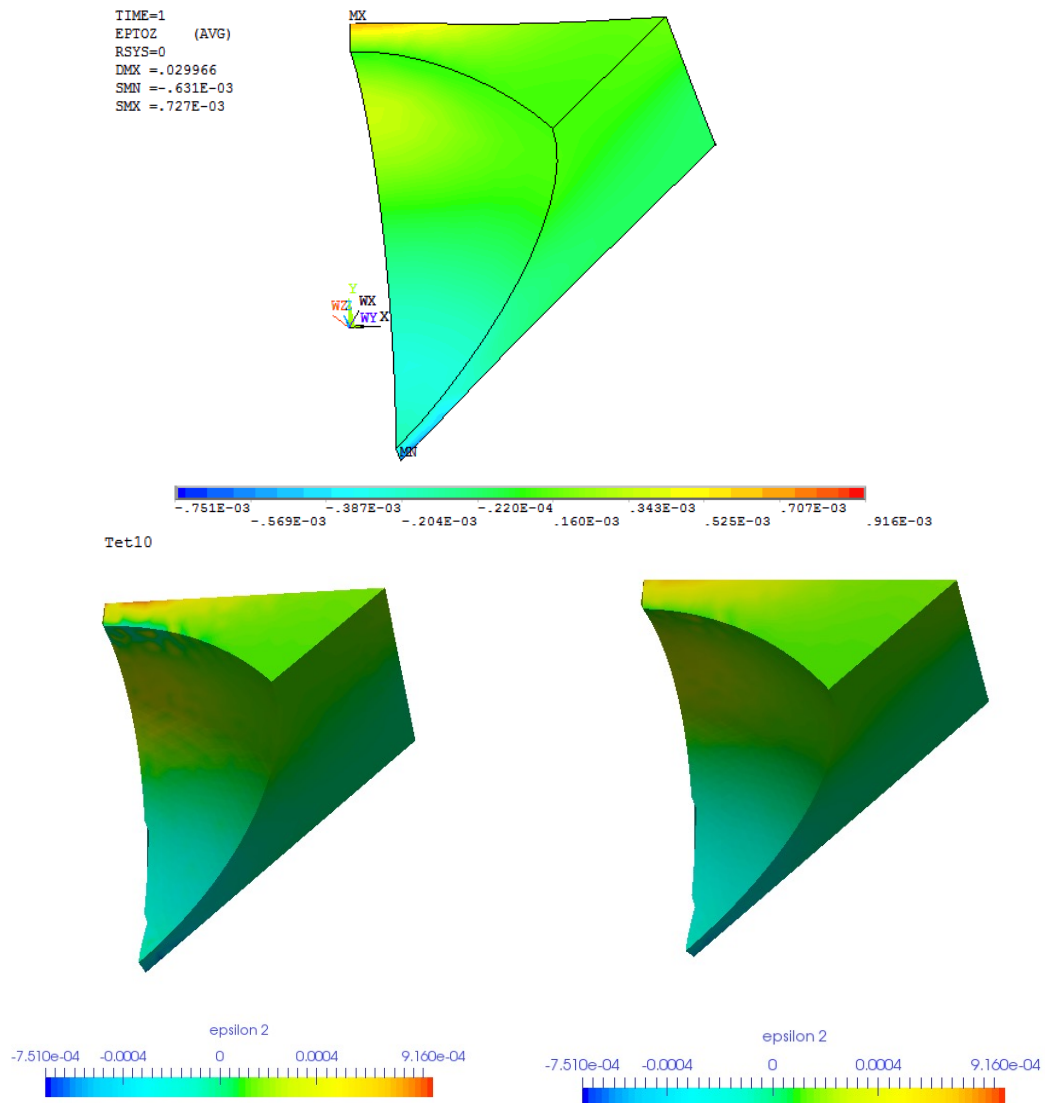


Figure 3.54: Mesh with Tet10, upper: contour plot of ϵ_{zz} in ANSYS; lower left: contour plot of ϵ_{zz} calculated without stress recovery in AMfe; lower right: contour plot of ϵ_{zz} calculated with stress recovery in AMfe

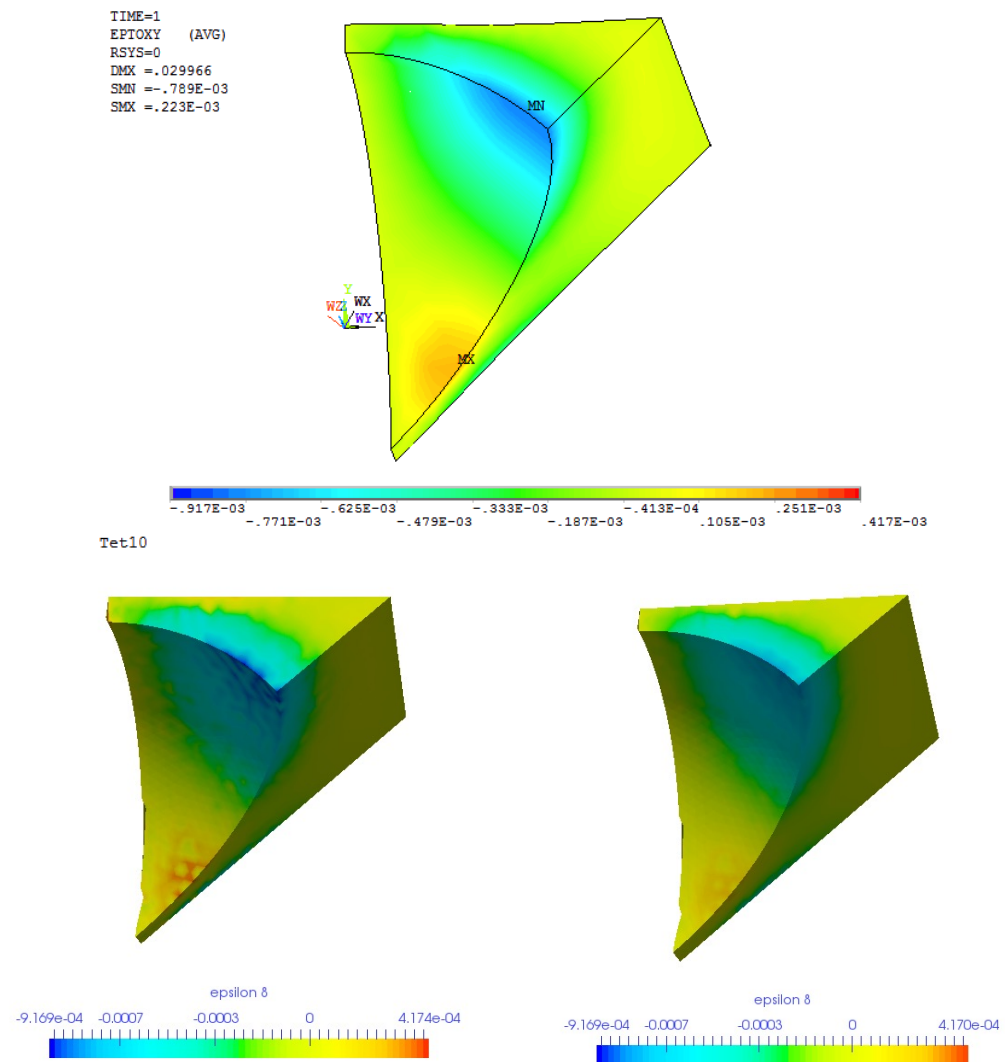


Figure 3.55: Mesh with Tet10, upper: contour plot of ϵ_{xy} in ANSYS; lower left: contour plot of ϵ_{xy} calculated without stress recovery in AMfe; lower right: contour plot of ϵ_{xy} calculated with stress recovery in AMfe

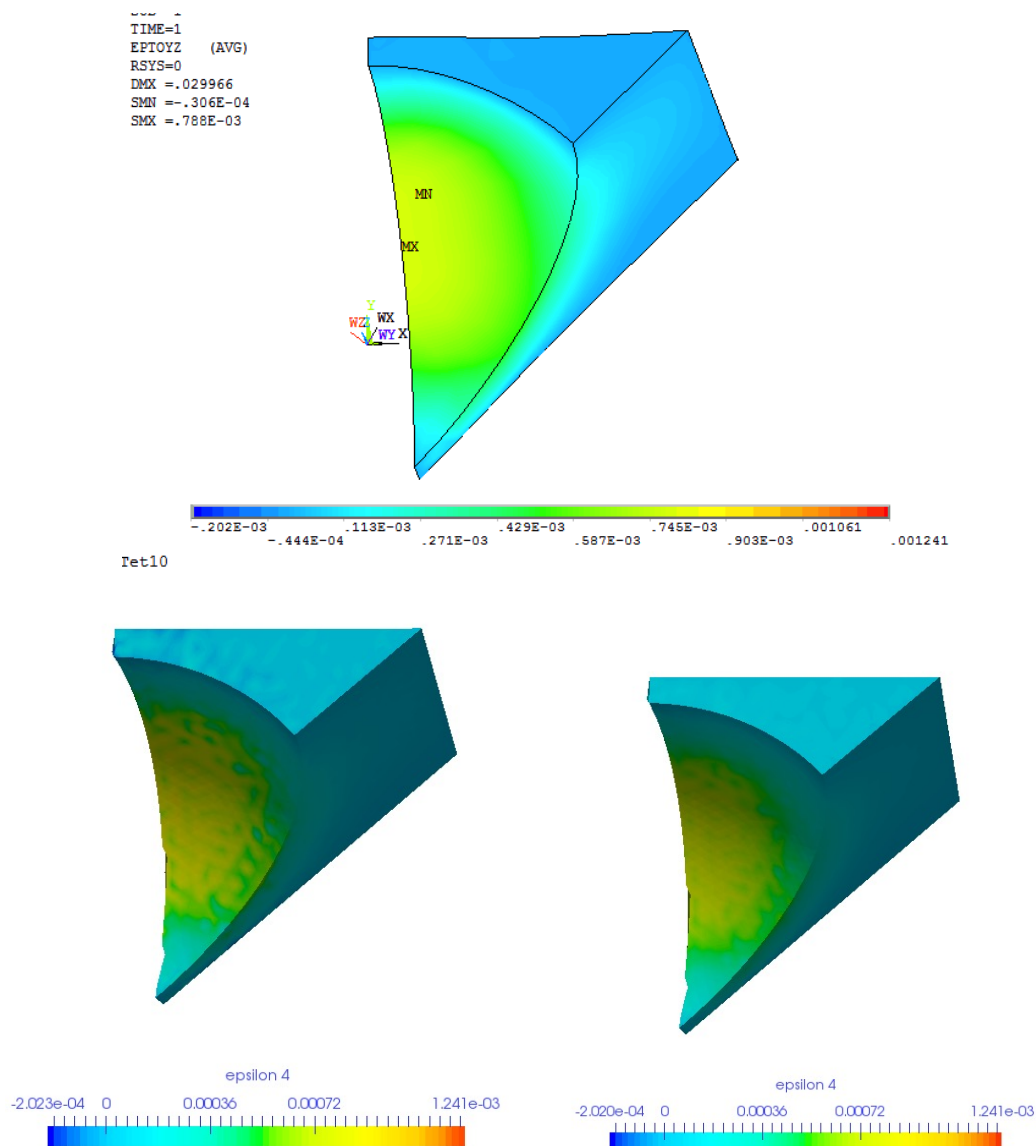


Figure 3.56: Mesh with Tet10, upper: contour plot of ϵ_{yz} in ANSYS; lower left: contour plot of ϵ_{yz} calculated without stress recovery in AMfe; lower right: contour plot of ϵ_{yz} calculated with stress recovery in AMfe

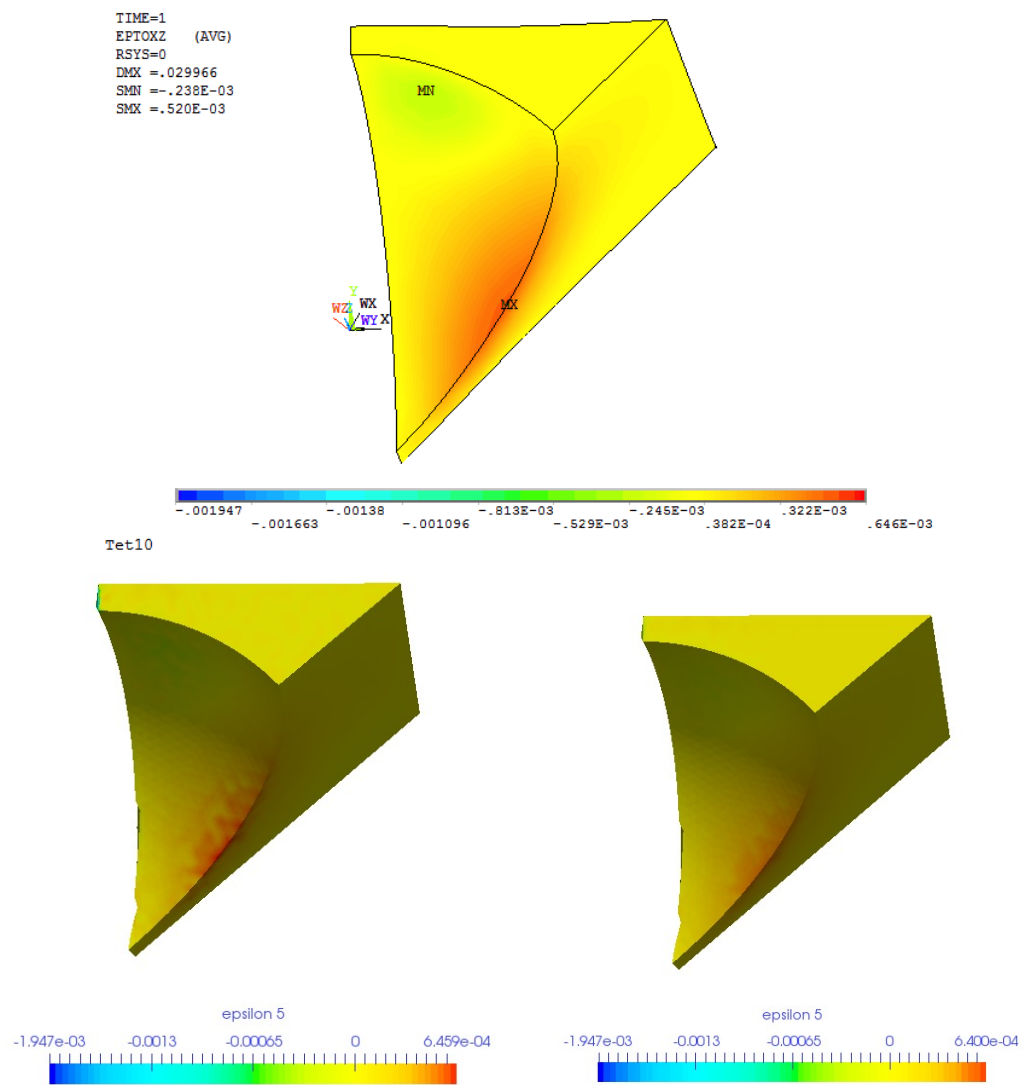


Figure 3.57: Mesh with Tet10, upper: contour plot of ϵ_{xz} in ANSYS; lower left: contour plot of ϵ_{xz} calculated without stress recovery in AMfe; lower right: contour plot of ϵ_{xz} calculated with stress recovery in AMfe

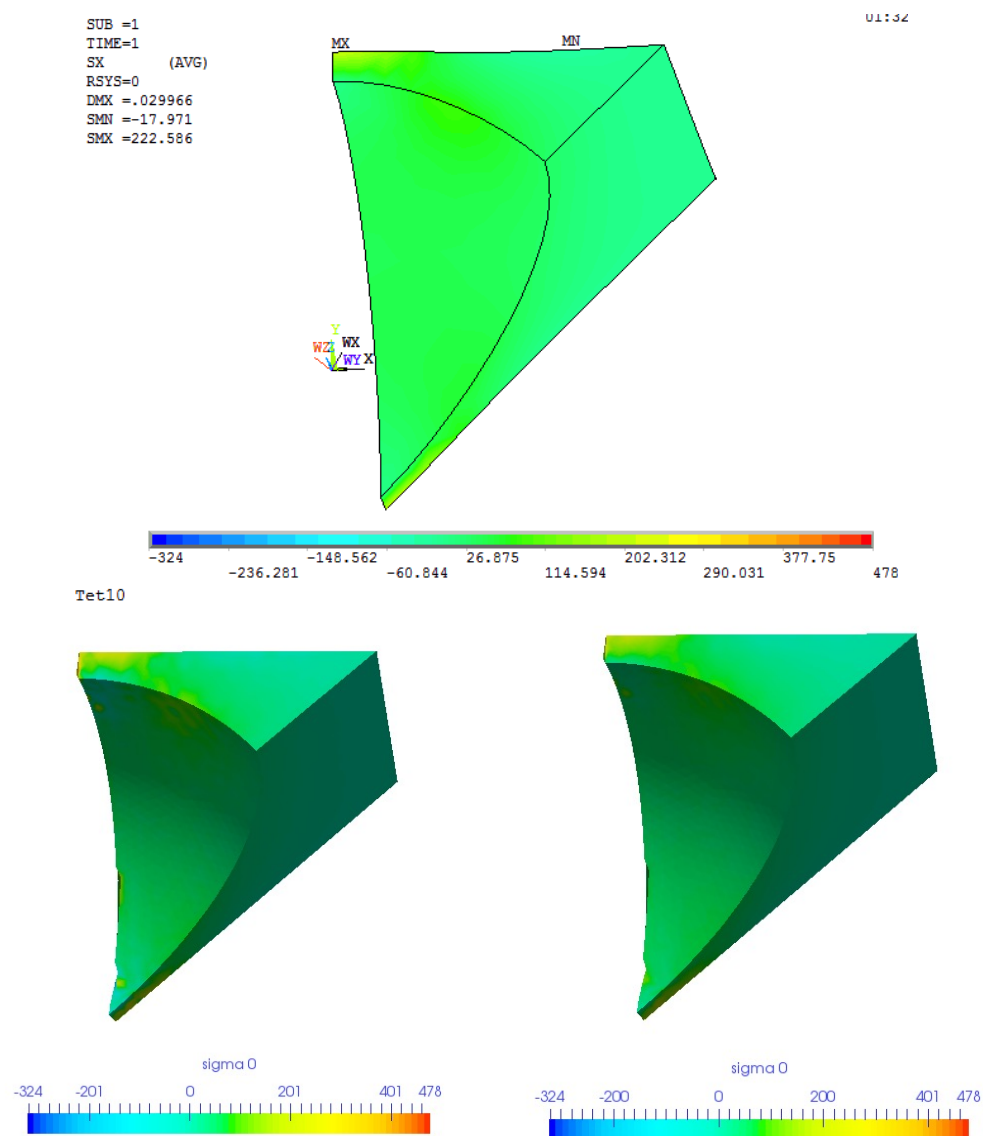


Figure 3.58: Mesh with Tet10, upper: contour plot of σ_{xx} in ANSYS; lower left: contour plot of σ_{xx} calculated without stress recovery in AMfe; lower right: contour plot of σ_{xx} calculated with stress recovery in AMfe

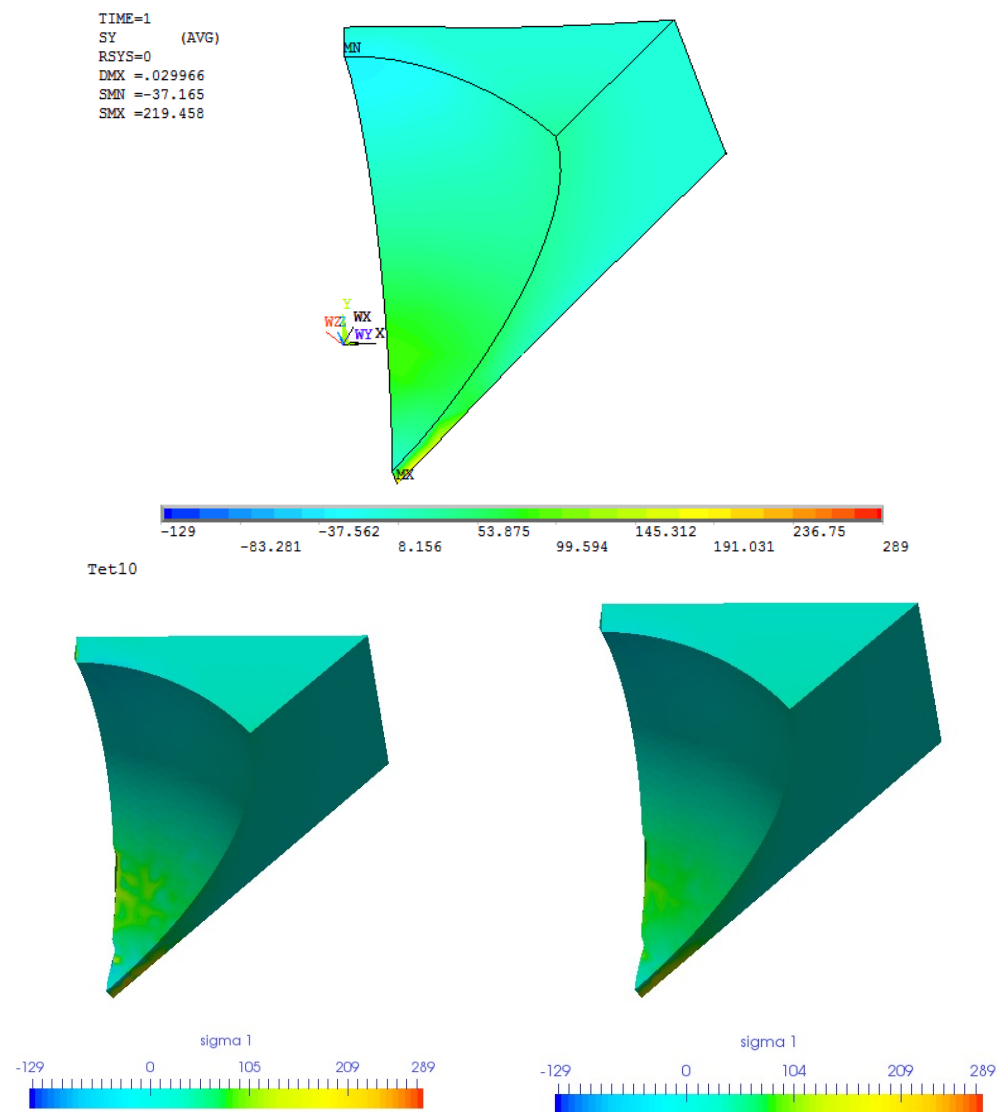


Figure 3.59: Mesh with Tet10, upper: contour plot of σ_{yy} in ANSYS; lower left: contour plot of σ_{yy} calculated without stress recovery in AMfe; lower right: contour plot of σ_{yy} calculated with stress recovery in AMfe

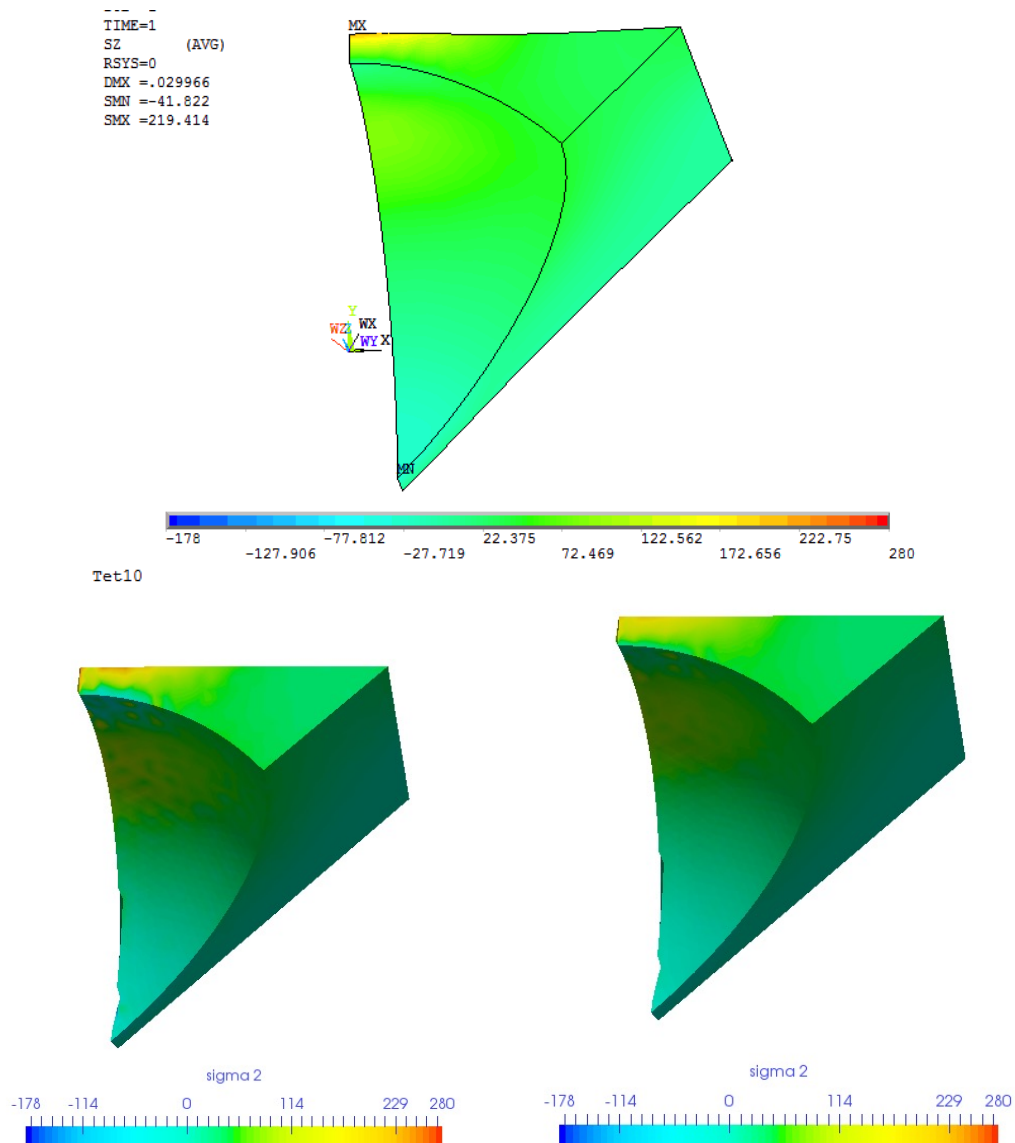


Figure 3.60: Mesh with Tet10, upper: contour plot of σ_{zz} in ANSYS; lower left: contour plot of σ_{zz} calculated without stress recovery in AMfe; lower right: contour plot of σ_{zz} calculated with stress recovery in AMfe

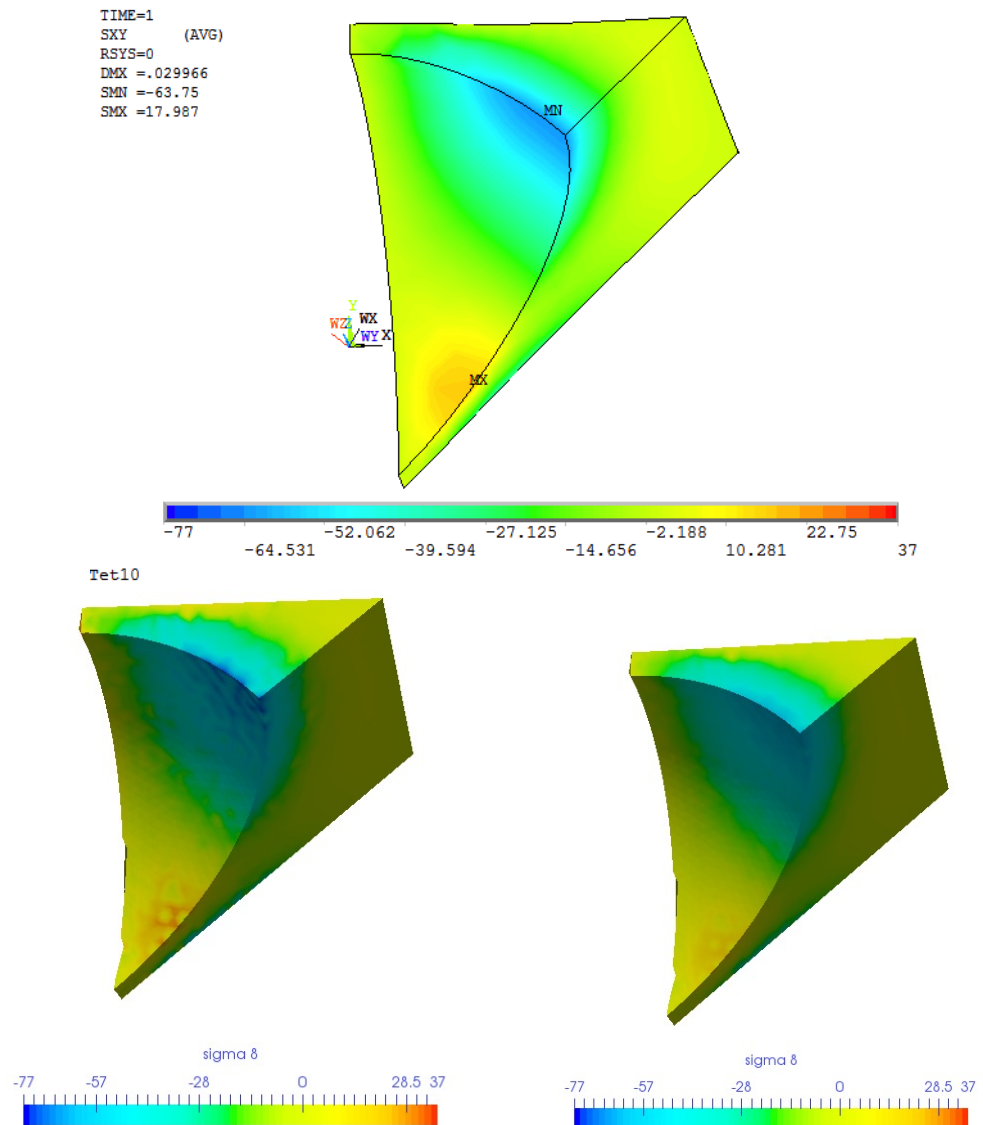


Figure 3.61: Mesh with Tet10, upper: contour plot of σ_{xy} in ANSYS; lower left: contour plot of σ_{xy} calculated without stress recovery in AMfe; lower right: contour plot of σ_{xy} calculated with stress recovery in AMfe

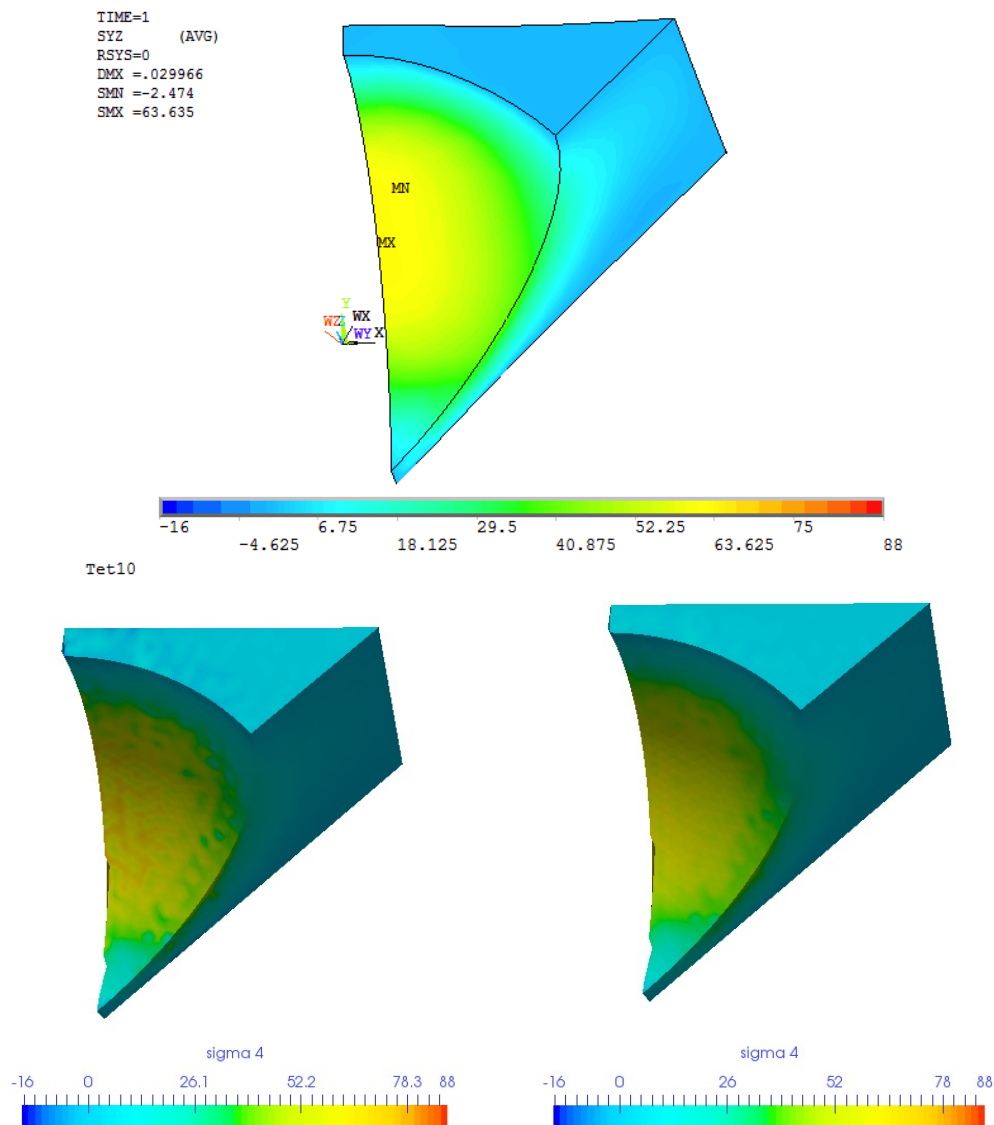


Figure 3.62: Mesh with Tet10, upper: contour plot of σ_{yz} in ANSYS; lower left: contour plot of σ_{yz} calculated without stress recovery in AMfe; lower right: contour plot of σ_{yz} calculated with stress recovery in AMfe

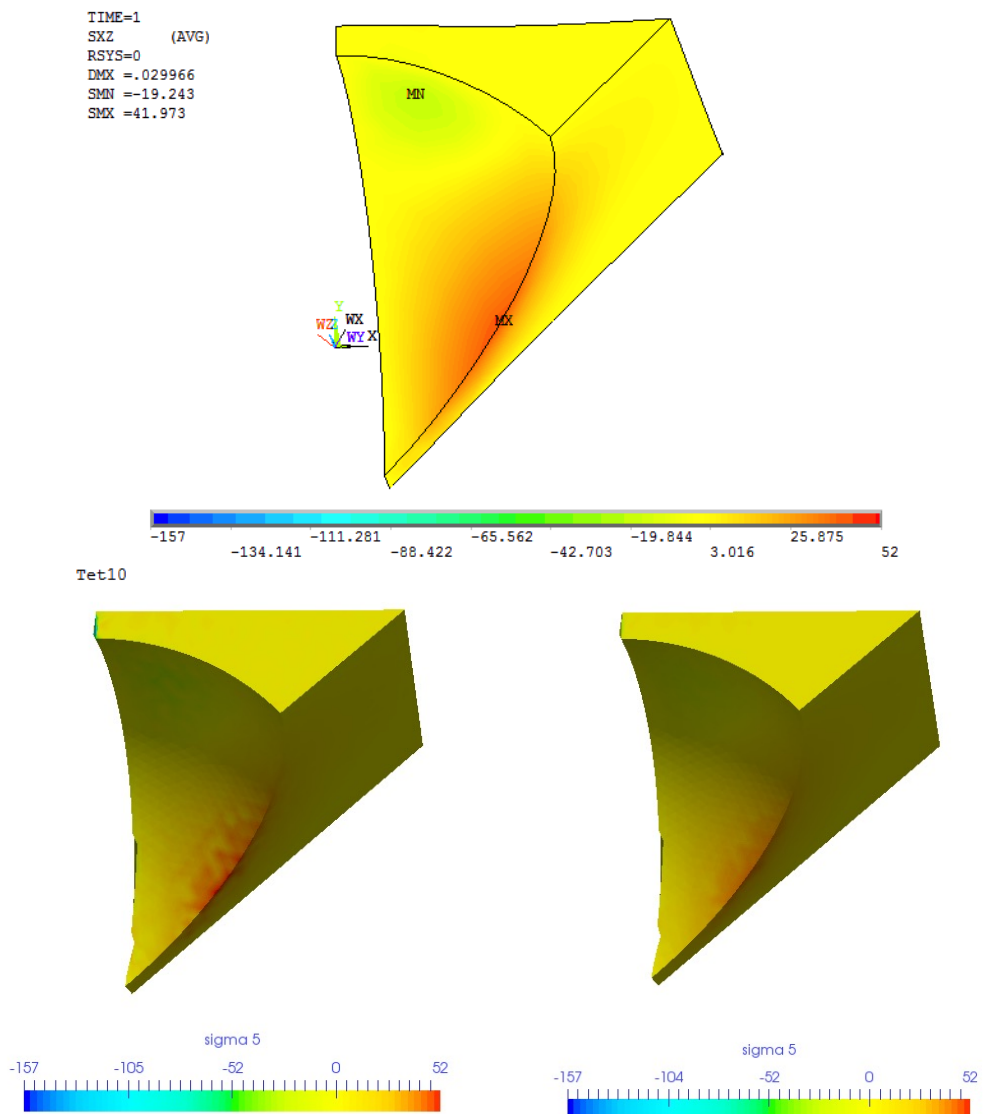


Figure 3.63: Mesh with Tet10, upper: contour plot of σ_{xz} in ANSYS; lower left: contour plot of σ_{xz} calculated without stress recovery in AMfe; lower right: contour plot of σ_{xz} calculated with stress recovery in AMfe

Chapter 4

Conclusion

4.1 Summary

There are two algorithms for calculating the approximation of nodal stress: one is called Direct-Evaluation-Algorithms and the other one is called Stress-Recovery-Algorithms. The latter is based on an extrapolation from the Gauss points to the corner nodes. According to the different element types, it is necessary to choose the suitable the coordinate systems. For quadrilateral elements, the Cartesian coordinate system is an appropriate choice. For triangular and tetrahedral elements, their own coordinate system is more appropriate for the calculation. The type of Gauss element for each element types is also available for selection. We make the selection as follows: 2×2 quadrilateral element with four Gauss points for Quad4; 3×3 quadrilateral element with nine Gauss points for Quad8; triangular element with three Gauss points for Tri3; triangular element with six Gauss points for Tri6; and tetrahedral element with four Gauss points for Tet4 and Tet10. The step after extrapolation of stress from Gauss points is to calculate the average value at each node by dividing the number of elements that share the same node. Then, the nodal stress is finally 'recovered'.

In the implementation part of this thesis, we export the Pre-Processing data from ANSYS modeling and import the above data into AMfe Toolbox for calculation. Then the solutions by Stress-Recovery-Algorithms and Direct-Evaluation-Algorithms are compared to the ANSYS solutions. A unit testing for calculating the Von Mises stress shows that only Tri3 and Quad4 have an acceptable accuracy of Von Mises stress values. Thus, we implement the displacement patch test for each element using both algorithms. All the element types using both algorithms have passed the patch test and Tri6, Quad8, Tet4, and Tet10 obtain the constant strain value of 1.5, which is expected to be 1. And the reason behind this issue has been found by debugging the code. The Pre-calculated strain at Gauss points is 1.5 when the modelling are meshed with Tri6, Quad8, Tet4, and Tet10. Hence, the nodal strain after extrapolation is also 1.5. This proves that the Stress-Recovery-Algorithms works well. In addition, the convergence analyses for displacement and Von Mises stress are also tested. The results of the displacement convergence analyses represent that all the element types converge to their exact solutions. The higher order elements (Tri6 and Tet10) have a relatively higher convergence rate than that of the lower order elements (Tri3 and Tet4). This characteristic is not that discernible in quadrilateral element types (Quad4 and

Quad8). The results of Von Mises stress convergence analysis represent that all the element types converge to the exact solutions and the elements with higher order (Tri6, Quad8, and Tet10) converge faster than the ones with lower order (Tri3, Quad4, and Tet4). The results also show that the Quad4 has a higher convergence rate than that of Tri3. The last test is to observe the performance of all the element types in a relatively complex model. We can compare not only the strain/stress contour plots between the solutions from Direct-Evaluation-Algorithms and the solutions from Stress-Recovery-Algorithms, but also the strain/stress contour plots between the solution from ANSYS and the solution from AMfe by the both algorithms. The comparisons among these three solution show that there is no difference between the solution by the both algorithms for Tri3 and Tet4, and the solutions from Stress-Recovery-Algorithms perform better than the solutions from Direct-Evaluation-Algorithms for the other element types (Tri6, Quad4, Quad8, and Tet10). The issue accompanying Direct-Evaluation-Algorithms is the deviation at the value around the extreme values. The values in the middle range appear closer to the ANSYS than the values at the ends do. In summary, Stress-Recovery-Algorithms provide higher accuracy in nodal stress for Tri6, Quad4, Quad8, and Tet10 than Direct-Evaluation-Algorithms do.

4.2 Recommendation

According to the work of Carlos A. Felippa [Felippa 2004 section 28 p.6], there are two methods in calculating the average nodal stress after stress recovery. One is the approach of unweighted averaging for the nodal stress, which we apply in this paper. The other is weighted averaging for the nodal stress, which allocates the weights to the contributions of element sharing the same node. Stress components and element types could affect their weights in selection.

According to the patch test in this paper, we found that the strains at Gauss points with element types Tri6, Quad8, Tet4, and Tet10 are problematic. Therefore, an investigation into the calculation of strain at Gauss points with these above mentioned element types is meaningful in improving the accuracy of nodal strain and stress.

In this thesis, we only discuss the case of extrapolation from one type of Gauss element. A comparison and discussion of the nodal stress among the extrapolation by using different types of Gauss element would be helpful for the further development of Stress-Recovery-Algorithms.

qwe Wang Felippa 2004qwe

Bibliography

- Felippa, Carlos A. (2004). *INTRODUCTION to Introduction to Finite Element Methods*. Boulder, Colorado 80309-0429, USA: University of Colorado.
- Dukkipati, Rao V. (2010). *Numerical Methods*. 4835/24 Ansari Road, Daryaganj, New Delhi: New Age International Publishers.
- ANSYS, Inc (2011). *ANSYS Parametric Design Language Guide*. Release 14.0. ANSYS, Inc. Canonsburg, PA 15317.
- Kurowski, P. M. (2012). *Von Mises Stress failure criterion*.
- Wall, W. A. (2014). *Finite Element*. Ed. by Svenja Schoeder. 9th ed. Lehrstuhl für Numerische Mechanik, Fakultät für Maschinenwesen, Technische Universität München.
- Fred L. Drake, Jr. (2016). *The Python Language Reference*. 3.51. Python Software Foundation.
- Mckinney, Wes (2016). *Pandas: powerful Python data analysis toolkit*. Release 0.18.1. PyData Development Team.
- Numpy (2016). *Numpy User Guide*. Release 1.11.0. Numpy community.
- Rutzmoser, Johannes (2016). “MEMO: Nichtlineare Finite Elemente”.

Disclaimer

I hereby declare that this thesis is entirely the result of my own work except where otherwise indicated. I have only used the resources given in the list of references.

Garching, 30.05.2016

(Signature)